

The Messenger



No. 141 – September 2010

On the difference between seeing and image quality
Measuring water vapour over Paranal and La Silla
The ESO Remote Galaxy Survey
Astronomical research by high school students



A New Coronagraph for NAOS–CONICA — the Apodising Phase Plate

Matthew Kenworthy¹
 Sascha Quanz²
 Michael Meyer²
 Markus Kasper³
 Julien Girard³
 Rainer Lenzen⁴
 Johanan Codona⁵
 Philip Hinz⁵

¹ Leiden Observatory, the Netherlands

² ETH Zurich, Switzerland

³ ESO

⁴ Max-Planck-Institut für Astronomie,
 Heidelberg, Germany

⁵ University of Arizona, USA

In April 2010, a new coronagraphic optical element, called an Apodising Phase Plate (APP), was installed in NAOS–CONICA (NACO). The APP coronagraph is optimised for use at $4.05\ \mu\text{m}$ with both narrow- and broadband filters. Unlike other types of coronagraph, it requires no alignment overhead and can be used immediately after switching from direct imaging for observing targets of interest where high contrast is required.

The Apodising Phase Plate (APP) is optimised for observations using the newly introduced IB4.05 filter in NACO (Rousset et al., 2003; Lenzen et al., 2003) and we have also demonstrated its performance at broader bandpasses around $4\ \mu\text{m}$ with the L' filter (Kenworthy et al., 2010). In this article, we describe the principle of the optical element, how it can be used for NACO observations and explain its strengths and weaknesses.

The goal of a coronagraph is to minimise the diffracted light from one astronomical source whilst letting through as much of the light as possible from a nearby, usually much fainter, source. The original Lyot coronagraph uses two optical elements within an astronomical camera to suppress light from the on-axis source. The image of the central star and a nearby planet, for example, is formed in a focal plane (FP), where a mask blocks light from the star out to a given radius (see Figure 1). The planet is ideally displaced off to one side of the star, and the light from the planet is not blocked by

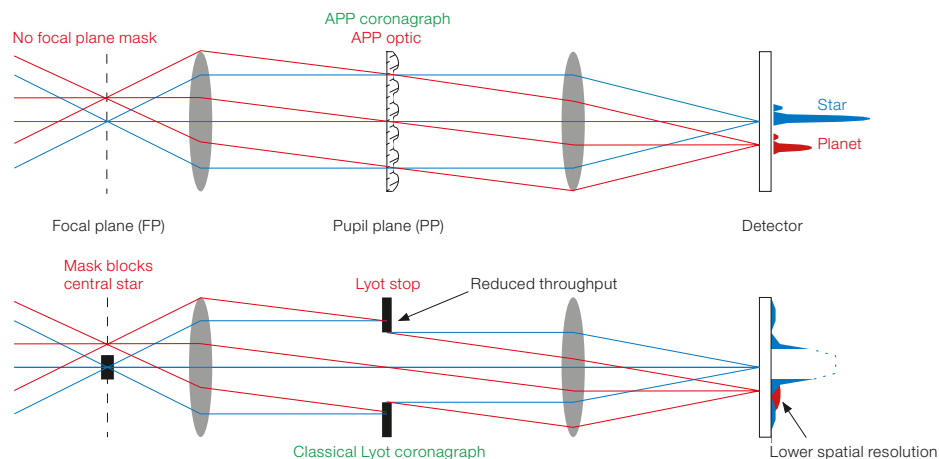


Figure 1. A comparison of the principles used in the Apodising Phase Plate coronagraph and in a classical Lyot coronagraph.

this mask. Reimaging optics form a pupil plane (PP) image (often coincident with the camera's filter wheel) and a Lyot stop then blocks light from the outer edge of the re-imaged telescope pupil, before going on to form the final image using another optical element at the science detector. Kasper et al. (2009) described pupil-stabilised Lyot coronagraphy at $4\ \mu\text{m}$ with NACO for exoplanet detection. The classical Lyot design is sensitive to the telescope's alignment of the star on the focal plane mask and there is a strong trade-off between angular resolution and achievable suppression: if the planet is too close to the star, the planet's light can also be blocked by the focal plane mask. Other coronagraphic designs, such as the four quadrant phase mask and phase-induced amplitude apodisation, significantly improve on the Lyot design, but still suffer from the tight tip-tilt alignment tolerances in the focal plane (for a review comparing many types of coronagraph, see Guyon et al., 2006).

How the APP works

The Apodising Phase Plate consists of just one optical element, rather than two, in the pupil plane of the telescope. It is a development of phase apodisation coronagraphy, originally developed by Johanan Codona at the University of Arizona (Codona & Angel, 2004; Codona, 2006) and initially tested at the 6.5-metre MMT (Kenworthy et al., 2007). Here, we

use light diffracted from the Airy core of the central star to cancel out the coherent light in the outer diffraction rings. Small sinusoidal ripples of phase added to the incoming wavefront act like a simple diffraction grating, creating a pair of “speckles” that can be adjusted to cancel out diffraction on one side of the star, but reinforcing it on the opposite side. Mathematically adding many of these virtual gratings together forms the resultant APP pattern, seen in Figure 2. Its effect on the Very Large Telescope (VLT) point spread function (PSF) is seen in the commissioning data in Figure 3. The APP optical element itself is shown in Figure 4 prior to installation.

It is important to note that every imaged object in the field of view — including any faint companions and extended structure — all have this new, modified APP PSF. Since energy from the Airy core is used in suppressing diffraction, there is an effective loss of transmission of the faint companion. We have designed the plate to use 40% of the Airy core flux to provide diffraction suppression, but this loss of planet flux is more than compensated by the much larger reduction of diffracted light from the central star. The measured throughput for the APP is 0.60 with an error of 0.02, consistent with the design specifications.

Since there is no focal plane mask that the target star has to be aligned behind, the greatest benefit for a NACO user is that there is no alignment overhead for the APP coronagraph. The target star can be beam-switched anywhere on the imaging array with no impact whatsoever on the

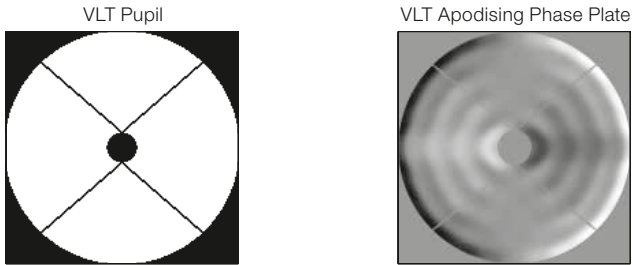


Figure 2. (Left) The APP phase plate pattern and its effect on the VLT point spread function.

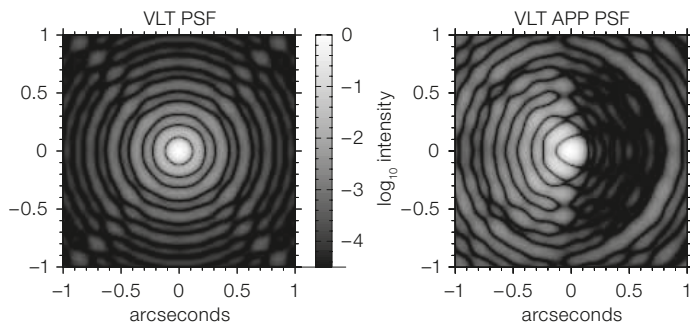
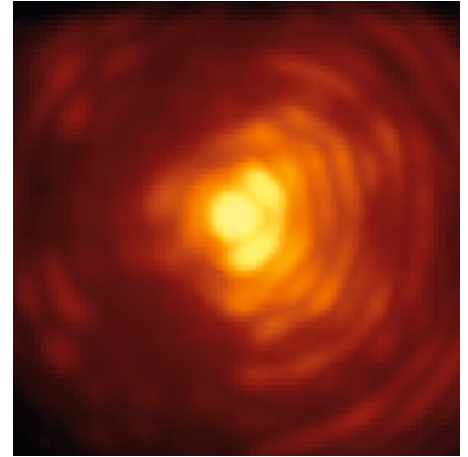


Figure 3. (Right) An image of the VLT PSF taken with the APP on NACO. The image has been logarithmically scaled for clarity.



coronagraph's performance. All coronagraphs represent a trade-off between inner working angle, planet flux throughput, and spatial resolution. In the case of the APP, it is designed to provide diffraction suppression from 0.180 arcseconds out to 0.750 arcseconds, moving the sky background limit up to three times closer to the central star than direct imaging observations. Beyond a radius of 0.750 arcseconds (the actual value varies with target star magnitude and adaptive optics [AO] correction) it is preferable to use direct imaging and related subtraction techniques.

Using the APP with NACO

The APP is used with the CONICA L27 camera nominally providing a field of view of 28 by 28 arcseconds. However, to prevent ghost reflections from the optics interfering with the coronagraphic mode, the APP has an optical wedge introduced into it. The practical result is that the APP can be used over the upper third of the detector area (i.e. no restrictions along the x-axis of the detector). There is no impact on the PSF quality and one can beam-switch along this part of the detector in a manner identical to direct imaging observational techniques. Observing with the APP does not increase the overhead of observations apart from that due to the reduced corona-

graphic throughput of 60%. If full field coverage around a target of interest is required, a second dataset with the field of view rotated by 180 degrees is required to cover both hemispheres around a target.

The APP can be used in pupil-tracking mode so that the fixed-pattern speckles of the telescope and instrument remain fixed with respect to the orientation of the APP PSF. A combination of angular differential imaging and/or PSF subtraction with a nearby reference star with similar colour and magnitude is required to minimise contributions from the uncorrected seeing halo produced by the adaptive optics system and to minimise any residual quasi-static speckles. The APP optical element is chromatic and is designed for a central wavelength of 4.05 μm , but the coronagraphic suppression only degrades slowly with increasing bandwidth, which was seen in the L' contrast curve determined during engineering time in April 2010.

In Figure 5, we show the contrast achieved in a 30-minute integration on HIP 61460 (an F2 V star with $L' = 6.2$ mag) using the L' filter (central wavelength 3.8 μm) with the observations made in pupil-tracking mode with detector integrations of DIT = 0.175 s, NDIT = 30 and NINT = 5, yielding five images at different dither positions. All images were in the

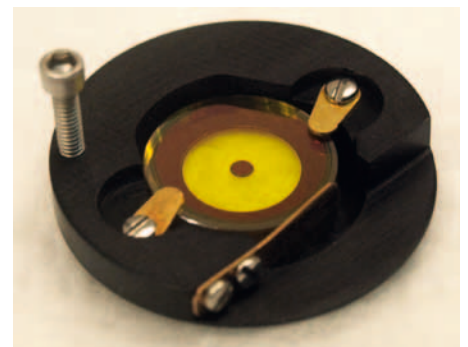


Figure 4. The APP optical element prior to installation in CONICA. The light yellow area is the transmissive ZnSe and the brown area is a gold coating that aids alignment in the pupil mask wheel.

linear detector regime (approximately one-third full well), the DIMM seeing varied between 0.7 and 0.8 arcseconds, and the airmass was less than 1.1. The contrast curve was calculated by stacking the images together and computing the root mean square (rms) per pixel in the stack. Using an aperture with a radius of 5 pixels, the mean flux per pixel in the core of the PSF was computed and then divided by the mean flux per pixel for a planet with a signal-to-noise ratio of 5 (estimated from the rms in a similar aperture at a given radial separation). The resultant L' contrast curve shows that the APP is working as expected and approximately as predicted from the simulations, and the contrasts are comparable to those from other coronagraphs. The steep drop of the contrast curve shows the specific strength of the APP, as we reach a 5σ point source detection limit of 10 magnitudes at 0.4 arcseconds offset.

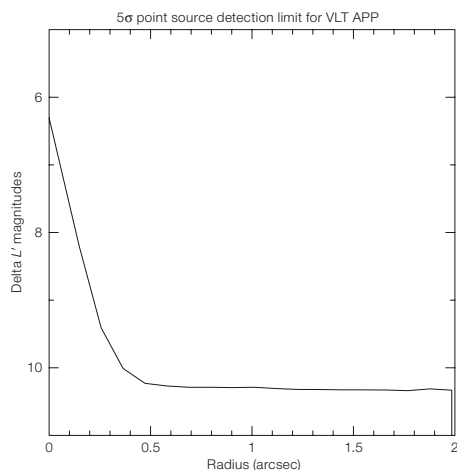


Figure 5. An L' contrast curve taken with the APP coronagraph. The curve shows the 5σ detection limit of a point source in L' -band as a function of angular separation from a star. The curve is calculated over a 150-degree wedge centred in the high contrast side of the APP PSF.

Further data on a brighter star will be taken to explore the contrast limit at larger radii, as in this dataset we are sky background limited at 0.5 arcseconds offset.

Thermal wavelengths are a natural regime for exoplanet searches, as the planet-to-star flux ratio falls more slowly with effective temperature than at shorter wavelengths (Hinze et al., 2006; Kasper et al., 2007). As telescope apertures increase, the red colours of exoplanets (see Heinze et al., 2010 for a fuller discussion) mean that the L' - and M -bands become more favourable for direct imaging contrast-limited searches around nearby stars.

The APP is available for general use with NACO, and some of the first results using the APP to obtain NB4.05 photometry of the planet beta Pictoris b (Lagrange et al., 2010) have been submitted (Quanz et al., 2010). Further developments include

an achromatised design suitable for working over broader wavelength ranges, and the potential for inclusion on the European Extremely Large Telescope (E-ELT) for thermal imaging of exoplanets with instruments such as METIS (see Brandl et al., 2010).

References

- Brandl, B. et al. 2010, *The Messenger*, 140, 30
 Codona, J. & Angel, J. R. P. 2004, *ApJL*, 604, 117
 Codona, J. et al. 2006, *SPIE*, 6269, 55
 Guyon, O. et al. 2006, *ApJS*, 167, 81
 Heinze, A. et al. 2010, *ApJ*, 714, 1570
 Hinze, P. et al. 2006, *ApJ*, 653, 1486
 Kasper, M. et al. 2007, *A&A*, 472, 32
 Kasper, M. et al. 2009, *The Messenger*, 137, 8
 Kenworthy, M. et al. 2007, *ApJ*, 660, 762
 Kenworthy, M. et al. 2010, *SPIE*, 7735, arXiv:1007.3448
 Lagrange, A.-M. et al. 2010, *Science*, 329, 57
 Lenzen, R. et al. 2003, *SPIE*, 4841, 944
 Quanz, S. et al. 2010, *ApJL*, submitted
 Rousset, G. et al. 2003, *SPIE*, 4839, 140

Credit: ALMA (ESO/NAOJ/NRAO)



Testing of the first two fully assembled European ALMA antennas, manufactured by the AEM consortium, has recently begun at the ALMA Operations Support Facility (OSF). The image shows a European antenna being moved by one of the ALMA transporters, Lore, at the OSF.

On the Difference between Seeing and Image Quality: When the Turbulence Outer Scale Enters the Game

Patrice Martinez¹
 Johann Kolb¹
 Marc Sarazin¹
 Andrei Tokovinin²

¹ ESO

² Cerro-Tololo Inter American Observatory, Chile

We attempt to clarify the frequent confusion between seeing and image quality for large telescopes. The full width at half maximum of a stellar image is commonly considered to be equal to the atmospheric seeing. However the outer scale of the turbulence, which corresponds to a reduction in the low frequency content of the phase perturbation spectrum, plays a significant role in the improvement of image quality at the focus of a telescope. The image quality is therefore different (and in some cases by a large factor) from the atmospheric seeing that can be measured by dedicated seeing monitors, such as a differential image motion monitor.

Seeing and *image quality* are two quantities that are frequently confused in the field of astronomical instrumentation. The first is an inherent property of the atmospheric turbulence, which is independent of the telescope that is observing through the atmosphere. The second, defined as the full width at half maximum (FWHM) of long-exposure stellar images, is a property of the images obtained in the focal plane of an instrument mounted on a telescope observing through the atmosphere. Without considering instrumental aberrations, one remaining property of the turbulence that affects the image quality is the outer scale: the size of the largest turbulent eddies present in the atmosphere. It has been observed that the image quality in a large telescope is always lower than the seeing, owing to the finite outer scale of the turbulence, as opposed to the commonly used Kolmogorov theory that considers an infinite outer scale.

In this article we discuss the dependence of atmospheric long-exposure resolution on the outer scale of the turbulence over the practically interesting range

of telescope diameters and wavelengths. We show that this dependence is efficiently predicated by a simple approximate formula introduced in the literature in 2002. The practical consequences for operation of large telescopes are discussed and an application to on-sky data is presented.

Background and definitions

In practice the resolution of ground-based telescopes is limited by the atmospheric turbulence, called “seeing”. It is traditionally characterised by the Fried parameter (r_0) – the diameter of a telescope such that its diffraction-limited resolution equals the seeing resolution. The well-known Kolmogorov turbulence model describes the shape of the atmospheric long-exposure point spread function (PSF), and many other phenomena, by this single parameter r_0 . This model predicts the dependence¹ of the PSF FWHM (denoted ϵ_0) on wavelength (λ) and inversely on the Fried parameter, r_0 , where r_0 depends on wavelength (to the power $-1/5$) and airmass (to the power $3/5$). In the following, we assume that r_0 and ϵ_0 refer to observations at the zenith. In addition, by adopting a standard wavelength of 500 nm, we can refer to ϵ_0 in place of r_0 for defining the strength of the turbulence, and this single parameter is nowadays usually called seeing. The equivalence between FWHM of a long-exposure image and seeing is indeed only valid in the Kolmogorov model, in which the energy is injected into the atmosphere at infinite scales, and is gradually transferred to smaller and smaller scales (a cascade process) until air viscosity dissipates it on scales of few mm (the inner scale l_0).

In reality, the physics of turbulence implies that the spatial power spectral density of phase distortions deviates from the pure power law at low frequencies, i.e. the energy is not injected into the atmosphere at infinite scales, but rather at finite scales. The popular von Kàrmàn turbulence model introduces an additional parameter, the outer scale L_0 , referring to a cut-off in the turbulence spectrum at low frequencies. The Kolmogorov model corresponds then to the particular case of L_0 of infinity.

A finite L_0 reduces the variance of the low order modes of the turbulence, and in particular decreases the image motion (the tip-tilt). The result is a decrease of the FWHM of the PSF. In the von Kàrmàn model, r_0 describes the high frequency asymptotic behaviour of the spectrum where L_0 has no effect, and thus r_0 loses its sense of an equivalent wavefront coherence diameter. The differential image motion monitors (DIMM; Sarazin & Roddier, 1990) are devices that are commonly used to measure the seeing at astronomical sites. The DIMM delivers an estimate of r_0 based on measuring wavefront distortions at scales of ~ 0.1 m, where L_0 has no effect. By contrast, the absolute image motion and long-exposure PSFs are affected by large-scale distortions and depend on L_0 . In this context the Kolmogorov expression for ϵ_0 ¹ is therefore no longer valid.

Proving the von Kàrmàn model experimentally would be a difficult and eventually futile goal as large-scale wavefront perturbations are anything but stationary. However, the increasing number of estimation campaigns worldwide over the past few years has firmly established that the turbulence phase spectrum does deviate from a power law (i.e. it does not match the Kolmogorov model at low frequencies), and the additional L_0 parameter provides a useful first-order description of this behaviour.

The purpose of this article is precisely to discuss the modifications of the Kolmogorov expression for ϵ_0 implied by the presence of a finite outer scale L_0 , and to further establish the difference between seeing and FWHM of a stellar image. A first order approximation of the FWHM of the atmospheric PSFs (ϵ_{vK}) under von Kàrmàn turbulence was proposed by Tokovinin (2002), with a dependence (see note²) on ϵ_0 scaled by an expression involving the ratio of r_0 and L_0 . The FWHM of long-exposure PSFs, ϵ_{vK} , is no longer equivalent to the seeing, but is a function of the seeing (ϵ_0), r_0 and L_0 . We recall that while r_0 depends on the wavelength, L_0 does not. In the following, we discuss the validity of using ϵ_{vK} rather than ϵ_0 , by presenting several results from extensive numerical simulations. At this point it is important to note that the FWHM ϵ_{vK} is independent of the telescope diameter.

Our investigations focus on telescope diameters ranging from 0.1 m to 42 m, with wavelength domain ranges from the *U*-band to *M*-band, while the seeing ranges from 0.1 to 1.8 arcseconds. Several L_0 cases were considered from 10 m to an infinite value. Our long-exposure PSFs are generated by Fourier transforms of 1000 atmospheric turbulence phase screen realisations adopting the von Kàrmàn model. The phase screens consist of 8192×8192 arrays to handle both atmospheric statistics and aliasing effects, and the same set is used for all telescope diameters. Several investigations were carried out on the phase screens to ascertain their properties (r_0 , L_0). For the sake of simplicity, we do not discuss the details of these investigations or the analytical treatment leading to the expression² for ϵ_{vK} . For more information one should refer to Martinez et al. (2010).

Outer scale and telescope diameter

Figure 1 aims at defining the general trend of atmospheric FWHM in large tele-

scopes in the presence of the outer scale of the turbulence. Several cases of L_0 are presented: 10 m, 22 m (Paranal median value), 50 m and 65 m. We compare the numerical FWHM (extracted from the simulated PSFs) to the analytical expectation, ϵ_{vK} , and the seeing, ϵ_0 . From Figure 1 it is straightforward to see that the FWHM is lower than the seeing ϵ_0 in all cases. In addition the FWHM nicely fulfilled the analytical approximation for ϵ_{vK} for all telescope diameters except small ones, where our treatment of the diffraction is too crude (the results are affected by coarse pupil sampling).

The validity of the expression² for ϵ_{vK} is hereby confirmed in an $L_0/r_0 > 80$ domain. As the outer scale L_0 gets smaller, the difference between FWHM and seeing increases. In all cases, the difference is significant and cannot be neglected. In addition, the effect of the outer scale is observable for all telescope diameters, and not only for large telescopes where diameters correspond to a significant fraction of L_0 (i.e., the common assumption that ϵ_0 is valid in a domain where

telescope diameters are smaller than L_0 does not hold). We found the expression² for ϵ_{vK} to be valid at least for $L_0/D \leq 500$. Very small telescope diameters do asymptotically converge to ϵ_0 , but for smaller diameters than usually considered and for very large outer scale L_0 values (e.g., $D = 0.1$ m and $L_0 = 100$ m, $D = 0.2$ m and $L_0 > 400$ m).

Wavelength and seeing dependence

Here we consider an 8-metre telescope, a fixed outer scale $L_0 = 22$ m, and 0.83 arc-second seeing at $0.5 \mu\text{m}$, while the imaging wavelength is varying from the *U*-band to the *M*-band ($0.365\text{--}4.67 \mu\text{m}$). The results are presented in Figure 2 (left), where a stronger dependence of the FWHM on wavelength compared to that expected by ϵ_0 is noticeable, and again an agreement with the expression for ϵ_{vK} is demonstrated. Considering the same value of L_0 and telescope diameter, but fixed wavelength ($0.5 \mu\text{m}$), we analysed the seeing dependency of the FWHM; the results are shown in Figure 2 (right). For

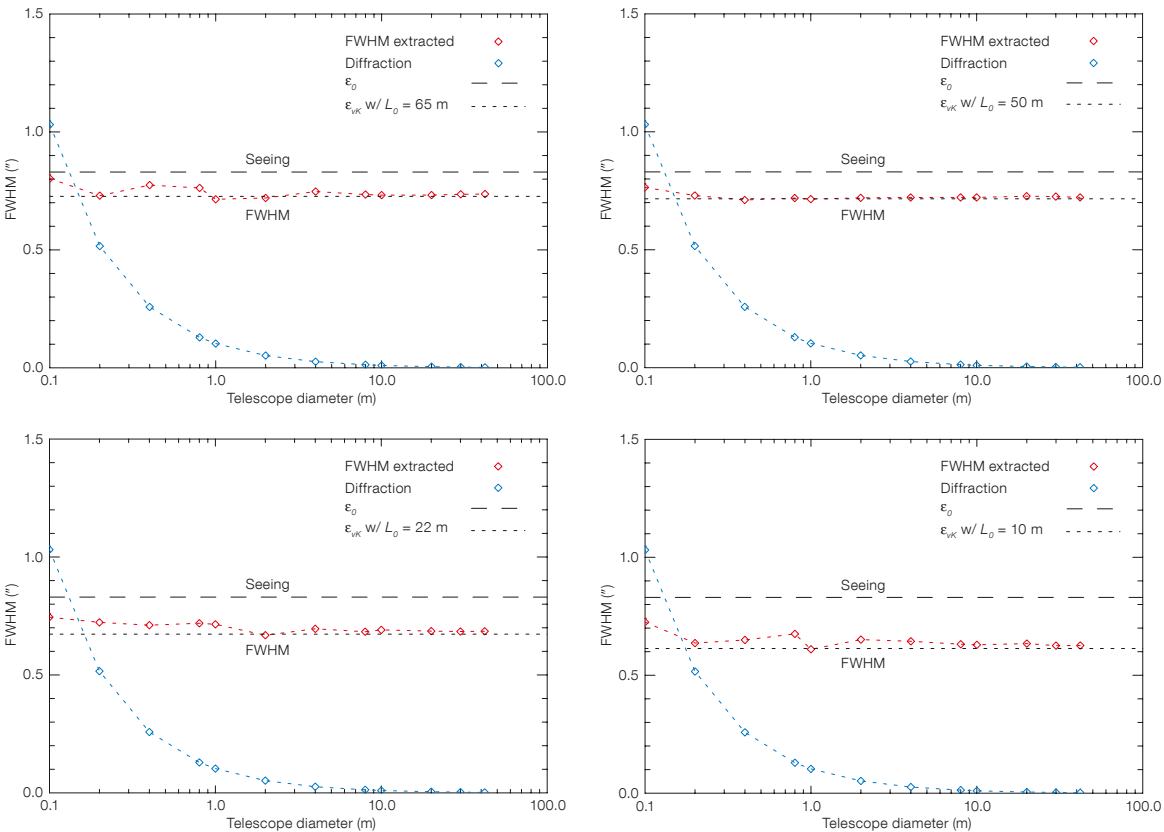


Figure 1. The atmospheric FWHM of simulated long-exposure PSFs versus telescope diameter for several turbulence outer scale L_0 values (10, 22, 50, and 65 m, for $\epsilon_0 = 0.83$ arcseconds at $\lambda = 0.5 \mu\text{m}$). The diffraction FWHM has been quadratically removed from the extracted FWHM.

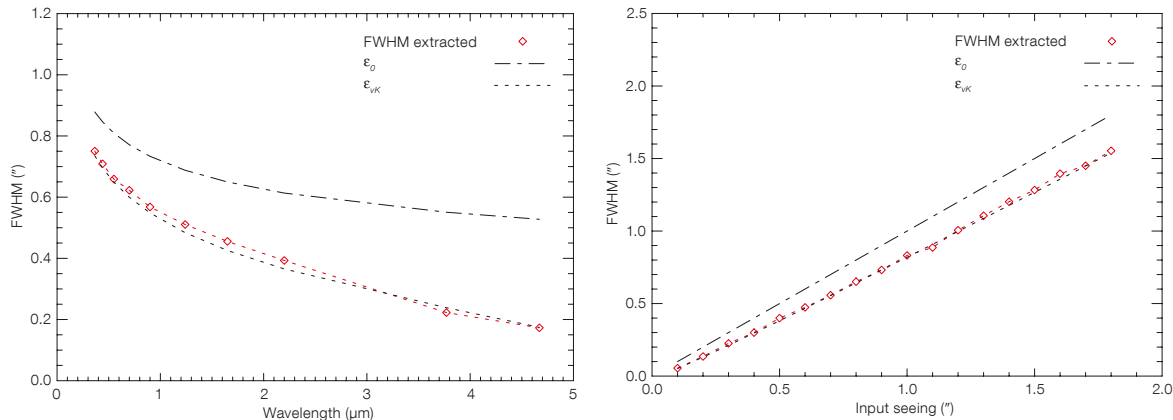


Figure 2. Dependence of the FWHM on wavelength (left, fixed $\epsilon_0 = 0.83$ arcseconds) and seeing (right, fixed $\lambda = 0.5 \mu\text{m}$). Other parameters are $L_0 = 22 \text{ m}$, $D = 8 \text{ m}$ (typical for the VLT).

all seeing values, the extracted FWHM clearly follows ϵ_{vK} and not ϵ_0 . The agreement with the expression² for ϵ_{vK} is therefore demonstrated for both wavelength ($L_0/r_0 > 10$) and seeing dependence ($L_0/r_0 > 20$). The FWHM of long-exposure PSFs is not the seeing.

Discussion of the case of Paranal

We discuss here the particular case of the VLT site at Paranal assuming standard seeing conditions (0.83 arcsecond at $0.5 \mu\text{m}$), and for several outer scale L_0 values including the Paranal median value (22 m) and its corresponding 1σ values (13 and 37 m). Figure 3 quantifies the ratio of the seeing ϵ_0 to the FWHM ϵ_{vK} for different wavelengths. The difference is substantial and can exceed a factor of two in the infrared (IR). For instance, the FWHM ϵ_{vK} is lower than ϵ_0 by 19% in the visible, and it is even more dramatic in the near-IR, where it is lower by 29.7% (H-band) and 36.3% (K-band). Figure 3 also strongly emphasises the importance of obtaining reliable estimation of L_0 at a telescope site, thus requiring simultaneous measurements of ϵ_0 and L_0 .

An intensive multi-instrument campaign of L_0 , surface layer, and seeing characterisation was carried out at Paranal in 2007 and has been recently presented in Dali Ali et al. (2010). This study has, for the first time, provided the profile of the outer scale $L_0(h)$ (where h stands for the altitude) at Paranal, enabling the whole profile of the atmospheric turbulence to be separated into the respective contributions from the free, ground and surface layers. In this extensive study, the authors

found outer scale L_0 values varying from a few metres ($\sim 10 \text{ m}$) in the ground layer to a maximum value of $\sim 35 \text{ m}$ appearing in the boundary layer (at 1 km). In addition, by comparing PSFs at visible and mid-IR wavelengths simultaneously, it is possible to extract the two parameters, ϵ_0 and L_0 , assuming that the telescope's contribution to the image degradation can be neglected (Tokovinin et al., 2007).

On-sky data application

To relate the previous results to real situations, we have evaluated several stellar FWHMs from an image of Omega Centauri recorded with the IR-camera of MAD (the ESO Multi-conjugate Adaptive Optics Demonstrator, formerly installed at the VLT UT3). The image was obtained on 29 March 2007 in open loop (i.e. no AO correction is applied) with a 65-sec-

ond integration time at a wavelength of $2.166 \mu\text{m}$ (bandwidth of $0.04 \mu\text{m}$). We use this example as it provides a well-sampled image of a large field of view (57 arcseconds \times 57 arcseconds).

The image is presented in Figure 4. The FWHM has been evaluated in the elongation-free direction of the stars, and derived using a 10th order polynomial fit to the radial profiles (a telescope PSF is a convolution of the atmosphere blur with diffraction, aberrations, guiding errors, etc. ... and none of these factors is described by a Gaussian). A mean FWHM value of 0.51 arcseconds has been measured. By converting this FWHM into a seeing value ϵ_{vK} assuming the Paranal outer scale median value of 22 m, and with a proper scaling for wavelength ($0.5 \mu\text{m}$) and airmass (1.1), we found that the seeing during the acquisition of the image was equal to 1.01 arcseconds.

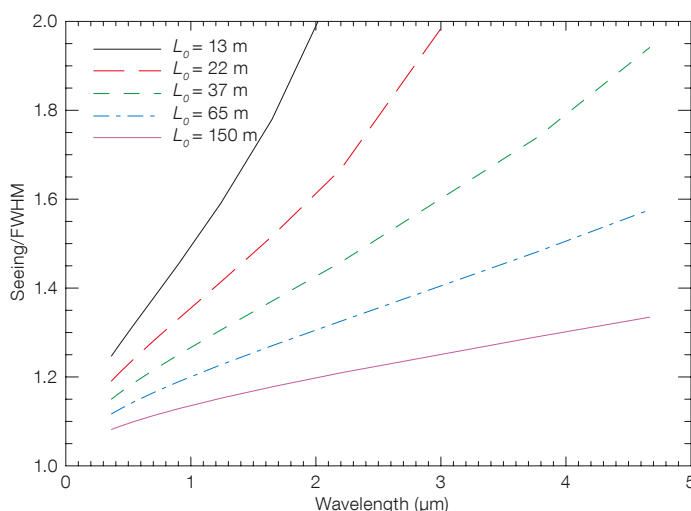


Figure 3. Ratio of seeing ϵ_0 to FWHM (ϵ_{vK}) as a function of the wavelength for several values of L_0 . The atmospheric seeing is set to the Paranal standard value of 0.83 arcsecond at $0.5 \mu\text{m}$.

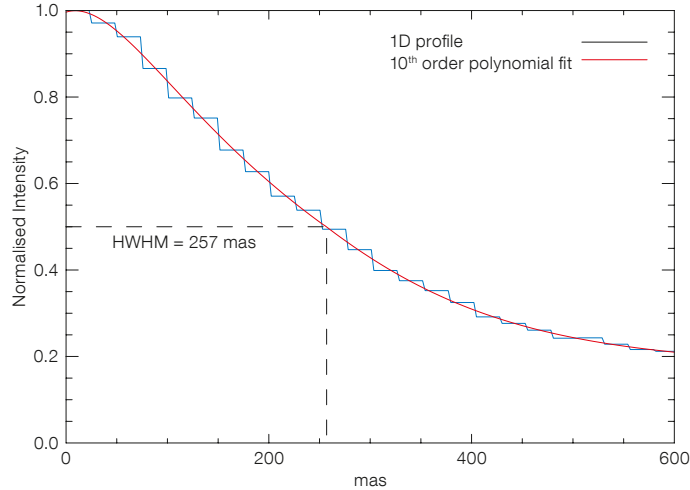
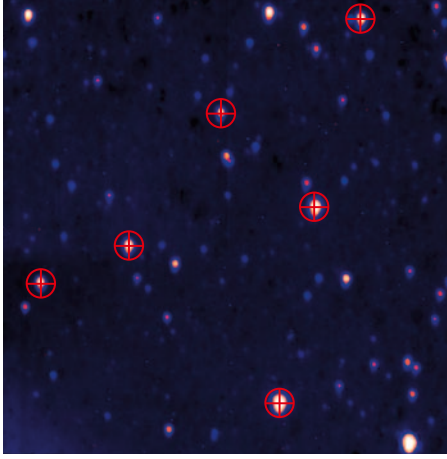


Figure 4. Left: VLT MAD image of Omega Centauri recorded in March 2007. The stars indicated were used for FWHM evaluation. Right: Normalised intensity profile of one star and the result of the FWHM evaluation (0.514 arcseconds) from a fit on the image minor axis.

DIMM seeing measurements were indeed evolving between 0.94 and 1.04 arcseconds (see Table 1) during this exposure. Not considering the outer scale presence (i.e. adopting ϵ_0), would have led to a value of 0.69 arcsecond seeing (wavelength and airmass corrected), more than 0.3 arcseconds different from the measured value ... quite a difference!

Although this test nicely supports the expression² for ϵ_{vK} , it relies on the chosen value of L_0 ; as a matter of fact we cannot guarantee that 22 m is a correct guess, nor did we consider potential internal telescope defects (a PSF is broadened by non-atmospheric factors as well). Indeed, optical aberrations and the outer scale of the turbulence act in opposite directions, and they can partially compensate for each other. Besides, the active optics also plays a role that is similar to the effect of the outer scale L_0 . In analogy with the finite outer scale impact, partially corrected wavefronts, resulting e.g., from tip-tilt compensation (fast guiding) or low order adaptive optics (AO) correction, lead to a small effective L_0 . All three effects — turbulence outer scale, partial AO correction and tip-tilt correction — reduce the low frequency content of the phase perturbation spectrum, but the gain in resolution over Kolmogorov turbulence is not cumulative. Therefore the search for an agreement with DIMM measurements should always be carefully considered, and would require statistical investigations, to prevent for example the surface layer (thin and time-varying turbulence layer occurring over the

mountain) to confuse the situation (see Sarazin et al., 2008).

On the other hand, by considering the DIMM seeing measurements during the acquisition of the image (0.94–1.04 arcseconds), one could retrieve the outer scale L_0 value occurring at that time and the measured FWHM. We thus obtained a value of L_0 confined between 25 and 45 m, which appears to be realistic considering the Paranal median value of 22 m, and measurements obtained in the 2007 campaign at Paranal and presented in Dali Ali et al. (2010). Floyd et al. (2010) derived the value of the outer scale of the turbulence at the Magellan telescopes likewise, and they found an outer scale L_0 of 25 m.

Conclusion

This study has confirmed several aspects of the difference between seeing and image quality at an optical telescope:

- the FWHM of long-exposure stellar images obtained at a telescope is not the seeing;
- the outer scale of the atmospheric turbulence plays a significant role in the relationship between the seeing and the FWHM of an image. The effect of the outer scale is apparent for all telescope diameters. The expression ϵ_{vK} proposed by Tokovinin (2002) accurately predicts the dependence of atmospheric long-exposure resolution on the outer scale.

By not considering the presence of the outer scale of the turbulence, one is currently: (a) overestimating the image size expected for a large telescope, i.e. our telescopes could perform better than we predict; (b) underestimating the seeing if deduced from the FWHM of a long-exposure PSF, i.e. the seeing is actually poorer than we predict.

FWHM (arcsecond)	0.51
Seeing (arcsecond) (ϵ_0)	0.69
Seeing (arcsecond) (ϵ_{vK})	1.01
DIMM seeing (arcsecond)	0.94–1.04

Table 1. Conversion of the FWHM obtained on the MAD image of Omega Centauri (1st row) into seeing values (assuming $L_0 = 22$ m) using the expression¹ for ϵ_0 (2nd row), the expression² for ϵ_{vK} (3rd row) and compared to DIMM seeing (4th row). All values are for a wavelength of 0.5 μ m and are corrected for airmass.

Reference

- Sarazin, M. & Roddier, F. 1990, A&A, 227, 294
 Tokovinin, A. 2002, PASP, 114, 1156
 Tokovinin, A. et al. 2007, MNRAS, 378, 701
 Sarazin, M. et al. 2008, The Messenger, 132, 11
 Martinez, P. et al. 2010, A&A, 516, A90
 Floyd, D. J. E. et al. 2010, PASP, 122, 731
 Dali Ali, W. et al. 2010, A&A, submitted

Notes

- ¹ The full expression for the FWHM of the Kolmogorov PSF is $\epsilon_0 = 0.976 \lambda / r_0$.
² The full expression for the FWHM of the van K arm an PSF is $\epsilon_{vK} \approx \epsilon_0 \sqrt{(1 - 2.183 (r_0/L_0)^{0.356})}$.

Balloons over the La Silla Paranal Observatory

Florian Kerber¹
 Richard Querel²
 Reinhard Hanuschik¹
 Arlette Chacón³
 Marc Sarazin¹
 on behalf of the project team*

¹ ESO

² Institute for Space Imaging Science (ISIS), Lethbridge, Canada

³ Grupo Astrometeorología, Universidad de Valparaíso, Chile

Precipitable water vapour (PWV) in the atmosphere is one of several key properties required to characterise overall quality of an astronomical site for observations at infrared wavelengths. Through analysis of archival data and by mounting a series of dedicated PWV measurement campaigns, we achieved our goal of establishing the Paranal Observatory as a reference site for evaluation of locations for the European Extremely Large Telescope (E-ELT) project. For the first time in an astronomical study, all measurement methods have been successfully validated with respect to balloon-borne radiosondes, the accepted standard in atmospheric research.

Atmospheric water vapour

Water vapour is the dominant source of opacity at infrared wavelengths (see Figure 1). Its vertical column abundance is expressed as precipitable water vapour in mm (Naylor et al., 2008). For reference, a “dry”, PWV-excellent night on Paranal may have 1 mm PWV or less, while middle-European conditions may easily offer > 30 mm. In order to better under-

stand the PWV above the La Silla Paranal Observatory, a collaboration was started in 2009 between ESO, the Institute for Space Imaging Science (ISIS) in Lethbridge, Canada, and the Astrometeorology Group of the Universidad de Valparaíso in Chile. In the context of astronomical observations, the amount of PWV above an observatory is of fundamental importance for successful scientific operations: on long time scales PWV determines how well a site is suited for IR astronomy, since low PWV values lead to drastically improved transmission in some wavelength domains (Smette et al., 2007); in fact such conditions can altogether open atmospheric windows that are completely opaque at higher values. In an operational sense, reliable knowledge of the content of PWV throughout a given night is critical for the success and quality of science observations (see Figure 2), and for their scheduling. As part of site testing and evaluation for the European Extremely Large Telescope (E-ELT), we have addressed primarily the aspect of long-term quality for infrared (IR) as-

tronomy. By comparing various methods to determine atmospheric PWV we also wanted to understand which methods were best suited to support IR science at the E-ELT in an operational sense.

History of PWV over La Silla Paranal Observatory

In order to reconstruct the history of PWV over the Paranal Observatory, we extracted about 1500 UVES flux standard observations from the archive, covering the period 2001 to 2008 (Figure 3). With their almost flat and featureless stellar continuum, these white dwarfs are particularly well-suited for this study (Kerber et al., 2010). While these pointed observations were originally reduced as flux standard star calibrations, we have reprocessed them for our project as science targets, with the same approach used in the UVES reprocessing project¹.

We have analysed the telluric absorption lines in the UVES flux-calibrated pipeline

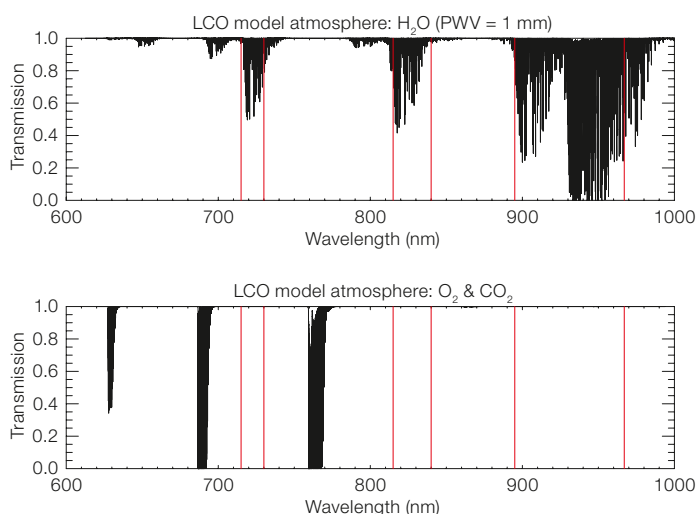


Figure 1. Atmospheric transmission in the optical to near-IR domain. Upper panel: absorption caused by 1 mm of H₂O. Lower panel: absorption resulting from O₂ and CO₂. The analysis described uses wavelength regions (denoted in red) in which absorption is from water vapour only, allowing the atmospheric content of PWV to be derived. This wavelength range was chosen for the analysis of the archival data, but suitable windows exist over a very wide wavelength extent.

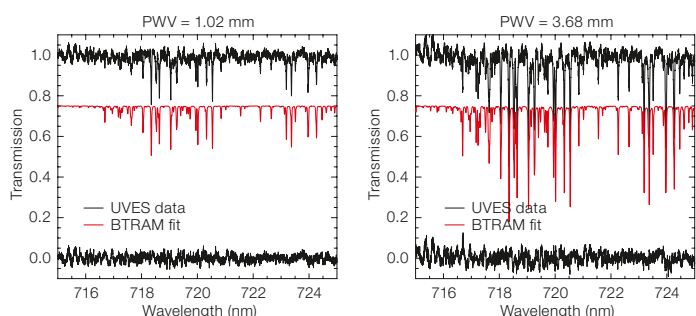


Figure 2. Sample UVES spectra analysed with the atmospheric model BTRAM illustrating conditions on Paranal: a) a dry night offering good conditions for IR observations, and b) a moderately wet night. From top to bottom are displayed: the UVES spectrum, the BTRAM fit, and the residuals between spectrum and fit.

* The Precipitable water vapour (PWV) project team consists of: Florian Kerber¹, Richard Querel², Reinhard Hanuschik¹, Arlette Chacón³, Gerardo Avila¹, Marta Caneo³, Lisette Cortes³, Omar Cuevas³, Michel Cure³, Carlos Guirao¹, Lizett Illanes³, Gaspare Lo Curto³, David A. Naylor², Marc Sarazin¹, Alain Smette¹, David Rabanus¹, Gregory Tompkins²

¹ ESO; ² ISIS, Canada; ³ Grupo Astrometeorología, Univ. Valparaíso, Chile

products by fitting an atmospheric radiative transfer model (BTRAM) developed by ISIS. A large number of weak and strong isolated and blended lines can be used for the analysis resulting in accurate and robust PWV values, see Figure 2. Standard star observations (~ 1700 spectra) taken with FEROS have been used to make an equivalent analysis for La Silla, described in detail by Querel et al. (2010).

From this analysis, we find a mean PWV value for Paranal of 2.4 ± 0.3 mm (after correcting for a dry-bias, since standard star observations are only done under clear sky conditions). There are pronounced seasonal variations, with periods of high PWV occurring during the southern summer months when the site is partially affected by the *invierno altiplánico* or Bolivian Winter (most pronounced in January and February) when winds from the east bring moisture from the Amazon basin and clouds may spill over the Andes to the west into northern Chile. The fraction of nights with $\text{PWV} < 2$ mm (good for IR observations) is 47%, while $\text{PWV} < 1$ mm occurs in 13.5% of nights. The corresponding mean PWV for La Silla is considerably higher at 3.7 ± 0.4 mm (see also Thomas-Osip et al., 2007; Querel et al., 2008).

Dedicated measurement campaigns

Three dedicated campaigns to measure PWV were conducted on La Silla (4–15 May 2009) and Paranal (31 July to 10 August and 9–20 November 2009). The goal was to operate several instruments in concert to gather independent measurements of PWV over a statistically relevant period of more than one week. We employed three main types of instruments: a) radiosonde launches to obtain atmospheric profiles; b) facility instruments for high resolution spectroscopy of telluric line systems; and c) high-cadence IR radiometer measurements. The IR radiometer (IRMA) was developed and built by ISIS (Naylor et al., 2008). It measures the transparency of the atmosphere around $20 \mu\text{m}$ in a pencil-beam column. In this carefully selected window, H_2O is the sole absorber (similar to Figure 1); by comparison with an internal black-body and the BTRAM atmospheric model, the PWV is directly derived.

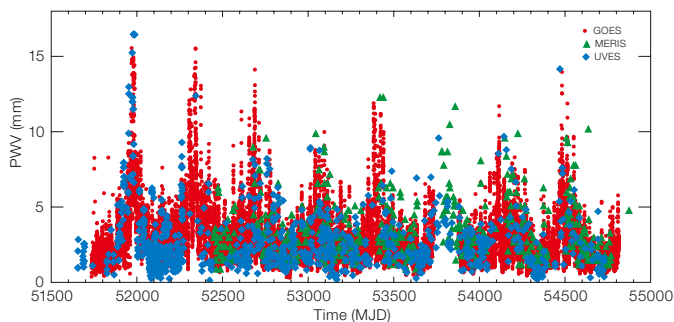


Figure 3. Record of precipitable water vapour over Paranal. Comparison of PWV data derived from UVES archival data and GOES and MERIS satellite data for the period 2001–8. Pronounced seasonal variations are evident as is the quantitative agreement between the different datasets.

The astrometeorology group at the Universidad de Valparaíso, with support from ESO, carried out the radiosonde launches (Figure 4). On Paranal we launched up to three times a day for a total of 52 radiosondes. Their schedule was carefully aligned with the scanning times of the geostationary GOES weather satellite providing infrared and, in particular, water vapour images, as well as with the daily radiosonde launch at Antofagasta airport. The full launch schedule had to be authorised four weeks in advance by the Chilean aviation authority. This permission was confirmed by phone 15 minutes before each launch. More details about the radiosonde campaigns are described in Chacon et al. (2010).

Radiosondes are the accepted standard method for atmospheric sounding. We have used their data to validate the various methods to measure PWV. The equipment employed in our campaign consisted of a Vaisala radiosonde RS92 (shown in Figure 4a) which comprises the following instrument package: a GPS receiver to track its location and deduce the wind speed, a silicon pressure sensor, a heated twin humidity sensor and a small fast temperature sensor; plus of course a transmitter for real-time telemetry to the mobile ground station at the launch site. The radiosonde payload is lifted by a helium-filled balloon with an initial diameter of about 1.5 m. During the 90-minute ascent the balloons drifted by as much as 80–150 km to the east. At an altitude of 20–25 km, the balloon — now more than 10 m in size — would finally burst, releasing the radiosonde package into free fall over the Cordillera de los Andes. Figure 4c shows an example record from one of the radiosonde ascents.

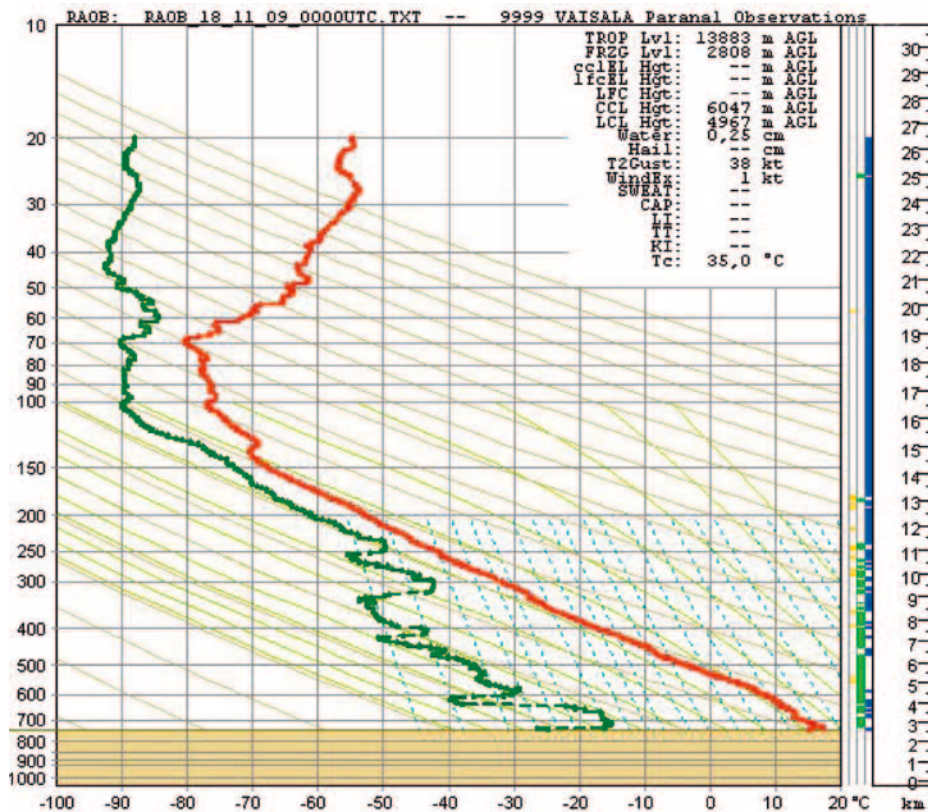
The absolute accuracy of PWV derived from radiosonde data is an important issue

in this context. In the literature an overall value of 5% is quoted, and of about 15% in very dry conditions (Schneider et al., 2010). One has to keep in mind that a radiosonde samples data along an ascent trajectory controlled by the prevailing wind pattern. PWV is then derived from the profile for the whole column, although water vapour is concentrated in the lowest few kilometres. Hence the radiosondes and astronomical spectrographs are not sampling the same column of air, and a 1:1 agreement between retrieved PWV values is not to be expected even under very stable conditions.

A total of 69 radiosondes have been successfully launched during the three campaigns on La Silla and Paranal. Since the balloons ascend at a rate of a few m/s only a relatively short window of about 60–90 minutes is available to conduct meaningful parallel observations with other methods. For a stand-alone high time resolution monitor such as IRMA, this is relatively easy to achieve, while for instruments on the VLT careful planning and flexibility is essential.

As for the VLT instruments, we have used a total of 21.5 hours of UVES technical time and obtained more than 900 spectra of white dwarf standard stars, with a cadence of up to 30 s. These data were taken with a 10-arcsecond slit width, providing essentially seeing-limited spectral resolution of 40 000–50 000. Periodic observations during the nights of the campaign were also performed by VISIR (65 spectra) and CRILES (110 spectra).

One IRMA unit was installed on Paranal, giving 350 hours of near-continuous coverage (with a cadence of seconds). A second IRMA unit was temporarily installed on Cerro Armazones, the designated site of the E-ELT, and provided



> 100 hours coverage. This IRMA unit was also used on Paranal for cross-correlation with the first IRMA.

Findings of the PWV campaigns

The main result from the comparison of the different instruments used during the campaigns is that all of them measure PWV with good fidelity (Figures 5 and 6). Using PWV values as derived by radiosonde as our reference, we find that agreement with the IR radiometer IRMA is excellent, providing results that are indistinguishable after taking into account the associated errors (Figure 6 left). Moreover, IRMA provides information pertaining to the air mass directly above the observatory. The internal precision of the IR radiometer data is ~ 3% while the accuracy is estimated at 5%, but not better than 0.25 mm. Relative agreement between the two IRMA units measuring in the same direction at the same site is extremely good on time scales of a few seconds up to several hours.

The variation of PWV over time is smooth, although significant changes can occur within one hour. Variations of PWV of a few percent were seen to occur on time scales of seconds or a few minutes as recorded by the IRMAs (see Figure 5). For Cerro Armazones a dry offset of 0.3 mm is found which can be mostly attributed to its difference in altitude ~ 400 m above Paranal. We saw local PWV variations of a few tenths of a millimetre, so horizontal variations are important even for closely adjacent sites.

The internal precision of PWV data from optical and IR spectroscopy is about 7%, whereas accuracy is estimated to be about 15–20%, but not better than 0.3 mm. Quantitative agreement between the individual ground-based remote sensing techniques and *in situ* measurements (radiosondes) is very good (10–20%). Structure in the spatial distribution of water vapour in the sky — at the few 0.1 mm level — can be directly detected as temporal variations in the observations of a transit instrument (IRMA) as well as by variations in the PWV found for pointed observations (from optical spectroscopy).

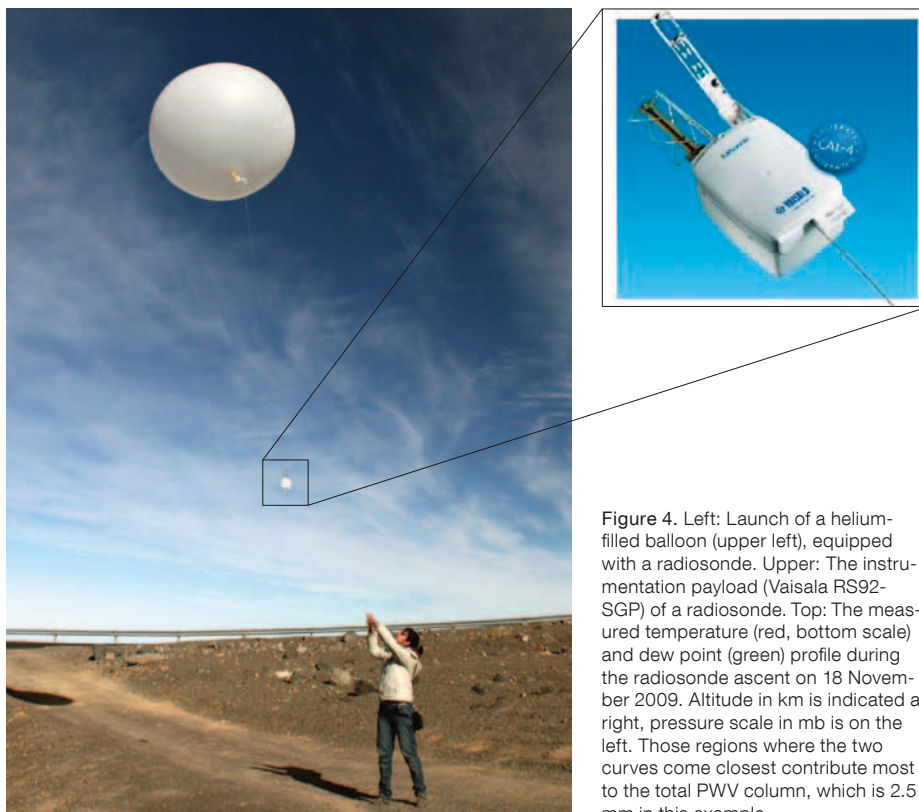


Figure 4. Left: Launch of a helium-filled balloon (upper left), equipped with a radiosonde. Upper: The instrumentation payload (Vaisala RS92-SGP) of a radiosonde. Top: The measured temperature (red, bottom scale) and dew point (green) profile during the radiosonde ascent on 18 November 2009. Altitude in km is indicated at right, pressure scale in mb is on the left. Those regions where the two curves come closest contribute most to the total PWV column, which is 2.5 mm in this example.

Comparison with the GOES satellite

We also compared the PWV data from the Geostationary Operational Environmental Satellite (GOES) that monitors the atmosphere with the results obtained from the radiosonde launches. In a statistical sense the agreement found is rather reasonable, while for a given day deviations can be significant. The numerical correlation values with the radiosondes are in fact excellent and fully consistent with the findings from the UVES archival data. Hence it is safe to assume that GOES data can be used successfully for the characterisation of sites in terms of PWV provided both a substantial timebase is used and the environment is very homogeneous, as is the case for northern Chile. These two conditions are fulfilled for Paranal and good agreement between GOES and other methods is found.

Continued PWV monitoring

In support of science operations on Paranal, PWV measurements taken with various VLT instruments are used in near real time. Whenever a flux standard star (on UVES), or a telluric standard star on CRILES, X-shooter or VISIR, are measured, automatic procedures are employed to analyse the pipeline-processed spectra and derive a new PWV data point. More details are provided on the ESO web^{2,3}. A similar procedure will soon become available for La Silla as well.

Implication for E-ELT site selection and future use of PWV measurements

Our multi-instrument campaigns in 2009 have produced a dataset that is unique in both quality and quantity. Very good agreement has been found for all methods, with IRMA delivering the best accuracy combined with the highest time resolution. From the results of our analysis, Paranal can be used as a reference site for northern Chile. For Cerro Armazones (Otárola et al., 2010) an offset of 0.3 mm with respect to the PWV at Paranal is found based on an altitude difference of about 400 m.

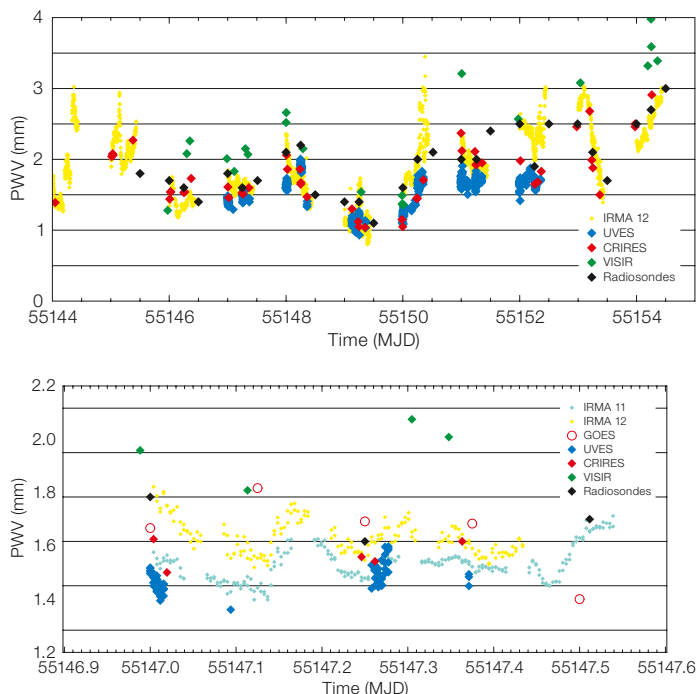


Figure 5. Top: Comparison of PWV data derived from the various methods during the PWV campaign on Paranal during November 2009. Bottom: enlarged section centred on MJD 55147.3 (12 November 2009), showing the limiting precision of about 0.25 mm. This plot includes data from both IRMA radiometers working in parallel on Paranal. The open circles represent data points from the GOES weather satellite.

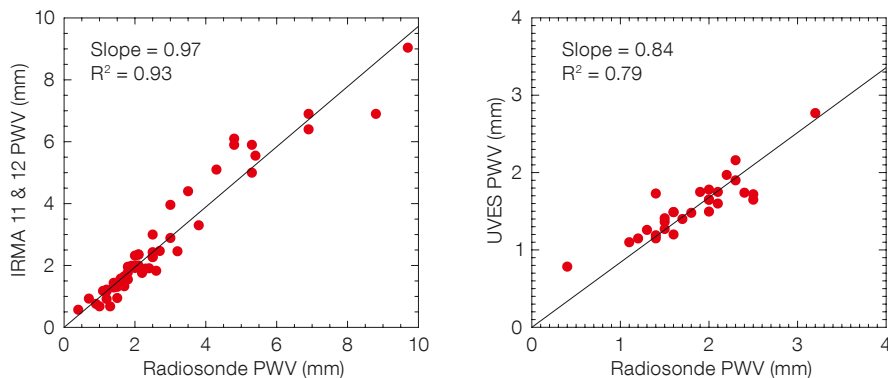


Figure 6. A comparison of PWV measured by IRMA (left) and UVES (right) with respect to the radiosonde data is shown as an example. Similar results have been derived for all other astronomical instruments (BACHES, CRILES, FEROS, HARPS, VISIR and X-shooter) validating all of them with respect to the established standard in atmospheric research.

The goals of the PWV project have been met in full. The results of this study have been communicated to the Site Selection Advisory Committee contributing directly to the site selection process for the future E-ELT. We continue to work on a detailed treatment of systematic effects which will result in better absolute accuracy of our PWV results.

From analysis of archival data and the results from the campaigns it is obvious that PWV can successfully be monitored. At present PWV values for Paranal are now routinely monitored using periodic spectra taken with CRILES, UVES, VISIR and X-shooter. We conclude that PWV could be used as a constraint in planning observations. Steps to this end are planned for the immediate future for Paranal Observatory. For the E-ELT a stand-alone high time resolution PWV monitor will be an essential part of the infrastructure in order to optimise the scientific output of the operations.

Acknowledgements

This work has been funded by the E-ELT project in the context of site characterisation. The measurements have been made possible by the coordinated efforts of the project team and each host observatory site. We would like to thank all of the technical staff, astronomers and telescope operators at La Silla and Paranal who have helped us in setting up equipment, operating instruments and supporting parallel observations. Similarly, we thank our colleagues at Las Campanas and GMT for the fruitful collaboration. We thank the Directors of the La Silla Paranal Observatory (Andreas Kaufer, Michael Sterzik, Ueli Weilenmann) for accommodating such a demanding project in the operational environment of the observatory and for granting technical time. Special thanks are due to the heads of science operations (Christophe Dumas, Ivo Saviane) for specifically adding flexibility to the scheduling, enabling us to achieve parallel observations between instruments and the

radiosondes. It is a pleasure to thank the Chilean Direction General de Aeronautica Civil (DGAC) for the helpful collaboration and for reserving airspace around the observatories to ensure a safe environment for the radiosonde balloon launches. Special thanks are due to the TMT project for providing on loan the two IRMA units used during our campaigns and the good collaboration. The authors would like to thank Brad Gom (ISIS) for his work with both IRMA and BTRAM.

References

- Chacón, A. et al. 2010, Proc. SPIE Astronomical Instrumentation, in press
Kerber, F. et al. 2010, Proc. SPIE Astronomical Instrumentation, in press
Naylor, D. A. et al. 2008, Int. J. of Infrared & Millimeter waves, DOI 10.1007/210762-008-9421-2
Otárola, A. et al. 2010, PASP, 122, 470

- Querel, R. R. et al. 2008, SPIE, 7014, 701457
Querel, R. R. et al. 2010, Proc. SPIE Astronomical Instrumentation, in press
Schneider, M. et al. 2010, Atmos. Meas. Tech., 3, 323
Smette, A. et al. 2008, The 2007 ESO Instrument Calibration Workshop, eds. A. Kaufer & F. Kerber, Springer, 433
Thomas-Osip, J. et al. 2007, PASP, 119, 697

Links

- ¹ UVES reprocessing project: <http://www.eso.org/qc/reproUVES/processing.html>
² PWV trend reporting: http://www.eso.org/observing/dfo/quality/GENERAL/PWV/HEALTH/trend_report_ambient_PWV_HC.html
³ Paranal PWV monitoring: <http://www.eso.org/sci/facilities/paranal/sciops/CALISTA/pwv/data.html>



The VLT Laser Guide Star facility in action, creating a guide star for adaptive optics correction. Image taken at Paranal in 2007.



An image of the Galactic H II region M8 (NGC 6523) taken with the 1.5-metre Danish telescope at the La Silla Observatory. This colour image combines observations in broadband *B*-, *V*- and *R*-filters, but the structure is dominated by the emission lines from the hot gas. A near-infrared image of M8 taken with the VISTA telescope can be found in the article by Saito et al. on p. 26.

The Outer Frontiers of the Solar System: Trans-Neptunian Objects and Centaurs

Maria Antonella Barucci¹
 Alvaro Alvarez-Candal²
 Irina Belskaya^{1,3}
 Catherine de Bergh¹
 Francesca DeMeo¹
 Elisabetta Dotto⁴
 Sonia Fornasier^{1,5}
 Frédéric Merlin^{1,5}
 Davide Perna⁴

¹ Observatoire de Paris, LESIA, France

² ESO

³ Institute of Astronomy, Kharkiv University, Ukraine

⁴ INAF–Osservatorio di Roma, Italy

⁵ Université de Paris VII–Diderot, France

The icy bodies in orbit beyond Neptune and known as Trans-Neptunian objects (TNOs), or Kuiper Belt objects, are the most distant objects of the Solar System accessible to direct investigation from the ground. The study of these objects, containing the least processed material of the Solar System, can help in understanding the still-puzzling accretion/evolution processes that governed planetary formation in our Solar System as well as in other dusty star discs. An ESO large programme has been devoted to obtaining simultaneous high quality visible and near-infrared spectroscopy and photometry of about forty objects with various dynamical properties. A few selected objects have also been observed with polarimetry to define their surface characteristics better and with detailed photometry to determine their rotational properties. The results provide a unique insight into the physical and surface properties of these remote objects.

Trans-Neptunian objects represent a newly identified population of pristine material in our Solar System. Discovered less than twenty years ago, these icy bodies revolutionised our understanding of the Solar System and most ideas on the evolution of the protoplanetary nebula. Located at the furthest frontiers of our planetary system observable with ground-based telescopes, these small bodies are considered to be the fossils of the protoplanetary disc and can provide unique information on the processes that domi-

nated the evolution of the early solar nebula as well as of other planetary systems around young stars.

TNO science has rapidly evolved in recent years, linking together different populations of small bodies in our planetary system. The attempt to determine the physical properties of this population is at present one of the most active research fields in planetary science. More than 1400 Trans-Neptunian objects, with different sizes, orbits and surface characteristics, have been discovered up to now. But many more must be present. A few of them belong to the newly defined population of dwarf planets.

The TNO population is classified into several dynamical groups (see Figure 1), depending on their distance from the Sun and their orbital characteristics: i) classical objects; ii) resonant objects; iii) scattering(ed) disc objects; and iv) detached objects. The first two groups are also known as the Kuiper Belt, containing objects with an average distance from the Sun of between 30 and 55 astronomical units (AU) and with low eccentricity orbits. The resonant objects are trapped in mean-motion resonances with Neptune in more than 20 resonances, with the 3:2 mean-motion resonance (hosting

Pluto) being the most densely populated. The scattering disc objects or scattered objects are considered to be those that have orbits with large eccentricities, and perihelion distances near the location of Neptune, while the detached objects are those with orbits at large eccentricities, and with perihelion distances out of Neptune's influence. The best example of this last category is (90377) Sedna, which has perihelion and aphelion distances of 76 and 927 AU, respectively. Another group of objects, the Centaurs (shown in orange in Figure 1), with unstable orbits between those of Jupiter and Neptune, can also be associated with the TNO population. Planetary perturbations and mutual collisions in the Kuiper Belt are probably responsible for the ejection of objects into Centaur orbits.

In order to investigate the surface properties of these remote and faint Solar System objects, a large programme has been carried out with the ESO Very Large Telescope (VLT) using, nearly simultaneously, the Unit Telescopes UT1, UT2 and UT4. The aim of this large programme was to obtain high signal-to-noise ratio (S/N), simultaneous visible and near-infrared (NIR) spectra for almost all objects that can be observed with the VLT. Forty objects have been studied, allowing a

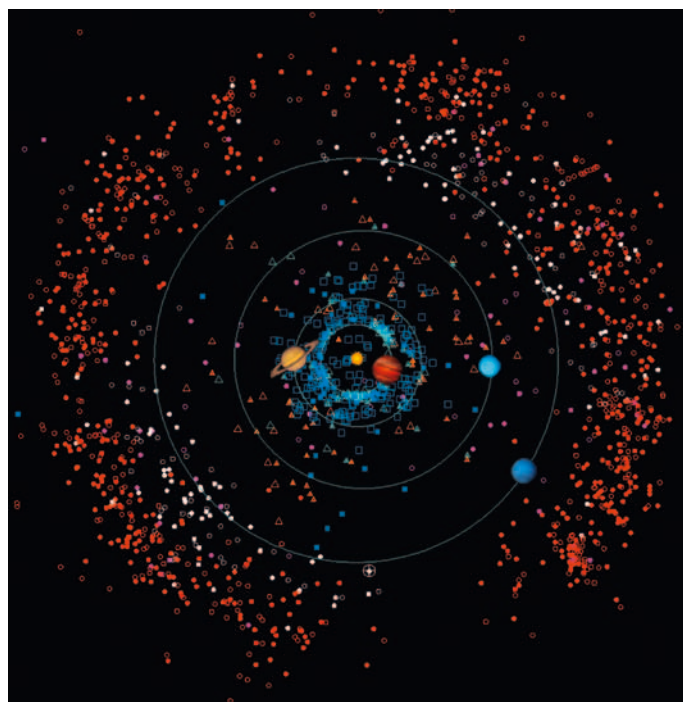


Figure 1. The location of TNOs (on 12 February 2010) are reported in different colours for different dynamical classes of objects. Unusual objects (high-ellipticity) are shown as cyan triangles, Centaurs as orange triangles, objects in 2:3 resonance with Neptune as white circles (Pluto is shown with the crossed white symbol), scattered-disc objects as magenta circles, while the classical objects are shown as red circles. Periodic comets are shown in blue squares. Objects observed at only one opposition are denoted by open symbols, while those with multiple opposition orbits are denoted by filled symbols. The orbits of the planets are shown in light blue with their respective images. (Adapted from a plot by the Minor Planet Center).

Figure 2. The lower left panel shows the distribution of the four TNO taxonomic groups (whose average photometric colours are represented in the upper left panel as reflectance values normalised to the Sun in the V-band) within each dynamical class. The right panel shows the distribution of the taxonomical groups, with respect to the orbital inclination relative to the ecliptic plane, for the “classical” TNOs.

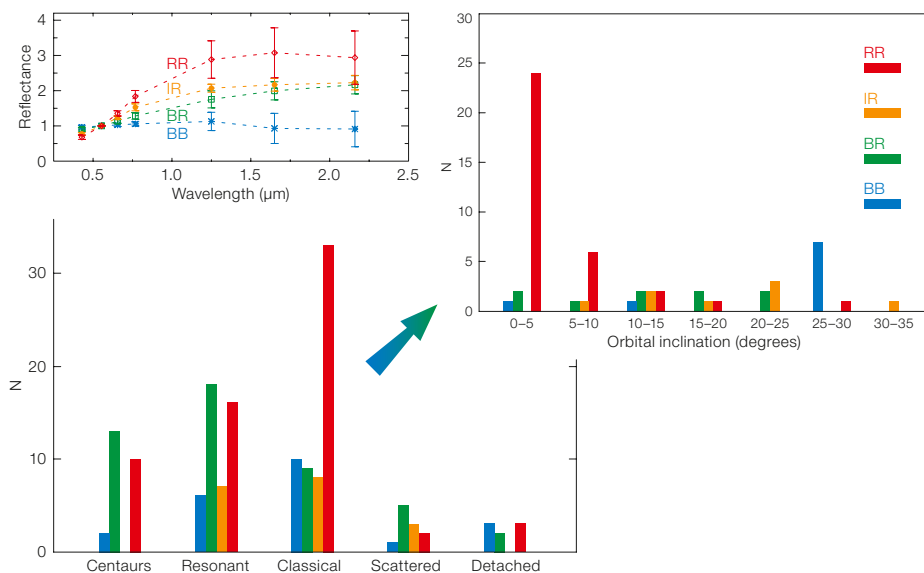
broad characterisation of the brightest TNOs. All the targets have also been observed by *V*, *R*, *I*, *J*, *H* and *K* photometry to determine their taxonomic classes.

Surface colours, taxonomy and rotation

Visible and NIR photometry of forty objects have been carried out with FORS and ISAAC. Based on the computed colour indices, we derived the taxonomic classification of 38 bodies (DeMeo et al., 2009; Perna et al., 2010), by applying the G-mode statistical method according to the Barucci et al. (2005) system. This scheme identifies four classes that reasonably indicate different compositions and/or evolutionary history, with increasingly red colours from BB (blue), BR (intermediate blue–red), IR (moderately red) to the RR (red) class. The observations performed in the framework of our ESO large programme were combined with the whole data sample presently available in the literature. We thus analysed a total of 151 taxonomically classified objects and performed a statistical analysis of the relationships between taxonomical and dynamical classification. The main results we obtained are (see Figure 2):

- i) the enlarged sample of analysed Centaurs confirms the colour bimodality suggested previously;
- ii) bodies belonging to the IR taxonomic class seem to be concentrated among the classical and resonant populations;
- iii) within the classical objects, the most spectrally red bodies (RR class) dominate the population at low orbital inclination, while blue objects (BB class) are more abundant at high orbital inclinations. These results confirm the previously suggested relationship between spectral behaviour and dynamical evolution, the red and blue colours being associated with the dynamically cold and hot populations, respectively.

In the framework of this large programme we also investigated the spin rates of



twelve bodies. Assuming ellipsoidal shapes with axes $a > b > c$, we derived a lower limit to the axis ratio a/b from the obtained light-curve amplitudes, under the hypothesis that the light curves are only affected by the shape elongation and that major albedo variations are not present on the surface of the observed bodies. From the rotational periods and light-curve amplitudes we also derived a range of variation of the density of the observed bodies, by applying the Chandrasekar theory for rotationally stable Jacobi ellipsoids under the simplified assumption of cohesionless and strengthless bodies (namely fluid objects). The obtained density values seem to confirm the existence of a magnitude/density trend with larger (brighter) TNOs being denser than smaller (fainter) ones, as had been suggested. However, this trend is strongly influenced by a single object (136 108 Haumea). The limited sample of densities currently available in the literature, together with the still unresolved ambiguity between brightness and size (due to the small number of reliable albedo measurements), prevent us from definitively assessing any relationship between TNO density and size.

Composition

Detailed information on the composition of TNOs can only be acquired from spectroscopic observations, especially covering the wavelength range between 0.4 and

2.4 μm . This spectral window provides the most sensitive technique to characterise from the ground the major mineral phases and ices present on Trans-Neptunian objects. Nearly simultaneous observations of FORS visible spectroscopy, ISAAC *J*-band and SINFONI *H*- and *K*-band spectroscopy been performed for forty objects selected among different dynamical groups. The exposure time required is generally long, and as the objects rotate around their principal axis, the resulting spectra often contain information coming from different parts of the object. The *V*-, *R*-, *I*-, *J*- and *H*-band photometry has been used to tie the different spectral ranges together.

The visible spectra are mostly featureless, showing, however, very large variations of their spectral slope, with colours from neutral to very red. The ultra-red slopes probably indicate the presence of complex organic material on the surface. A few big objects, like Eris and Pluto, show signatures of CH_4 in their spectra. We identify in a few other objects (10 199 Chariklo, 42 355 Typhon, and 2003 AZ84) new faint and broad absorption features that are, in general, associated with aqueous altered silicates on the surfaces of these bodies, by analogy with features present in the spectra of some main belt dark asteroids. Hydrous silicates are also known to be present in interplanetary dust particles (IDPs). The NIR 1–2.4 μm window provides powerful diagnostics for the study of astrophysical ices.

Radiative transfer models have been used to investigate TNO surface composition, and to interpret features and spectral behaviour using intimate or geographical mixtures of organics, silicate minerals, carbonaceous assemblages, ices, and/or light hydrocarbons. The red spectral slopes are typically well-reproduced by assuming the presence of organic compounds on the surface, such as kerogens (complex dark organic compounds) and tholins (Titan and Triton materials — substances formed in the laboratory by irradiation of gaseous mixtures of methane and nitrogen in different proportions) or ice tholins (formed by irradiating mixtures of essentially water and hydrocarbon ices). Other physical properties such as porosity and rugosity (the numerical measure of roughness) can, in principle, be derived from these models, but the observation of unresolved sources and the small phase angle coverage, due to the large heliocentric distance of these bodies, limit considerably confidence in the results. These models utilise numerical algorithms that fit the object spectra by reduced chi-squared minimisation. This minimisation provides the best set of parameters among the input free parameters (such as concentration and particle size). The models can provide insights into the chemical composition and the dilution state of the various compounds, or constraints on the way they are mixed (intimate mixtures, areal mixtures, combinations of both, etc.). They also provide information on the stratification state of the subsurface layers providing strong evidence of volatile transport or on limits on the irradiation level, depending on the depth.

The main results obtained during the ESO large programme on the forty objects observed spectroscopically, and the models of their surface by radiative transfer models, can be summarised by subdividing the targets into three main groups according to their composition:

1) Water ice group

More than 50% of the targets show the presence of water ice on their surface. The best-fit compositional models of these objects include water ice in the crystalline state as well as in the amorphous state. The majority of spectra with high S/N ratios show the presence of a feature at 1.65 μm due to crystalline

water ice. It is still a matter of debate whether water ice was amorphous or crystalline in the protosolar nebula. The presence of crystalline water ice implies that the ice has been heated above 100–110 K. This heating could have resulted from impacts, or the ices might have formed in the warmer deep interiors and were then exposed on the surface. The quality of the observations of fainter objects is not sufficient to distinguish between amorphous or crystalline water ice. Nonetheless, when trying to model the spectra the best-fit model is usually obtained when using a combination of the two water ice states.

2) Other ices group

Methane ice is present on the largest TNOs such as Eris, Pluto, Sedna and Quaoar. The spectra of some objects, such as Pluto and probably Eris, show that some of the methane ice must be dissolved in nitrogen. Methane is present at the surface of these large objects because their gravity is high enough to retain such a volatile component, but it may also be present in lower quantities on smaller objects. A small amount of ethane (a by-product of methane ice irradiation) has also been detected on Quaoar. Some objects, such as Pholus and (55638) 2002 VE95, show spectra with methanol features. In addition, many objects show spectra with a decreasing slope beyond 2.2 μm , implying the possible presence of methanol or similar molecules, even if these faint objects have spectra with a low S/N, especially in the *K*-band. The presence of ammonia or ammonia hydrate in the spectra of a few objects (Charon, Orcus) has been suggested. A firm detection of ammonia would have important implications on the composition of the primitive solar nebula in low density regions far from the Sun.

3) Featureless spectra group

Many objects have featureless spectra in the NIR, with a wide range of colours. These objects could be mantled by a surface rich in organics or carbon. As all these objects are supposed to be at least partly made of ices, irradiation processes have to be responsible for these properties. C-bearing molecules progressively lose their hydrogen atoms, which results in a polymerisation

of the surface layer, and the formation of a crust.

The largest objects

The largest TNOs, many of which are also labelled as dwarf planets, have distinctly different surface compositions compared with the rest of the population. Specifically, they have strong signatures of methane or crystalline water ice in their spectra (see Figure 3). During this ESO large programme we managed to observe several of the largest TNOs: Pluto, Eris, Sedna, Quaoar, Charon and Orcus.

On Pluto we detect volatile species such as methane, nitrogen, and carbon monoxide. From our investigation, we confirm that the level of dilution of methane in nitrogen is different on different parts of the heterogeneous surface of Pluto. On Eris, the largest dwarf planet, we indirectly detect nitrogen on the surface based on the wavelength position of some of the bands of methane (Merlin et al., 2009). The data indicate that the dilution of methane ice in nitrogen changes as a function of depth below the surface. This suggests the formation of a temporary atmosphere around Eris when close to perihelion, as is observed for Pluto. Modelling of the data also suggests a large quantity of irradiated material and evolved chemistry on the surface, as well as the presence of a small amount of ethane that could be formed either in the atmosphere or on the surface.

Orcus has large amounts of crystalline water ice on its surface. Barucci et al. (2008) detected a signature attributed to hydrated ammonia, similar to the case of Charon, the satellite of Pluto, on which large amounts of water ice also exist in crystalline form. These observations suggest processes that are able to renew the surface with fresh and non-irradiated icy materials. For the largest objects evolutionary models indicate that cryovolcanism is possible (if enough radiogenic sources were present in their interiors). Non-disruptive collisions could also play a role in renewing the surface, as well as catastrophic collisions such as that at the origin of the Haumea family, which could explain the presence of fresh crystalline water ice even on small members of the family.

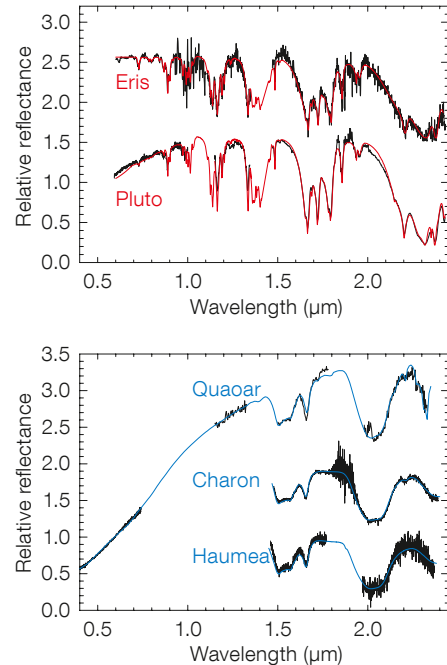
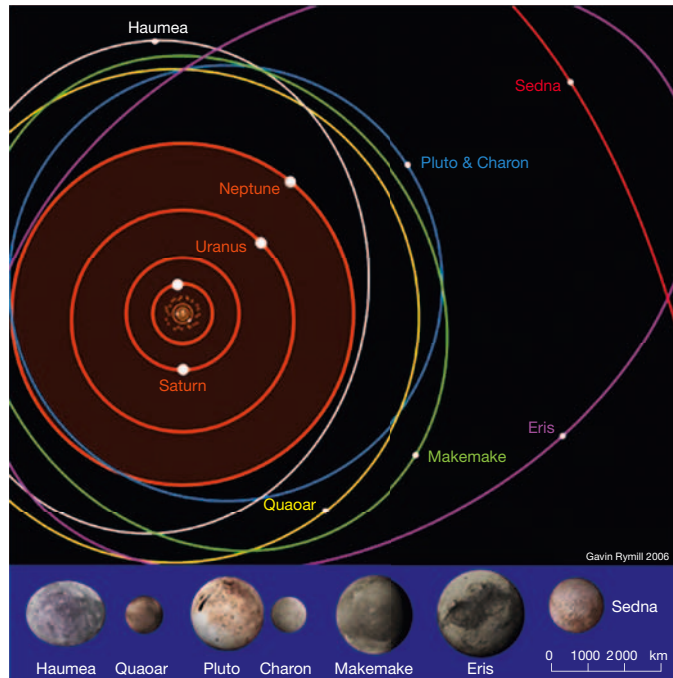


Figure 3. The image on the left (adapted from Gavin Rymill, 2006) shows the circular orbits of the eight planets versus the eccentric orbits of the biggest TNOs (Pluto, Eris, Quaoar, Sedna, ...) On the right are shown the two groups of TNO spectra: Eris and Pluto with methane ice dominated spectra and Quaoar, Haumea and Charon with water ice dominated spectra.

Although Quaoar's spectrum displays clear water ice features in the crystalline form, there is a strong red slope in the visible and other weak features in the NIR that suggest a small amount of methane on the surface and small grains of irradiated material. Dalle Ore et al. (2009) model a spectrum from the visible to the NIR, including the additional constraints of Spitzer data, and find a best-fit model consisting of crystalline and amorphous water ice, methane, nitrogen and ethane ices with, in addition, Triton and Titan tholins. Sedna, which is significantly further from the Sun (~ 90 AU) than most known TNOs (30–50 AU), also exhibits one of the reddest visible spectra, and weak features in the near-infrared that suggest a surface covered by water ice, methane and nitrogen ice, as well as small grains of irradiated material mainly formed via impacts of cosmic rays and interstellar medium particles (Sedna's orbit often takes it beyond the heliopause).

Surface properties

To investigate the surface characteristics of TNOs better we carried out polarimetric observations of eight objects belonging to different dynamical groups. These include dwarf planets Eris and Haumea, the classical object (2000) Varuna, the resonant

object (38628) Huya, the scattered disc object (26375) 1999 DE9, and Centaurs (2060) Chiron, (5145) Pholus and (10199) Chariklo. The polarimetric characteristics of the scattered radiation contain much more accurate and specific information concerning the microscopic properties of the surface. We found that all observed bodies revealed negative polarisation, where the polarisation plane of linearly polarised light coincides with the scattering plane. It is a characteristic feature for surfaces with a complex structure, as observed for the majority of planetary surfaces. However, the measured polarisation phase angle behaviour of TNOs and Centaurs was found to be unique among other Solar System bodies observed so far. Objects with a diameter smaller than 1000 km exhibit a negative polarisation that rapidly increases (in absolute value) with the phase angle and reaches about -1% at phase angles as small as 1° . The largest TNOs exhibit a small fraction of negative linear polarisation that does not noticeably change in the observed phase angle range. It has been suggested that the different types of polarimetric behaviour are related to different albedos and different capabilities for retaining volatiles for large and small TNOs (Bagnulo et al., 2008). The modelling of the polarimetric behaviour of the largest objects suggests that their topmost surface layer consists

of large (compared to the observation wavelength) inhomogeneous particles (Belskaya et al., 2008). Smaller size TNOs, characterised by a pronounced branch of negative polarisation, revealed a similar polarisation behaviour regardless of the fact that they have different surface albedos and belong to different dynamical groups. The presence of a thin frost layer of submicron ice crystals on a dark surface is considered as one of the possible ways to explain the particular polarisation properties of these distant objects.

The overall picture

These results provide unique insights into the global population of these faint and distant objects. Important advances in elucidating the surface composition of TNOs have been achieved. Observations performed with SINFONI in the *H* and *K* regions have allowed us to detect spectral signatures, revealing the presence of surface deposits of ices such as H_2O , CH_4 , CH_3OH , C_2H_6 , NH_3 and N_2 . We find that most of the largest objects have ices on their surface (water ice or ices of more volatile species), whatever their dynamical class (see Figure 4) and whatever their colours, although objects with neutral colours tend to be covered by water ice. The colours are very variable, from slightly blue

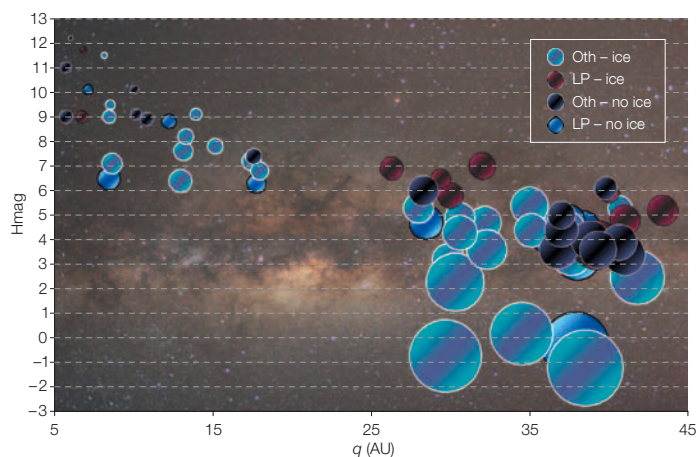


Figure 4. The absolute magnitude (in *H*-band) of the TNOs and Centaurs (with and without ice detected on their surface) is plotted as a function of the perihelion distance (*q*, in astronomical units). The dimension of the symbol is related to the diameter of the object (for clarity the scale used is not linear). The smallest size of the Centaurs is 20 km, while the biggest TNO has a diameter close to 2500 km.

to have formed from a disc of debris ejected during the collision of Pluto with a body of almost equal size.

In addition, the high albedos and the detection of volatiles on the surfaces on some TNOs indicate the possible presence of an atmosphere, even if only as a transient phenomenon. The only Trans-Neptunian object observed thus far with a seasonal atmosphere is Pluto, but other large objects like Eris or Sedna may have one as well. A cometary-type activity (outburst) has also been suggested for the Centaur Chariklo to explain differences in spectra obtained at different times (Guilbert et al., 2009).

Our understanding of the population of these faint and distant objects is, however, still limited. The observations that have been made so far lead to a lot of questions. If major differences in composition between the very large objects and the others can be attributed to a size effect, it is very hard to explain differences among smaller objects. The next generation of more powerful instruments on 10-metre-class telescopes will start giving us some answers, but most of the answers will probably come with the next generation of telescopes, the ELTs, which will open the study of smaller objects. These smaller objects are those that carry most of the information about the dynamical/collisional evolution of the Solar System. The definitive evidence for atmospheres can come only from occultations or direct spectroscopic detection with spacecraft. A major step in the study of this population is the New Horizons–NASA mission that will fly by Pluto in 2015 and will enable the detailed study of Pluto and its three satellites, Charon, Nix and Hydra. The New Horizons spacecraft will continue on into the Trans-Neptunian population to fly by one or more TNOs.

References

- Bagnulo, S. et al. 2008, *A&A*, 491, L33
- Barucci, M. A. et al. 2005, *AJ*, 130, 1291
- Barucci, M. A. et al. 2008, *A&A*, 479, L13
- Belskaya, I. et al. 2008, *A&A*, 479, 265
- Dalle Ore, C. M. et al. 2009, *A&A*, 501, 349
- DeMeo, F. et al. 2009, *A&A*, 493, 283
- Guilbert, A. et al. 2009, *A&A*, 501, 777
- Fornasier, S. et al. 2009, *A&A*, 508, 457
- Merlin, F. et al. 2009, *AJ*, 137, 315
- Perna, D. et al. 2010, *A&A*, 508, 457

to very red (Fornasier et al., 2009). The wide difference in surface composition and colour within the TNO population could be connected to different original compositions and/or the different processes they have experienced, as well as to their size. Even if TNOs are considered as the most pristine objects in the Solar System, over the 4.5 Gy of the Solar System's life they have experienced various modifying processes.

It is clear that the surface of these objects has been affected by bombardment by cosmic ray and solar wind ions and/or micrometeorites (space weathering), with the consequence that the molecular complexes are structurally changed and the molecular compositions of ice and minerals are altered over time. Laboratory experiments on plausible materials for TNOs show the formation of an irradiation mantle (forming a crust), breaking bonds in ice molecules, allowing the formation of radicals, escape of hydrogen and formation of a carbon-rich layer of low albedo. This can easily mask the presence of volatiles and the crust thus formed would hide the real composition of these icy bodies. The statistics do not, however, show any strong correlation between the surface properties and dynamical classes or orbital properties of TNOs. Many objects from the reddest class (RR), which are the reddest objects in the Solar System, have probably been heavily irradiated. The slopes of the spectra of these objects, which have typically low albedos, have been modelled with complex organic compounds such as Titan, Triton or ice tholins, or terrestrial-type kerogens, but

the real nature of the organics present on these objects is still a matter of debate. The red class (RR) objects are present in all dynamical populations, with a higher concentration in the classical group. They are found amongst the Centaur population as well as in the detached population, as for example Sedna, which is considered as part of the inner Oort Cloud.

Other processes must be at work that could affect some objects more than others. Models of the interiors of TNOs indicate that cryovolcanism, which is considered to be the most probable form of geological activity on some satellites of the outer planets, may be possible on the larger Trans-Neptunian objects (diameter > 800 km). This could explain, for instance, the surface composition of Orcus which includes both water ice in the crystalline state, which is not supposed to exist at such low temperatures (around 30 K), and ammonia, which is easily destroyed by irradiation. Furthermore, the water ice in the crystalline state should be quickly amorphised by irradiation, as indicated by various laboratory studies.

Collisions must have also played an important role in the evolution of this population, inducing heating and chemical changes. The consequence of collisions is not only the alteration of the surface properties, but also the modification of the internal structure of the targets. Collisions are important both for small and large objects. A typical example is Charon, a moon of Pluto, but completely different in composition (see Figure 3), which is supposed (according to numerical models)

The APEX Telescope Large Area Survey of the Galaxy (ATLASGAL)

Frédéric Schuller¹
 Henrik Beuther²
 Sylvain Bontemps³
 Leonardo Bronfman⁴
 Philipp Carlhoff⁵
 Riccardo Cesaroni⁶
 Yanett Contreras⁴
 Tímea Csengari⁷
 Lise Deharveng⁸
 Guido Garay⁴
 Thomas Henning²
 Fabrice Herpin³
 Katharina Immer¹
 Bertrand Lefloch⁹
 Hendrik Linz²
 Diego Mardones⁴
 Karl Menten¹
 Vincent Minier⁷
 Sergio Molinari¹⁰
 Frédérique Motte⁷
 Quang Nguyen Luong⁷
 Lars-Åke Nyman¹¹
 Jill Rathborne⁴
 Vincent Reveret⁷
 Christophe Risacher¹²
 Delphine Russeil⁸
 Peter Schilke⁵
 Nicola Schneider⁷
 Jochen Tackenberg²
 Leonardo Testi¹³
 Tobias Troost¹
 Tatiana Vasyunina²
 Malcolm Walmsley⁶
 Marion Wienen¹
 Friedrich Wyrowski¹
 Annie Zavagno⁸

¹ Max-Planck-Institut für Radioastronomie, Bonn, Germany

² Max-Planck-Institut für Astronomie, Heidelberg, Germany

³ Laboratoire d'Astrophysique de Bordeaux, France

⁴ Universidad de Chile, Santiago, Chile

⁵ University of Cologne, Germany

⁶ Osservatorio Astrofisico di Arcetri, Firenze, Italy

⁷ IRFU/SAP, Commissariat à l'énergie atomique, Saclay, France

⁸ Laboratoire d'Astrophysique de Marseille, France

⁹ Laboratoire d'Astrophysique de l'Observatoire de Grenoble, France

¹⁰ INAF–Istituto di Fisica dello Spazio Interplanetario, Roma, Italy

¹¹ ALMA, Santiago, Chile

¹² SRON, Groningen, Netherlands

¹³ ESO

Thermal emission from dust at submillimetre wavelengths is a direct tracer of high column densities and, thus, of dense cloud regions in which new stars are forming. Surveys of the Galactic Plane in thermal dust emission have the potential to deliver an unbiased view of high-mass star formation throughout the Milky Way. The Atacama Pathfinder Experiment (APEX) telescope is ideally located for mapping the inner Galaxy. Using the Large APEX Bolometer Camera (LABOCA), we have recently completed the APEX Telescope Large Area Survey of the Galaxy (ATLASGAL). This survey, which covers 360 square degrees at 870 μm , provides the first unbiased sample of cold dusty clumps in the Galaxy at submillimetre wavelengths and reveals the clumpy structure of the cold interstellar medium over very large scales that have previously been little explored.

Trying to understand the early stages of star formation is an important topic of modern astrophysics. While significant progress has been achieved in the field of low-mass star formation, both from theoretical and observational aspects, the quest for the earliest phases of massive star formation remains a major challenge. The prime reason for this is the short lifetime of massive stars, which makes them rare, so that most high-mass star-forming regions are located at distances greater than 1 kpc. Therefore, systematic surveys on the scale of the full Galaxy are required to provide large samples of massive pre- and proto-stellar objects.

The advent of large arrays of bolometers has made it possible to map large areas in the sky at submillimetre (sub-mm) and millimetre (mm) wavelengths. Using the Max-Planck Millimeter Bolometer (MAMBO) array at the IRAM 30-metre telescope, Motte et al. (2007) obtained a complete 3 by 2 degree map covering the Cygnus-X complex at 1.2 mm. They could derive statistically significant results and lifetimes for the evolutionary phases of high-mass star formation. In particular, no high-mass analogue of pre-stellar dense cores was found by this study, implying a very short lifetime for the earliest phases of dense cores in

which high-mass stars are being formed. Whether this is representative can only be revealed by an unbiased survey of the complete Galactic Plane, providing large samples, which will allow us to place far stronger constraints on the early stages of high-mass star formation.

Located at one of the driest sites on Earth, and at a latitude of -23° , the 12-metre diameter APEX telescope (Güsten et al., 2006) is ideally located to observe the inner two quadrants of the Galactic Plane. Equipped with the 295-pixel LABOCA instrument (Siringo et al., 2007; Siringo et al., 2009), APEX can map hundreds of square degrees at 870 μm in reasonable time. Making the best possible use of this “mapping machine”, a consortium involving the Max-Planck-Institut für Radioastronomie (MPIfR) in Bonn, the Max-Planck-Institut für Astronomie in Heidelberg, the ESO community and the Universidad de Chile has embarked on the APEX Telescope Large Area Survey of the Galaxy (ATLASGAL). The LABOCA observations have just been completed, covering 360 square degrees of the inner Galactic Plane. Several follow-up projects have already been started.

The first systematic survey of the inner Galactic Plane in the submillimetre range

In the past decade, several bolometer arrays have been used by various teams to map individual star-forming complexes. For example, Johnstone et al. (2004) used SCUBA to map the Ophiuchus and Perseus clouds, and Enoch et al. (2006) covered Perseus, Ophiuchus and Serpens with BOLOCAM. Unlike these targeted observations, the ATLASGAL project aims at mapping the entire Galactic Plane accessible from APEX at 870 μm . A similar survey of the northern Galactic Plane has recently been completed with BOLOCAM at the Caltech Submillimeter Observatory (CSO) at 1.1 mm (Rosolowsky et al., 2010). Only such blind surveys have the potential to deliver unbiased samples of cold dusty cores.

The ATLASGAL observations started in 2007. A large programme was conducted in 2008–9, using observing time from MPIfR, from ESO and from Chile. The

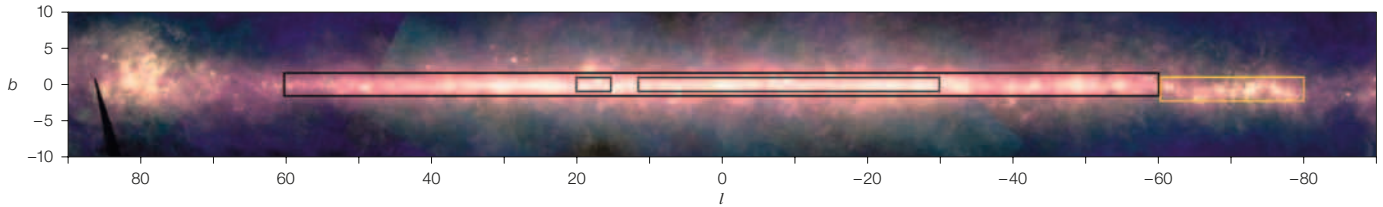


Figure 1. The coverage of the ATLASGAL observations is shown in Galactic coordinates (l, b) in degrees, on top of an IRAS false-colour image (blue: 12 μm , green: 60 μm , red: 100 μm). The large black frame shows the 360 sq. degrees mapped to date; the smaller frames inside the larger one show the data obtained in 2007 and presented in Schuller et al. (2009). The frame in yellow delineates the additional region being mapped in 2010.

current data cover the $\pm 60^\circ$ range in Galactic longitude, over $\pm 1.5^\circ$ in latitude (see Figure 1). To complete the coverage of the most active regions in the inner Galaxy, another small programme was accepted in 2010. Observations of the -80° to -60° range in longitude are still ongoing.

The telescope patterns are linear on-the-fly maps, where the telescope scans at (typically) 3 arcminute/s along a line, and the step between lines is 1.5 arcminutes. The 11-arcminute field of view and 295 pixels of LABOCA ensure a high redundancy in a single map. In addition, each position in the sky is covered by at least two different maps, observed with different scanning angles. More details on the observing strategy and data reduction can be found in Schuller et al. (2009). The noise level in the final maps is usually around 50 mJy/beam. Assuming a dust temperature of 15 K and typical properties for dust, this

corresponds to a 5σ detection of individual clumps of $10 M_\odot$ at 2 kpc, and $100 M_\odot$ at the distance to the Galactic Centre.

Compact sources and long filaments

The LABOCA maps reveal thousands of compact sources, as well as extended objects, many of them showing filamentary structures. Such filaments have a width of just a few parsecs, and can extend over 100 pc. A typical example is shown in Figure 2.

With a spatial resolution of 19 arcseconds, the LABOCA data can spatially resolve objects with sizes of 0.3 pc and larger, for typical distances of 3 kpc or more. Most of the compact objects are actually resolved by our observations, with full width at half maximum generally of order 30 arcseconds. This corresponds to massive clumps, which will probably give birth to groups or clusters of stars: most clumps have total gas+dust masses of a few $100 M_\odot$, and the most extreme have a few $10^4 M_\odot$. Only with interferometers that provide a resolution of order 1 arcsecond is it possible to resolve such clumps into individual star-forming cores (today, for example with the Plateau de Bure interferometer, e.g., Beuther et al., 2007, and in the future with the Atacama

Large Millimeter/submillimeter Array, ALMA).

Many of these compact sources are embedded in extended emission on the arcminute scale, as can be seen in the close-up examples in Figure 3. Our 5σ sensitivity of 0.25 Jy/beam corresponds to a hydrogen column density of order 10^{22} cm^{-2} , or, to a visual extinction of about 10 magnitudes. We note that, due to the subtraction of correlated noise during data reduction, uniform emission on scales larger than 2.5 arcminutes is filtered out and is not present in the final maps (more details are given in Schuller et al., 2009). Observations in the sub-mm continuum are nevertheless complementary to the infrared extinction techniques, which are sensitive to larger scales, but “saturate” in the densest regions.

The long filaments seem sometimes to connect large molecular complexes together (e.g., near the M16 nebula, see Figure 4), or to trace the boundaries of supergiant bubbles.

Nature of the sources

Because thermal emission from dust in the submillimetre range is optically thin, the emission seen with LABOCA directly

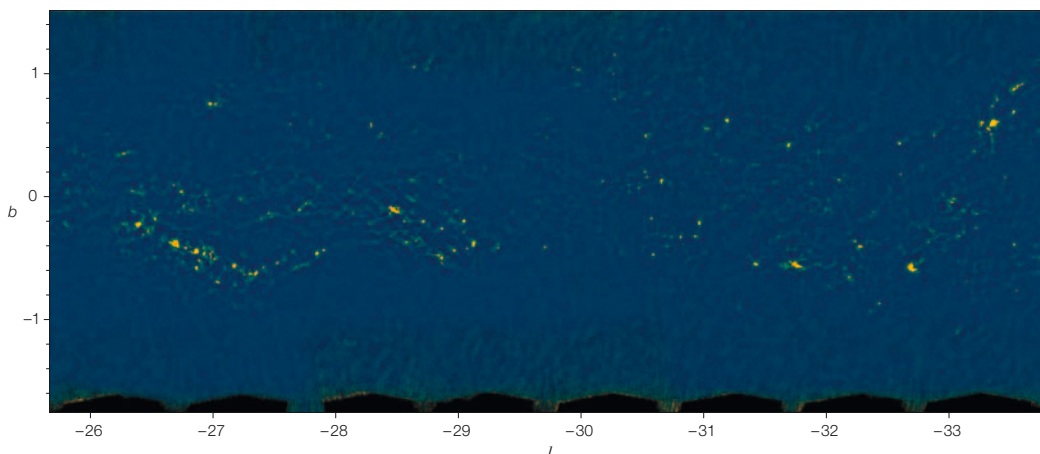
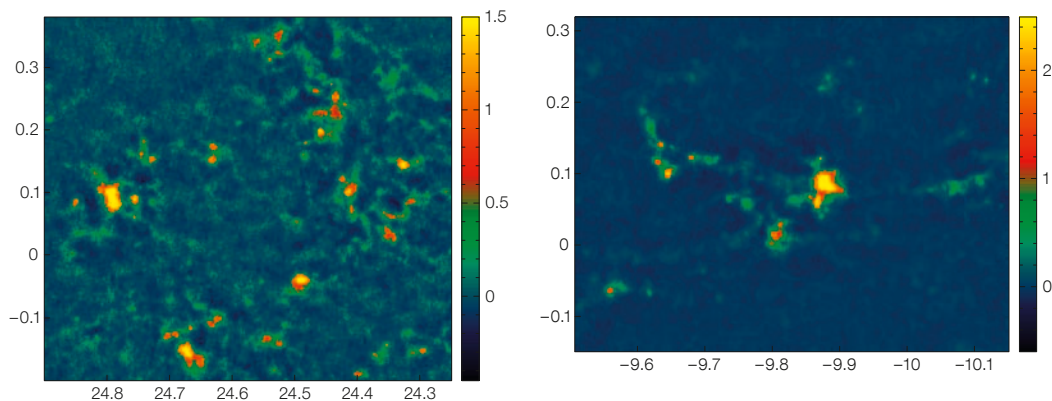


Figure 2. Example ATLASGAL map at 870 μm , in the direction of the Norma arm, showing about 20 square degrees, or 6% of the surveyed area (in Galactic coordinates). Compact objects and filamentary structures are prominent.

Figure 3. Close-up views of representative regions, towards Galactic longitudes $+24.6^\circ$ (left) and -10° (right). The intensity scale (in Jy/beam) is linear, as shown on the right of each panel. Galactic coordinates (l, b) shown in degrees.



scales with the amount of matter along the line of sight. Therefore, our survey is primarily sensitive to massive star-forming clumps. We cannot exclude, however, that some of our compact sources are nearby low-mass clumps (our 5σ detection limit corresponds to a one solar mass clump at a distance of 1 kpc). Evolved stars, such as post-asymptotic giant branch (AGB) or supergiant stars, also have large amounts of dust in their envelopes and can therefore appear bright at $870\ \mu\text{m}$. However, only a few sources are unresolved in our maps, and could correspond to evolved stars.

During their early evolution, star-forming clumps increase in temperature, as the protostar starts to warm the inner part of the clump. The peak of the thermal emission then moves from the sub-mm to the far- and mid-infrared. We have systematically searched for infrared counterparts to our compact sources in the Infra-Red Astronomical Satellite (IRAS) and the Mid-course Space Experiment (MSX) point-source catalogues. Only about 10% of ATLASGAL sources could be associated with mid- and far-infrared IRAS sources, and one third have a counterpart within a 30-arcsecond search radius in the MSX mid-IR database (Figure 5).

Sources with infrared counterparts are relatively warm, and correspond to later stages of star formation, when one or several protostar(s) have already been formed, and a molecular hot core or a compact H II region has developed. On the other hand, the majority of ATLASGAL sources have no bright IR counterpart (they may however be detected at $24\ \mu\text{m}$ with the superior sensitivity of the Spitzer surveys). These sources are likely to be

very cold, and to represent the earliest stages of massive star formation, and, in particular, the pre-stellar phase.

A first version of the ATLASGAL catalogue of compact sources will soon be published (Contreras et al., in preparation). Associations with IRAS and MSX point sources will be included. This catalogue will allow the distribution of massive star-forming clumps in the inner Galactic Plane to be studied in a systematic way for the first time. The catalogue will later be cross-associated with databases at other wavelengths, e.g., the Spitzer GLIMPSE and MIPS GAL surveys, and with the Herschel Hi-GAL data when they become available.

Star formation triggered by expanding H II regions

The Spitzer–GLIMPSE images at $8\ \mu\text{m}$ have unveiled a “bubbling Galactic disc”. More than 600 bubbles with diameters of a few arcminutes have been catalogued by Churchwell et al. (2006, 2007). As shown by Deharveng et al. (2010), more than 85% of these $8\ \mu\text{m}$ bubbles enclose H II regions and contain hot dust emitting at $24\ \mu\text{m}$. Taking advantage of the simple morphology of these bubbles, Deharveng et al. (2010) used ATLASGAL to search for dense neutral shells and condensations surrounding the H II regions. A sample of one hundred bubbles from the Churchwell et al. (2006) catalogue was studied. Among the 65 regions for which the angular resolution of the ATLASGAL observations is high enough, they find that 40% of the bubbles are surrounded by cold dust (accumulated at their borders during the expansion of the central

H II region); another 28% contain condensations clearly interacting with the ionised gas. Thirteen bubbles exhibit ultra-compact H II regions associated with the dust condensations found adjacent to their ionisation fronts. Another five show 6.7 GHz methanol masers, tracers of very young embedded high-mass proto-stars, in similar condensations.

The conclusion from this study is that more than a quarter of the bubbles could have triggered the formation of massive objects. Star formation triggered by H II regions has long been thought to be an important process, especially for the formation of massive stars, but so far little systematic evidence was available. We now plan to use complementary data to characterise the properties (such as mass and evolutionary stage) of the young sources formed on the borders of these regions.

Follow-up projects

Based on a preliminary extraction of the compact sources, several follow-up projects in spectral lines have been started. In particular, observations of the inversion lines of ammonia (NH_3) with the Effelsberg radio telescope for the northern sources, and with the Parkes telescope for the south, provide the most efficient way to measure radial velocities and to derive kinematic distances. These lines of NH_3 also provide rotation temperatures, which give an estimate of the gas temperature in the clumps. So far, more than 1000 sources have been observed in NH_3 (Wienen et al., in preparation). These observations show that the compact sources are not randomly distrib-

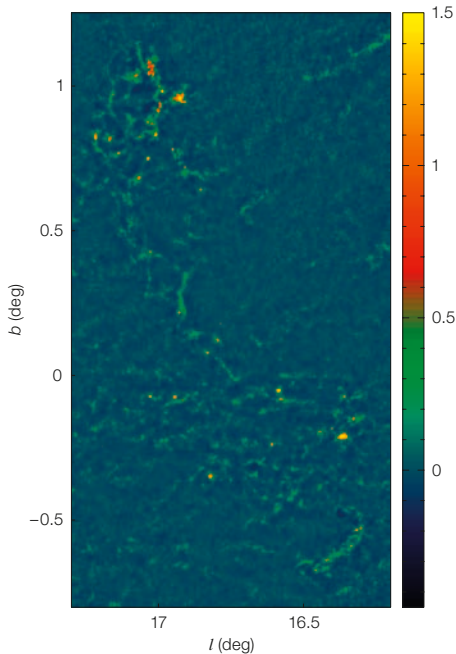


Figure 4. Example ATLASGAL map in the vicinity of the M16 (Eagle) nebula. The intensity scale is linear, as shown on the right, in Jy/beam.

uted at all possible distances, but they are rather found to gather within coherent complexes, at a given distance. Such complexes extend over several hundreds of parsecs.

We have also observed a large sample of over 600 sources at 3 mm with the Australian Mopra telescope. This telescope, equipped with an 8 GHz wide spectrometer, allows many molecules to be detected simultaneously (e.g., SiO, N₂H⁺, HCN, HCO⁺, NH₂D, ...), tracing a broad range of physical conditions. Such a large dataset also provides valuable information on the chemical processes occurring within the sources. A detailed analysis of these data is in progress (Wyrowski et al., in preparation). A smaller sample was also observed in the 1 mm window with the APEX telescope. These observations are highly complementary to the Mopra data, since they allow us to observe, at a similar spatial resolution, higher energy transitions of the same molecules.

Since maser emission is known to be another good tracer of massive star formation, we have started to follow up a

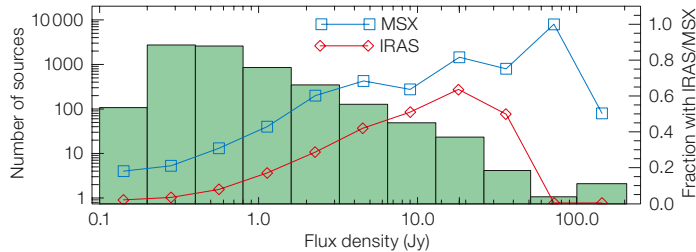


Figure 5. Distribution of peak fluxes from a preliminary extraction of 6000 ATLASGAL compact sources. The fraction of sources in each bin for which a counterpart in the IRAS or MSX catalogues could be found is shown in red or blue, respectively.

large sample of bright ATLASGAL sources in the H₂O maser line at 22 GHz, with the Effelsberg 100-metre radio telescope. In 2009, we observed 140 sources, and water maser emission, tracing outflow activity, was detected in about two thirds of the sources, including many new detections.

Finally, we have observed a sample of about 100 bright sources at 350 μ m, using the Submillimeter APEX Bolometer Camera, SABOCA (Siringo et al., 2010). The combination of LABOCA and SABOCA data allows us to compute the dust spectral index. This is found to vary between ~ 2 and values above 4, which could trace an evolution of the dust properties. Moreover, the spatial resolution of APEX at 350 μ m is 7 arcseconds, significantly better than that of LABOCA. Therefore, the SABOCA data make it possible to study the fragmentation of star-forming cores. These observations took place in May 2010, and a detailed analysis is ongoing (Troost et al., in preparation). We are also planning to use the SABOCA instrument to map large regions of the Galactic Plane, in order to study core fragmentation and dust properties on large scales, mostly unexplored so far.

Perspectives: a long-lasting legacy database

The SABOCA and LABOCA data, when combined with the available Spitzer GLIMPSE and MIPS GAL surveys at 3.6 to 24 μ m, provide spectral energy distributions (SEDs) for a very large sample of sources, from the near-IR to the sub-mm range.

Currently, the Herschel Space Observatory is mapping the same area of the Galactic Plane as observed for ATLASGAL in the wavelength range from 70 to 500 μ m, as part of the Hi-GAL project

(Molinari et al., 2010). We plan to combine the Hi-GAL and ATLASGAL data, in order to build SEDs for thousands of compact Galactic sources. Using also the Spitzer data, we will then obtain complete SEDs from 3.6 μ m to 870 μ m. This dataset will remain unique for many years to come. The catalogue of compact sources with identifications at other wavelengths will be available to the public upon completion, as well as the reduced calibrated maps. We also plan to include results from follow-up observations in this public database. This will give a high legacy value to the survey, providing well characterised samples of targets for many possible studies.

Last but not least, the first ALMA antennas should be available soon for early science. This will be the perfect time for conducting follow-up studies of carefully selected samples at an unprecedented spatial resolution. The ATLASGAL catalogue will provide ALMA with several thousand compact sources, including hot cores, high-mass proto-stellar objects, and cold pre-stellar cores. Thus ATLASGAL is expected to trigger numerous follow-up studies with ALMA, aimed at characterising the physical conditions and the chemistry of the massive star formation process at the smallest possible scales.

References

- Beuther, H. et al. 2007, A&A, 466, 1065
- Churchwell, E. et al. 2006, ApJ, 649, 759
- Churchwell, E. et al. 2007, ApJ, 670, 428
- Deharveng, L. et al. 2010, A&A, accepted, arXiv:1008.0926
- Güsten, R. et al. 2006, A&A, 454, L13
- Enoch, M. L. et al. 2006, ApJ, 638, 293
- Johnstone, D. et al. 2004, ApJ, 611, L45
- Molinari, S. et al. 2010, A&A, 518, L100
- Motte, F. et al. 2007, A&A, 476, 1243
- Rosolowsky, E. et al. 2010, ApJS, 188, 123
- Schuller, F. et al. 2009, A&A, 504, 415
- Siringo, G. et al. 2007, The Messenger, 129, 2
- Siringo, G. et al. 2009, A&A, 497, 945
- Siringo, G. et al. 2010, The Messenger, 139, 20

VISTA Variables in the *Vía Láctea* (VVV): Current Status and First Results

Roberto Saito¹
 Maren Hempel¹
 Javier Alonso-García¹
 Ignacio Toledo¹
 Jura Borissova²
 Oscar González³
 Juan Carlos Beamin¹
 Dante Minniti^{1,4}
 Philip Lucas⁵
 Jim Emerson⁶
 Andrea Ahumada^{7,3,8}
 Suzanne Aigrain^{9,24}
 Maria Victoria Alonso⁷
 Eduardo Amôres¹⁰
 Rodolfo Angeloni¹
 Julia Arias¹¹
 Reba Bandyopadhyay¹²
 Rodolfo Barbá¹¹
 Beatriz Barbuy¹³
 Gustavo Baume¹⁴
 Luigi Bedin¹⁵
 Eduardo Bica¹⁶
 Leonardo Bronfman¹⁷
 Giovanni Carraro³
 Márcio Catelan¹
 Juan Clariá⁷
 Carlos Contreras¹
 Nicholas Cross¹⁸
 Christopher Davis¹⁹
 Richard de Grijs²⁰
 István Dékány¹
 Janet Drew^{5,21}
 Cecilia Fariña¹⁴
 Carlos Feinstein¹⁴
 Eduardo Fernández Lajús¹⁴
 Stuart Folkes²
 Roberto Gamen¹⁴
 Doug Geisler²²
 Wolfgang Gieren²²
 Bertrand Goldman²³
 Andrew Gosling²⁴
 Guillermo Gunthardt¹¹
 Sebastian Gurovich⁷
 Nigel Hambly¹⁸
 Margaret Hanson²⁵
 Melvin Hoare²⁶
 Mike Irwin²⁷
 Valentin Ivanov³
 Andrés Jordán¹
 Eamonn Kerins²⁸
 Karen Kinemuchi²⁹
 Radostin Kurtev²
 Andy Longmore¹⁸
 Martín López-Corredoira³⁰
 Tom Maccarone³¹
 Eduardo Martín³⁰
 Nicola Masetti³²
 Ronald Mennickent²²
 David Merlo⁷

Maria Messineo³³
 Félix Mirabel^{34,35}
 Lorenzo Monaco³
 Christian Moni Bidin²²
 Lorenzo Morelli³⁶
 Nelson Padilla¹
 Tali Palma⁷
 Maria Celeste Parisi⁷
 Quentin Parker^{37,38}
 Daniela Pavani¹⁶
 Pawel Pietrukowicz³⁹
 Grzegorz Pietrzynski^{22,40}
 Giuliano Pignata⁴¹
 Marina Rejkuba³
 Alejandra Rojas¹
 Alexandre Roman-Lopes¹¹
 Maria Teresa Ruiz¹⁷
 Stuart Sale^{1,2}
 Ivo Saviane³
 Matthias Schreiber²
 Anja Schröder^{42,43}
 Saurabh Sharma²
 Michael Smith⁴⁴
 Laerte Sodré Jr.¹³
 Mario Soto¹¹
 Andrew Stephens⁴⁵
 Motohide Tamura⁴⁶
 Claus Tappert²
 Mark Thompson⁵
 Elena Valenti³
 Leonardo Vanzì⁴⁷
 Walter Weidmann⁷
 Manuela Zoccali¹

¹ Departamento de Astronomía y Astrofísica, Pontificia Universidad Católica de Chile, Santiago, Chile
² Departamento de Física y Astronomía, Universidad de Valparaíso, Chile
³ ESO
⁴ Vatican Observatory, Italy
⁵ Centre for Astrophysics Research, University of Hertfordshire, Hatfield, UK
⁶ School of Mathematical Sciences, Queen Mary, University of London, UK
⁷ Observatorio Astronómico de Córdoba, Argentina
⁸ Consejo Nacional de Investigaciones Científicas y Técnicas, Buenos Aires, Argentina
⁹ School of Physics, University of Exeter, UK
¹⁰ SIM, Faculdade de Ciências da Universidade de Lisboa, Portugal
¹¹ Departamento de Física, Universidad de La Serena, Chile
¹² Department of Astronomy, University of Florida, USA

¹³ Universidade de São Paulo, Brazil
¹⁴ Facultad de Ciencias Astronómicas y Geofísicas, Universidad Nacional de La Plata, Argentina
¹⁵ Space Telescope Science Institute, Baltimore, USA
¹⁶ Universidade Federal do Rio Grande do Sul, Porto Alegre, Brazil
¹⁷ Departamento de Astronomía, Universidad de Chile, Santiago, Chile
¹⁸ Institute for Astronomy, The University of Edinburgh, UK
¹⁹ Joint Astronomy Centre, Hilo, USA
²⁰ Kavli Institute for Astronomy and Astrophysics, Peking University, China
²¹ Astrophysics Group, Imperial College London, UK
²² Departamento de Astronomía, Universidad de Concepción, Chile
²³ Max-Planck Institute for Astronomy, Heidelberg, Germany
²⁴ Department of Astrophysics, University of Oxford, UK
²⁵ Department of Physics, University of Cincinnati, USA
²⁶ School of Physics & Astronomy, University of Leeds, UK
²⁷ Institute of Astronomy, University of Cambridge, UK
²⁸ Jodrell Bank Centre for Astrophysics, The University of Manchester, UK
²⁹ NASA-Ames Research Center, Moffett Field, USA
³⁰ Instituto de Astrofísica de Canarias, Tenerife, Spain
³¹ School of Physics and Astronomy, University of Southampton, UK
³² Istituto di Astrofisica Spaziale e Fisica Cosmica di Bologna, Italy
³³ ESTEC, Noordwijk, the Netherlands
³⁴ Service d'Astrophysique — IRFU, CEA-Saclay, France
³⁵ Instituto de Astronomía y Física del Espacio, Buenos Aires, Argentina
³⁶ Dipartimento di Astronomia, Università di Padova, Italy
³⁷ Department of Physics, Macquarie University, Sydney, Australia
³⁸ Australian Astronomical Observatory, Epping, Australia
³⁹ Nicolaus Copernicus Astronomical Center, Warsaw, Poland
⁴⁰ Warsaw University Observatory, Poland
⁴¹ Departamento de Ciencias Físicas, Universidad Andres Bello, Santiago, Chile
⁴² SKA/KAT, Cape Town, South Africa
⁴³ Hartebeesthoek Radio Astronomy Observatory, South Africa

⁴⁴ The University of Kent, Canterbury, UK

⁴⁵ National Astronomical Observatory of Japan, Tokyo, Japan

⁴⁶ Gemini Observatory, Hawaii, USA

⁴⁷ Departamento de Ingeniería Eléctrica, Pontificia Universidad Católica de Chile, Santiago, Chile

VISTA Variables in the *Vía Láctea* (VVV) is a public ESO near-IR variability survey aimed at scanning the Milky Way Bulge and an adjacent section of the mid-plane. VVV observations started in October 2009 during ESO science verification. Regular observations for the first year of the survey have been conducted since February 2010 and will cover a total area of 520 square degrees in five passbands and five epochs. Here we address the first results obtained from the VVV Survey as well as the current status of the observations.

Introduction

VISTA Variables in the *Vía Láctea* is one of the six ESO Public Surveys selected to operate with the new 4-metre Visible and Infrared Survey Telescope for Astronomy VISTA¹ (Emerson & Sutherland, 2010). VVV is scanning the Milky Way (the *Vía Láctea*) Bulge and an adjacent section of the mid-plane, where star formation activity is high. The survey will take 1929 hours of observations during five years (2010–14), covering $\sim 10^9$ point sources across an area of 520 square degrees, including 33 known globular and ~ 350 open clusters; the survey area is shown in Figure 1. The final product will be a deep near-infrared (NIR) atlas in five passbands and a catalogue of more than 10^6 variable point sources (Minniti et al., 2010). Detailed information about the VVV Survey can be found at the survey web page².

Science verification

Some VVV data were obtained on 19–30 October 2009, during ESO science verification (SV) of VISTA (Arnaboldi et al., 2010), following the same observing strategy as the VVV survey. The observations consisted of multi-colour imaging, Z- (0.87 μm), Y- (1.02 μm), J- (1.25 μm), H-

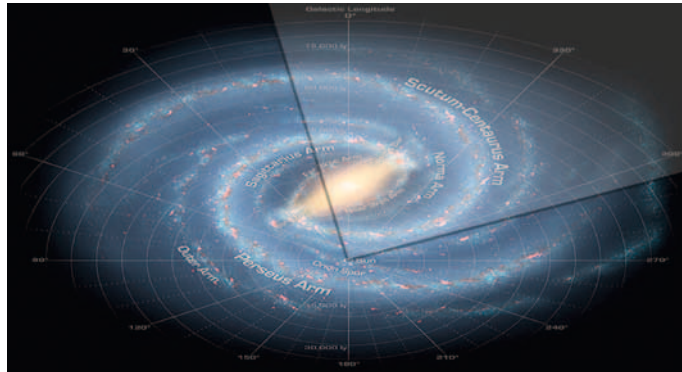


Figure 1. Illustration showing the Milky Way galaxy and the area being observed by the VVV Survey (based on Figure 16 of Churchwell et al., 2009).

(1.64 μm) and Ks- (2.14 μm) bands of a field at Galactic coordinates $l = 2.2^\circ$, $b = -3.1^\circ$. An additional thirteen epochs in Ks-band were also taken, since the variability study will be done only in this band. This is one of the most crowded fields in the Galactic Bulge, allowing us to test whether there are too many saturated stars. It is also known to contain numerous variable stars, allowing us to test their detectability. In addition to this field we also observed three other tiles (each tile corresponds to a sky field of $1 \times 1.5 \text{ deg}^2$) in the Bulge in Ks-band to test different sky subtraction strategies.

Regular observations

Regular observations for the first year started in February 2010 and will cover the total survey area in the five passbands. An additional set of five Ks-band exposures will also be taken. Table 1 shows the number of Observational Blocks (OBs), each of which corresponds to one tile, scheduled for observation during the first period, as well as the current status of the observations. The OBs named “colour” contain observations in more than one filter.

Table 1. Overview of VVV observations: first year.

	Planned for 2010	Executed by 1 July 2010	Fraction %
Bulge			
Colour ZY	196	40	20
Colour JHKs	196	170	87
Variability Ks	1004	92	9
Disc			
Colour ZY	152	121	80
Colour JHKs	152	152	100
Variability Ks	760	507	67
Total	2460	1082	44

Pipeline processing and calibration of the VVV data are performed by the UK Cambridge Astronomy Survey Unit (CASU) using the VISTA Data Flow System (VDFS) pipeline³. The VISTA Science Archive (VSA) at the Wide Field Astronomy Unit (WFAU) in Edinburgh⁴ performs: (i) image stacking to produce stacked and subtracted tiles; (ii) photometric and astrometric calibration; (iii) source merging; (iv) quality control; and (v) identification of variable sources. Photometric calibration on the VISTA system is done via thousands of unsaturated Two Micron All Sky Survey (2MASS) stars present in every VVV tile, including for Z and Y filters (not observed by 2MASS) where colour equations are used. The method is similar to that used for WFCAM (Hodgkin et al., 2009). Our project takes advantage both of the VDFS team’s experience in handling the WFCAM/UKIRT and VISTA data, and the experience of the VVV team members, who are leading participants in other surveys such as OGLE and in routine data processing and delivery to ESO.

Figure 2 shows a J-, H- and Ks-band colour-composite image centred on the Galactic HII region M8 (NGC 6523). Figure 3 (top panels) shows a small portion of a VVV image centred on the globular cluster Palomar 6, compared with 2MASS (Skrutskie et al., 2006). VVV images are usually a combination of J-, H- and Ks-band observations. However, some early images (including this one of Palomar 6) were created using Z-, H- and Ks-band colours. The higher quality of the VVV data stands out in this comparison. As another example of the superior quality of the VVV data, the lower panels of Figure 3 show colour images of the Bulge planetary nebula NGC 6629, located in a field centred at $l = 9.8^\circ$,

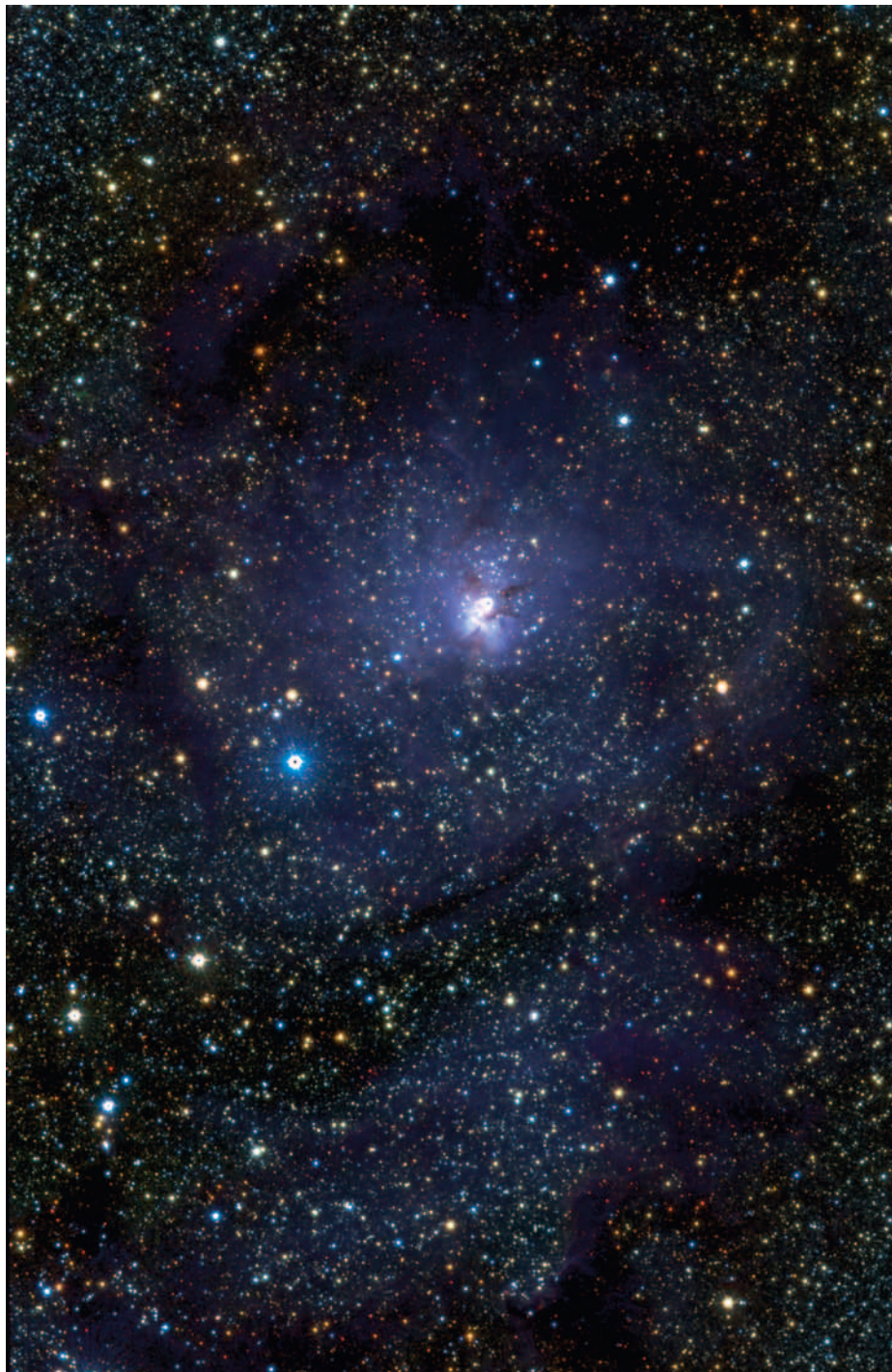


Figure 2. VVV image of the Lagoon Nebula (NGC 6523), a giant interstellar cloud in the constellation of Sagittarius, towards the Bulge of our Galaxy. This colour image was made combining *J*- (blue), *H*- (green) and *Ks*-band (red) observations. Saturated objects show a black dot in the centre. Credit: Ignacio Toledo and Dante Minniti.

Colour–magnitude diagrams

The left-hand panel of Figure 4 shows a colour–magnitude diagram (CMD) for the SV field in the Bulge located at $l = 2.2^\circ$, $b = -3.1^\circ$, in one of the most crowded regions of our Galaxy. In spite of the high stellar density and large number of giants, high precision photometry is possible over most of the field. This figure shows the dominant Bulge red giant branch along with the main sequence track of the foreground Disc, and it is evident that the VVV photometry is about 4 magnitudes deeper than 2MASS in this field, almost reaching the Bulge main sequence turn-off. About a million stars are measured in total in this 1.5 deg^2 field. CMDs like this can be used to study the stellar populations across the Bulge, as well as the 3D structure of the inner Milky Way.

The right-hand panel of Figure 4 illustrates the CMD of the first Galactic Plane field observed. Located at $l = 295.4^\circ$, $b = -1.7^\circ$ (in the outskirts of Carina), this field suffers from large and very inhomogeneous extinction. The Disc main sequence dominates and numerous reddened giants are also seen. We stress that 2MASS is very complementary to our survey, providing the external photometric and astrometric calibration, and photometry for the brighter sources ($K_s < 10$), which saturate even in the short (4 s) VVV exposures. The depth of the VVV allows us in many cases to see all the way through the Plane of the Milky Way. In fact, very often our CMDs show numerous background galaxies. CMDs like these can also be used to study the 3D structure of the Milky Way Plane, as well as the spiral arms, the edge of the Disc and the outer warp. About half a million stars are measured in this 1.5 deg^2 field. Taking into account that the VVV Survey covers over 520 deg^2 in total, we will provide photometry for $\sim 5 \times 10^8$ sources in the Bulge and Disc of our Galaxy.

$b = -5.3^\circ$. Clearly, even though the survey is not designed to detect or map emission line objects, it turns out that planetary nebulae (PNe) are also prominent in the VVV images. The colour is typical of most PNe, due to the intense emission

lines present in our filters, particularly Paschen β in the *J*-band and Brackett γ in the *Ks*-band. We expect to identify a few hundred PNe in our fields in the inner Disc and Bulge.

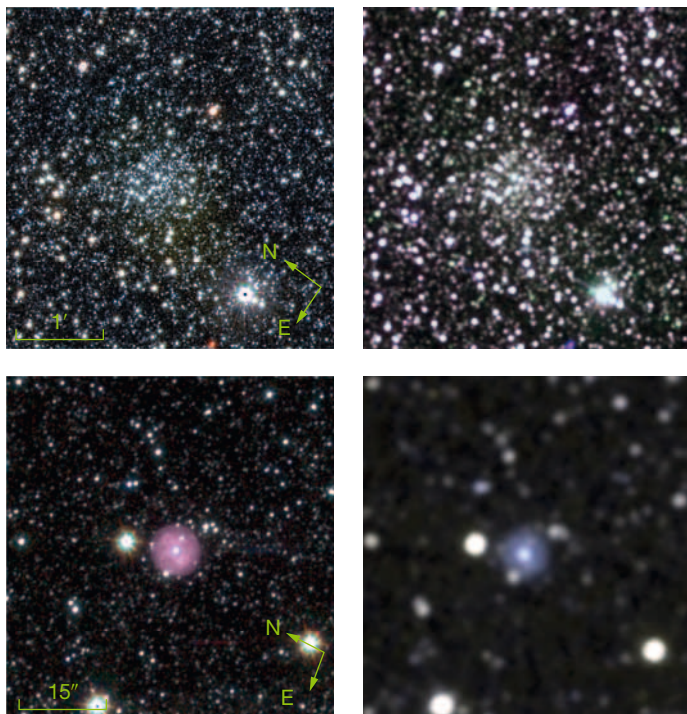


Figure 3. Upper panels: Comparison between VVV (left) and 2MASS (right) images of the globular cluster Palomar 6. Lower panels: VVV image (left) of the planetary nebula NGC 6629 compared with 2MASS (right).

in *I*-band, as expected. The photometric accuracy of the data points in the light curve is ~ 0.05 mag. Our simulations show that, at a typical magnitude of $K_s \sim 15$ – 16 mag, we should be able to detect RR Lyrae stars with amplitudes down to 0.03 – 0.05 mag, using 100 phase points over the time frame of five years of the VVV Survey.

In parallel with the main VVV Survey, we are also obtaining a large database of high quality (“template”) light curves in the *Ks*-band for different variability classes, using a variety of other telescopes. This will allow us to automatically classify an important fraction of the $\sim 10^6$ VVV *Ks*-band light curves. While automated classification is routinely accomplished in other variability surveys (e.g., Debosscher et al., 2007; 2009), the VVV Survey is the first of its type to be carried out in the NIR, where the required light-curve templates are, for the most part, not available in the literature.

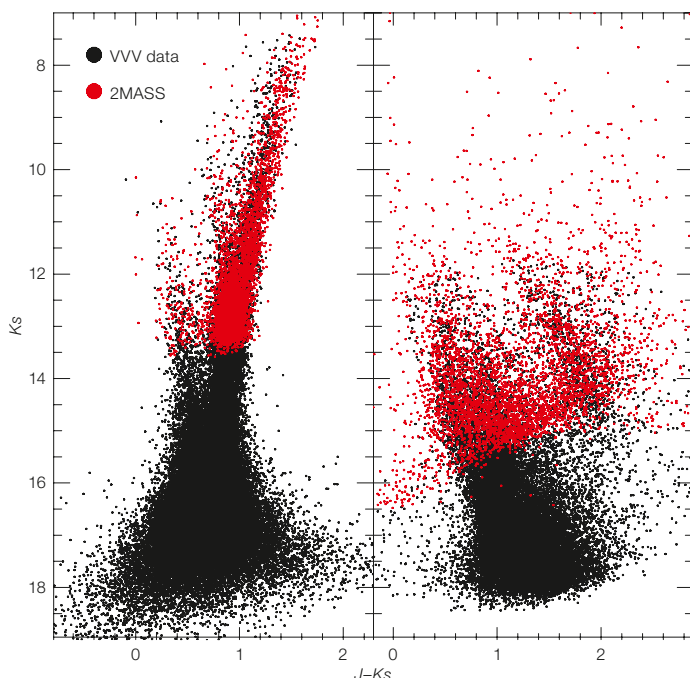


Figure 4. Colour-magnitude diagrams comparing VVV data (black) and 2MASS (red) for two extreme examples. The left-hand panel shows one of the most crowded Bulge fields (SV field), while the right-hand panel shows one of the Disc fields that are most heavily and inhomogeneously reddened (see text for further details).

First moving object

The VVV Survey will allow the detection of Solar System objects down to $K_s \sim 18$ mag. We are searching for Trans-Neptunian objects (TNOs), Jupiter Trojan asteroids (L5Js), Neptune Trojan asteroids (N5Js), Main Belt asteroids (MBAs), and near-Earth objects (NEOs). Since the VVV Bulge fields lie just on the Ecliptic, our search is limited to this region. Satellite tracks are also common and readily identified, even in the short VVV exposures.

As an example, Figure 6 shows MBA 199 Byblis, the first moving object detected by the VVV Survey while making the colour tiles. The sequence of observations (in this case taken on 23 October 2009) started with the *H*-band (green), 3 minutes later the *Ks*-band (red) was exposed, and finally 13 minutes later the *Z*-band (blue). The object was also recovered in *Ks*-band images acquired on 22 and 24 October 2009. 199 Byblis shows a magnitude of $K_s = 12.12$ mag and a motion of about 0.22 arcminutes/day. The excellent VISTA image quality (typically full width at half maximum < 1 arcsecond) and scale (0.34 arcseconds/pixel), also allows us to identify high proper motion stars with the survey baseline of 4–5 years

First VVV RR Lyrae light curve

The detection of variable stars and the monitoring of their variability is the main goal of the VVV Survey. In Figure 5 we present the first, and preliminary, light curve of an RR Lyrae star obtained from

the VVV SV data. The object, OGLE 189770, is an ab-type RR Lyrae star with a period $P = 0.72949$ days and an amplitude of 0.33 mag (Collinge et al., 2006). In *Ks*-band the minimum magnitude is $K_s \sim 14.2$ mag, with an amplitude of ~ 0.20 mag, smaller than that observed

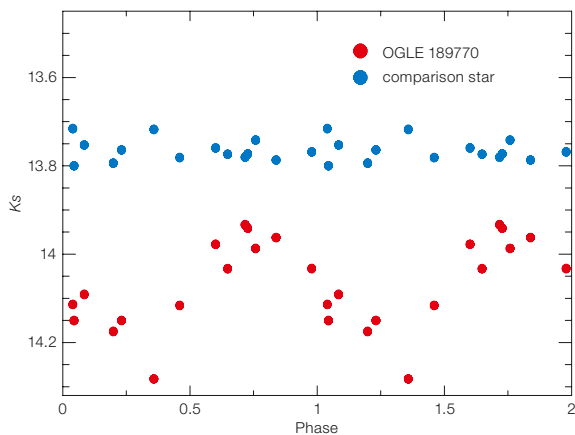


Figure 5. (above) First VVV light curve for a Bulge RR Lyrae, obtained from the SV data. This ab-type RR Lyrae was identified from the OGLE sample, and has a period $P = 0.72949$ days (Collinge et al., 2006). The data are repeated in phase for better visualisation.

for faint objects, and with a baseline of more than ten years for bright objects with 2MASS. As a complementary project, we will also search for background QSOs in some selected fields, to provide an extragalactic frame for accurate astrometry.

Searching for new clusters and streams

Another goal of the VVV is to search for new star clusters of different ages. To trace the early stages of star cluster formation, we are carrying out a survey of infrared star clusters and stellar groups. These are found towards known massive star formation regions associated with methanol maser emission and hot molecular cores. Using the list of star-forming regions provided in Longmore et al. (2009), we have already identified 25 small star cluster candidates by visual inspection. Almost all of them seem indeed very young, because most of the mass is still concentrated in the gas. A typical example of a newly identified cluster candidate is shown in Figure 7. We are also studying the old metal-poor stellar population histories of the Milky Way Disc and Bulge, with the aim to find and study disrupted stellar streams produced during past accretion events.

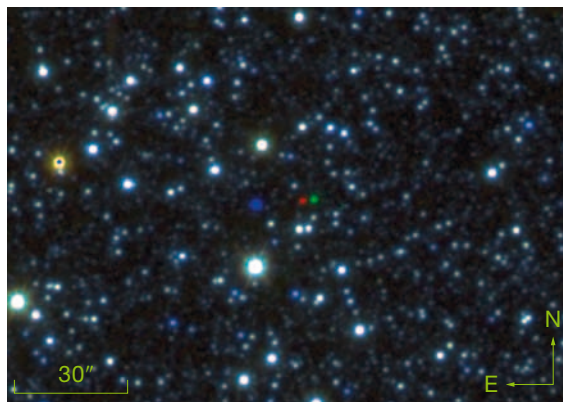


Figure 6. Main Belt asteroid 199 Byblis, the first moving object detected by the VVV Survey. It is the central object seen from left to right in filters Z (blue), K_s (red), and H (green). Bright saturated stars have $K_s < 10$ mag, and show a black dot in the centre.



Figure 7. Star cluster candidate identified in the VVV Survey. This cluster is located in a Disc field. The faintest stars in this picture have $K_s \sim 17$ mag.

Acknowledgements

The VVV Survey is supported by the European Southern Observatory, the BASAL Center for Astrophysics and Associated Technologies (PFB-06), the FONDAP Center for Astrophysics (15010003) and the MIDEPLAN Milky Way Millennium Nucleus (P07-021-F). We would like to thank the staff of CASU and WFAU, who provide the pipeline processing, data calibration and archive. Some VVV tiles were made using the Aladin sky atlas, SExtractor software and products from the TERAPIX pipeline (Bertin et al., 2002). This publication makes use of data products from the Two Micron All Sky Survey, a joint project of the University of Massachusetts and IPAC/CALTECH, funded by NASA and NSF.

References

Arnaboldi, M. et al. 2010, *The Messenger*, 139, 6
 Bertin, E. et al. 2002, *ADASS XI*, 281, 228
 Churchwell, E. et al. 2009, *PASP*, 121, 213

Collinge, M. J. et al. 2006, *ApJ*, 651, 197
 Emerson, J. & Sutherland, W. 2010, *The Messenger*, 139, 2
 Debosscher, J. et al. 2007, *A&A*, 475, 1159
 Debosscher, J. et al. 2009, *A&A*, 506, 519
 Hodgkin, S. T. et al. 2009, *MNRAS*, 394, 675
 Longmore, S. N. & Burton, M. G. 2009, *PASA*, 26, 439
 Minniti, D. et al. 2010, *New Astronomy*, 15, 433
 Skrutskie, M. F. et al. 2006, *AJ*, 131, 1163

Links

¹ Visible and Infrared Survey Telescope for Astronomy (VISTA): <http://www.vista.ac.uk>
² VISTA Variables in the *Vía Láctea* project page: <http://www.vvvsurvey.org>
³ VISTA Surveys page at the Cambridge Astronomical Survey Unit (CASU): <http://casu.ast.cam.ac.uk/surveys-projects/vista>
⁴ Wide Field Astronomy Unit (WFAU) of the University of Edinburgh: <http://horus.roe.ac.uk/vsa/>

A Wide-angle VIMOS Survey of the Sagittarius Dwarf Spheroidal Galaxy

Giuliano Giuffrida¹
 Luca Sbordone^{2,3}
 Simone Zaggia⁴
 Gianni Marconi⁵
 Piercarlo Bonifacio^{3,6}
 Carlo Izzo⁵
 Thomas Szeifert⁵
 Roberto Buonanno^{1,7}

¹ ASI Science Data Center, Frascati, Italy

² Max-Planck-Institut für Astrophysik, Garching, Germany

³ GEPI, Observatoire de Paris, Meudon, France

⁴ INAF–Osservatorio Astronomico di Padova, Italy

⁵ ESO

⁶ Istituto Nazionale di Astrofisica, Osservatorio Astronomico di Trieste, Italy

⁷ Università di Roma, Italy

Using VIMOS in imaging and spectroscopy modes and FLAMES spectroscopy data, we have mapped the Sagittarius dwarf spheroidal galaxy (Sgr dSph) photometrically and spectroscopically over eight fields along the galaxy minor and major axes. We have found, for the first time, striking evidence of multiple populations in the peripheral zones of this near companion of the Milky Way. These data, together with previous analyses of the Sgr dSph core and streams, supply a detailed picture of this galaxy, and will give us the opportunity to reconstruct the history of this object and its influence on the evolution of the Milky Way.

Sagittarius dSph

For many decades two competing scenarios for the formation of the Milky Way (MW) have been presented. In the “monolithic collapse” scenario (Eggen, Lynden-Bell & Sandage, 1962, hereafter ELS) our Galaxy formed quickly through the collapse of an isolated protogalactic cloud. Early star formation populated the Halo and the globular clusters (hereafter GCs), while dynamical friction led the bulk of the gas to form a thin disc. In the competing “hierarchical merging” scenario (Searle & Zinn, 1978, hereafter SZ), the Galaxy would have formed by the coalescence of a large number of sub-

structures over a timescale of many gigayears.

At the moment there is no universally accepted scenario for the formation of the Milky Way, although some progress was made towards a description which, not surprisingly, appears as a compromise between the ELS and SZ models. The Galactic Halo was formed by hierarchical merging of substructures, while the thin and thick Disc components formed as the result of the monolithic infall of a diffuse gaseous component that was ejected from the substructures prior to the merging event.

In 1994 Ibata et al., during a spectroscopic study of the Milky Way Bulge, discovered a new dwarf spheroidal galaxy at only 25 kpc from the Sun, the Sagittarius dSph, hereafter Sgr dSph. This object is orbiting inside the MW Halo with a period of about 1 Gyr, and probably was captured about 10 Gyr ago (Ibata et al., 1997). It was quickly theorised that the Sgr dSph should be in the process of being tidally destroyed by its interaction with the MW, its stellar content being dispersed in the Halo along a massive stellar stream. The stream was indeed observed, and constitutes the most prominent Halo substructure detected by wide field surveys such as the Two Micron All Sky Survey and the Sloan Digital Sky Survey. The Sgr dSph and its stream now constitute the most dramatic evidence (albeit not the only piece) that hierarchical merging processes have contributed heavily to the build up of the MW, and continue to do so today.

The residual, bound Sgr dSph main body is still a remarkable object. Four globular clusters (M54, Terzan 7, Terzan 8 and Arp 2) are currently associated with it and M54 is the second most massive GC known in the MW, lying at the centre of Sgr dSph main body (Bellazzini et al., 2008). At least one more GC (Pal 12) almost certainly originated in the Sgr dSph system and was consequently stripped (Sbordone et al. [2007] and references therein). Spectroscopic studies of stars in the very centre of the Sgr dSph showed that the galaxy underwent an impressive degree of chemical evolution. The central population has a mean metallicity, $[Fe/H]$ of -0.5 , unusually high for a dSph,

a sizeable metal-rich population at $[Fe/H] \approx 0$, and a metal-poor tail likely reaching down to almost $[Fe/H] = -3$. The associated GCs also span about two orders of magnitude in metallicity, between $[Fe/H] = -2.6$ in Terzan 7 and $[Fe/H] = -0.6$ in Terzan 8 (Sbordone et al., 2007; Mottini et al., 2008).

Except for the analyses in the associated GCs, the large size (roughly 15×7 degrees on the sky) and low surface density of the Sgr dSph have so far prevented any large-scale photometric and spectroscopic study outside a tiny central region. Thus the kinematics, star formation history and chemical composition remain unexplored over most of the galaxy. In the present article, and in forthcoming papers, we describe the first attempt to map the Sgr dSph stellar populations and chemical composition over most of its surface.

A wide-angle VIMOS survey

The main body of Sgr dSph is located near the Milky Way disc, and on the opposite side of our Galaxy, so discriminating between MW and Sgr dSph stars is a real challenge. Fortunately, by combining photometric and spectroscopic data it is possible to select an almost uncontaminated sample of Sgr dSph stars. Given the impressive angular size of the Sgr dSph, we decided to concentrate our efforts on its centre and on seven peripheral fields located along the minor and major axis of the galaxy (see Figure 1 for the positions of these fields).

Photometrically, the red giant branch (RGB) stars of the Sgr dSph are clearly visible as a nearly vertical sequence on a colour–magnitude diagram (CMD) of the area, and are separated from the bulk of the MW Disc and the Bulge+Halo population. But this is not enough, because a large number of Bulge and Halo stars could be present in that region of the CMD. A further selection can only be performed dynamically: Sgr dSph stars are co-moving along their orbital trajectories due to gravitational interaction with the Milky Way, and this common motion is identifiable through radial velocity measurements, distinguishable from the motions of MW stars. This

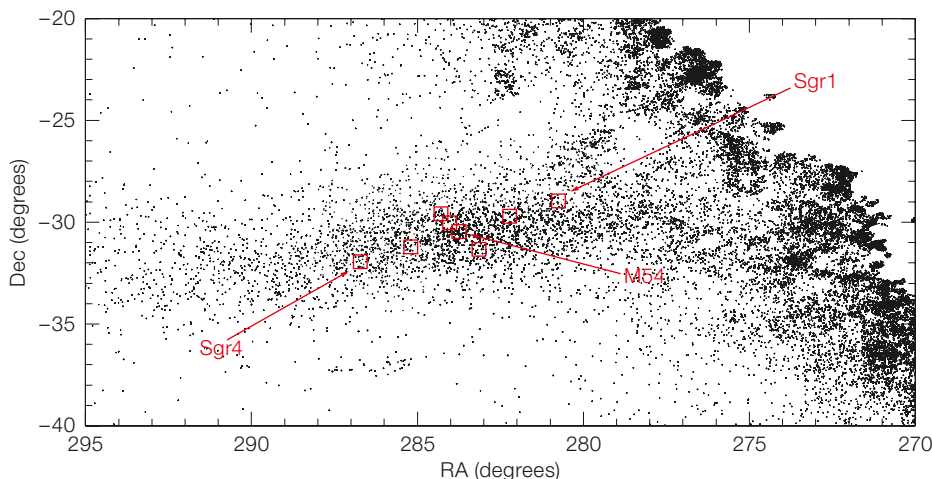


Figure 1. Map of the catalogued stars and clusters in the Sgr dSph galaxy obtained from 2MASS and UCAC catalogues selected in K and $J-K$ (see Majewski et al. [2003] for the selection criteria). The boxes show the position of the fields observed with VIMOS and FLAMES.

uncontaminated sample of stars could be successively observed with a high resolution spectrograph to characterise in detail the dynamics and chemical content of the Sgr dSph.

The programme for sampling the stellar populations across the Sgr dSph was performed in three steps. We secured the first images of the eight selected fields with VIMOS on the ESO Very Large Telescope (VLT); second, we selected targets from the RGB of Sgr dSph and other luminous stars to observe with the VIMOS Multi Object Spectroscopy (MOS) with the high resolution red grism (645–860 nm, $R = 2500$) mode, with an exposure time of 600 s for each pointing. With these data a first dynamical selection has been performed: while the bulk of contaminant MW stars have

radial velocities (V_{rad}) not exceeding 90–100 km/s, the Sgr dSph stars have a narrow V_{rad} distribution centred around 140 km/s (see Figure 2). Finally, we performed a follow-up spectroscopic analysis with FLAMES of candidate Sgr dSph members in the seven peripheral fields. We decided not to include the central M54 field in the FLAMES follow-up, since a large number of observations were already available for that field.

Imaging observations with VIMOS were obtained over five different nights. Each pointing consisted of two exposures: a 10 s exposure in the I -band, and a 15 s exposure in the V -band. Atmospheric seeing, evaluated using the full width at half maximum (FWHM) of the observed point spread function for a sample of bright, isolated stars, was in the range 0.7 to 1.3 arcseconds, perfectly suited for our purposes. The analysis of this photometric data reveals a fairly homogeneous scenario (Giuffrida et al., 2010): all the Sgr dSph fields appear to be characterised by the presence of a dominant

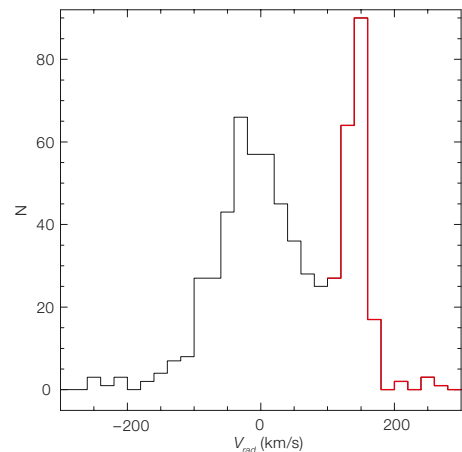


Figure 2. The radial velocity distribution of the FLAMES sample of stars observed in the direction of the Sag dSph. In red the candidate Sgr dSph members; the other stars belong to the Milky Way.

population whose progeny is the ubiquitous RGB, visible also in the border fields (Sgr1 and Sgr4). In Figure 3 we show the CMD obtained from three of our fields: Sgr4, M54 and Sgr1. It is interesting also to observe the different MW contribution to these fields: from the less contaminated (Sgr4), to the most contaminated one (Sgr1). The central field is characterised by the presence of the M54 GC superimposed on the general Sgr dSph population: along with the RGB of the Sgr dSph population, the RGB of the M54 population is clearly visible; finally the highly populated horizontal branch is visible only in this central field. The combination of imaging and multi-object spectroscopy with VIMOS and multi-object spectroscopy with FLAMES Medusa mode guarantees a sample of more than 200 confirmed Sgr dSph stars localised in the seven peripheral fields (Giuffrida et al., 2010).

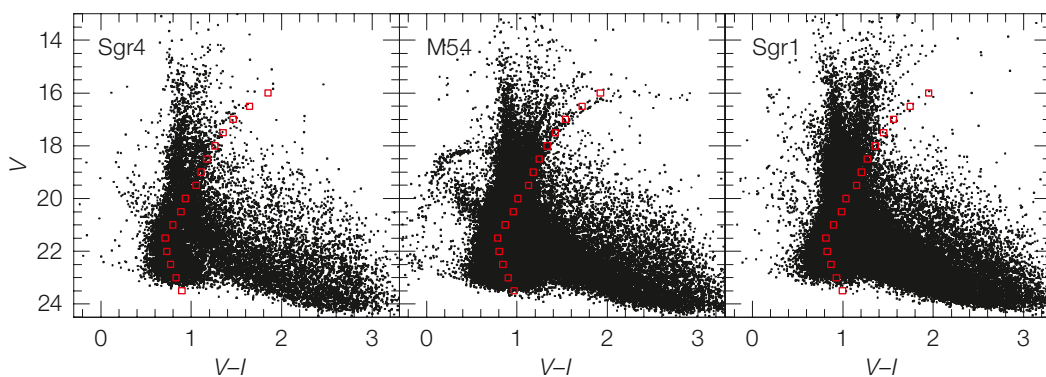


Figure 3. VIMOS colour-magnitude diagrams (CMD) for three of the observed fields are shown with, superimposed, the fiducial line of the dominant Sgr dSph population. Left: CMD for the Sgr4 field; centre: CMD of the central (M54) field; right: CMD of the Sgr1 field.

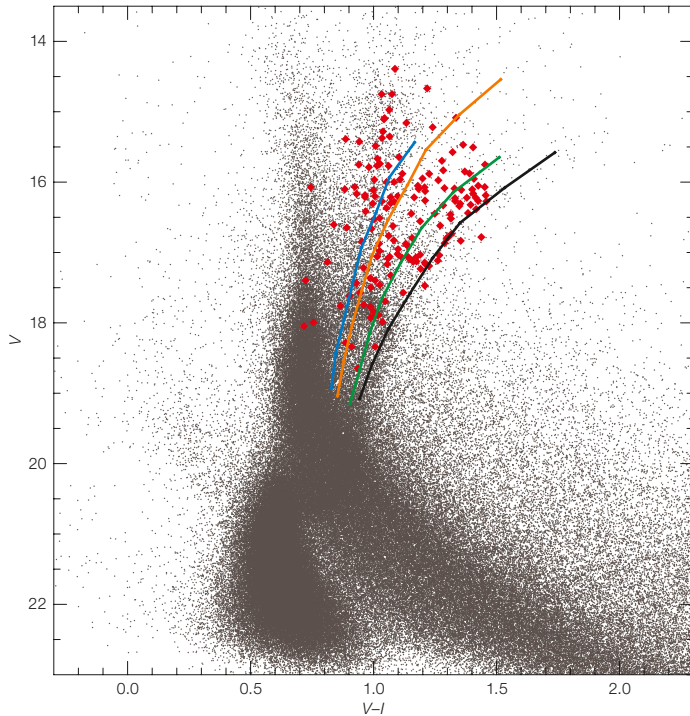


Figure 4. Colour-magnitude diagram for all the stars detected in the seven Sgr dSph peripheral fields with, over-plotted, the stars observed with FLAMES and showing radial velocities compatible with a membership of the Sgr dSph. Fiducial lines of three galactic globular clusters are superimposed. From left to right: M92, M5 and 47 Tuc characterised by $[Fe/H] = -2.52$, -1.24 and -0.67 respectively. The bold black line follows the position of the RGB of Sgr dSph main population.

In Figure 4 we superimpose the confirmed (radial velocity) Sgr dSph members observed with FLAMES over the global CMD (obtained joining all the data of the seven peripheral fields). An inspection of this figure reveals a complex scenario: while many stars are located on the main RGB of Sgr dSph, a large number of them are located on different sequences. To better characterise these populations, we superimposed fiducial lines of three well-known Galactic GCs,

namely M92, M5 and 47 Tuc. These GCs are representative of a metal-poor population (M92, $[Fe/H] = -2.52$), intermediate metallicity population (M5, $[Fe/H] = -1.24$) and a metal-rich population (47 Tuc, $[Fe/H] = -0.67$). This large metallicity span is in agreement with the data collected on the Sgr dSph core, with two remarkable exceptions, namely the presence of a well-populated intermediate population ($[Fe/H] \approx -1$) and large numbers of bright stars lying at

the blue edge of the RGB ($17 < V < 14$ mag and $0.9 < V-I < 1.1$ mag) that cannot be reproduced with a “M92-like” population. The hypothesis that these “blue-edge” stars are high velocity halo interlopers cannot be rejected, but they can also correspond to a very metal-poor Sgr dSph population: the results from the high resolution abundance analysis will allow us to clarify this question.

We are completing the analysis of the FLAMES spectra, and dynamical and chemical measurements are currently underway; there are still many open questions regarding this galaxy, such as a possible rotation of the main body around one of the axes, or the presence of an ultra metal-poor population ($[Fe/H] < -2.5$). Unveiling the history of this fascinating companion to the Milky Way will be extremely useful for our understanding of both the local and the distant Universe.

References

- Bellazzini, M. et al. 2008, ApJ, 136, 1147
- Eggen, O. J., Lynden-Bell, D. & Sandage, A. R. 1962, ApJ, 13, 748
- Giuffrida, G. et al. 2010, A&A, 513, 62
- Ibata, R. A. et al. 2001, ApJ, 551, 294
- Ibata, R. A. et al. 1997, AJ, 113, 634
- Ibata, R. A. et al. 1995, MNRAS, 277, 781
- Ibata, R. A. et al. 1994, Nature, 370, 194
- Majewski, S. R. et al. 2003, ApJ, 599, 1082
- Mottini, M. et al. 2008, AJ, 136, 614
- Searle, L. & Zinn, R. 1978, ApJ, 225, 357
- Sbordone, L. et al. 2007, A&A, 465, 815



The interacting galaxy NGC 4027 (Arp 22) is shown in this colour composite image formed from exposures in three broadband filters (B , V and R) and two narrowband filters ($H\alpha$ and $[O\text{III}] 5007\text{\AA}$) taken with EFOSC on the NTT. This barred spiral galaxy is a member of the NGC 4038 Group and shows evidence of interaction from its distorted northern spiral arm.

Studying the Properties of Early Galaxies with the ESO Remote Galaxy Survey

Malcolm Bremer¹
 Matthew Lehnert²
 Laura Douglas^{1,2}
 Elizabeth Stanway¹
 Luke Davies¹
 Douglas Clowe³
 Bo Milvang-Jensen⁴
 Mark Birkinshaw¹

¹ H. H. Wills Physics Laboratory,
 University of Bristol, UK

² GEPI, Observatoire de Paris Meudon,
 France

³ Ohio University, USA

⁴ Dark Cosmology Centre, University of
 Copenhagen, Denmark

We present a discussion of and results from the ESO Remote Galaxy Survey (ERGS), a spectroscopic survey of Lyman-break galaxies with $z \sim 5$ and above. The survey directly explores the properties of these early star-forming galaxies, increasing the observational detail in our picture of early galaxy evolution. The survey provides a sample of galaxies ideally matched in spatial distribution to the capabilities of current and imminently available instrumentation. We discuss the results of the first follow-on studies of the sample in the mm/sub-mm that signpost the potential of these facilities for exploring early galaxy evolution.

Over the last decade, the observational frontier of galaxy evolution research has been pushed back from two billion years after the Big Bang (at redshifts $z \sim 3$) to one billion years or less (at $z \sim 5$ and higher). While the difference in the cosmological time between these redshifts may seem insignificant, it is thought that during this early epoch the most massive galaxies in the local Universe underwent their first significant star formation episode. If this is so, what physical mechanisms drove this early collapse of galaxies and their first major episodes of star formation?

Much of our progress in developing understanding of the nature of galaxies in the early Universe has been made possible by extending the Lyman-break technique pioneered by Steidel and collaborators at $z \sim 3$ to higher redshifts. This photometric tech-

nique is, in principle, very efficient at identifying galaxies in the early Universe, but one must always be cautious of potential contamination by interloping lower redshift galaxies or stars that have similar red colours, and of the broad distribution in redshift inherent in such selection techniques. Both of these problems potentially undermine conclusions based on purely photometric samples — spectroscopic confirmation is crucial to remove contaminants, to investigate the clustering properties of galaxies and to understand the nature of their line emission. Perhaps most importantly, spectroscopic confirmation of regions with a large number of sources at similar redshifts enables detailed and efficient follow-up using facilities with comparatively small fields of view or limited spectral coverage. It is through the study of spectroscopically-confirmed samples well-matched to the capabilities of upcoming facilities that we will make progress in understanding the nature of the earliest galaxies.

In order to assemble a reliable sample of $z \sim 5$ Lyman-break galaxies (LBGs) that can be explored in detail at multiple wavelengths, we have carried out the ESO Remote Galaxy Survey (Douglas et al., 2007; 2009; 2010), building on our earlier work (e.g., Lehnert & Bremer, 2003; Stanway et al., 2004). In addition to determining the properties of both individual galaxies and the sample as a whole, we wanted to explore whether and how the galaxies cluster in three dimensions, as might be expected if they are the progenitors of massive galaxies at lower redshifts. Our previous analysis of $z \sim 5$ LBGs (Verma et al., 2007) showed that their stellar mass surface densities were extremely high, comparable to those found at the centres of massive galaxies today, lending support for this possibility.

The need to trace any clustering constrains observations to a high surface density of spectroscopically-confirmed sources, using multiple spectroscopic masks on a single field if necessary. This approach also has a clear benefit for follow-up studies with current and future instruments that have a limited field of view, where maximising the number of targets per pointing improves the scientific return of each observation. We also wanted to draw sources from multiple equatorial fields. Not only does this allow exploration of and

mitigation of cosmic variance, but also has the practical effect of helping to avoid the RA-congestion inherent in concentrating any follow-up observations of only a few comparatively large public fields.

The ESO Remote Galaxy Survey large programme

Our large programme targeted ten fields previously imaged with FORS2 by the ESO Distant Cluster Survey (EDisCS) survey (White et al., 2005; Poggianti et al. 2009) in the V -, R - and I -bands and supplemented this with further imaging in the z -band. Although we have obtained imaging in longer wavebands for these fields, only the optical imaging data was used to select potential LBGs with $z \sim 5$ and above. Simple colour cuts (most importantly $R-I > 1.3$ mag) along with an I -band magnitude cut of $I_{AB} = 26.3$ were used to identify prime candidate LBGs, but where the available space on spectroscopic masks allowed, even these criteria were relaxed. The colour cut and I -band magnitude limit were chosen to select galaxies with $z > 4.8$ and to probe to luminosities the equivalent of one magnitude below L^* for $z \sim 3$ LBGs, thus allowing us to measure possible evolution in the UV luminosity function.

Our observing strategy enabled the widest range of candidate LBGs to be targeted by spectroscopic follow-up, minimising the number of true $z \sim 5$ galaxies rejected from our sample before spectroscopy. The number of spectroscopic masks used on any one field was guided by the number of photometric candidates in that field, varying from one mask for the poorest to five masks for the richest field. Objects were prioritised for spectroscopy using the multi-wavelength data in each field, but given the number of masks, completeness was generally very good. This approach, coupled with the liberal selection technique generally maximised the surface density of spectroscopically-confirmed LBGs in the fields. In addition, given the relatively high completeness of this approach, we are able to use the spectroscopically-confirmed sample to infer the global statistical properties of the set of objects that either were untargeted spectroscopically or failed to yield a reliable redshift, despite being subjected to spectroscopy.

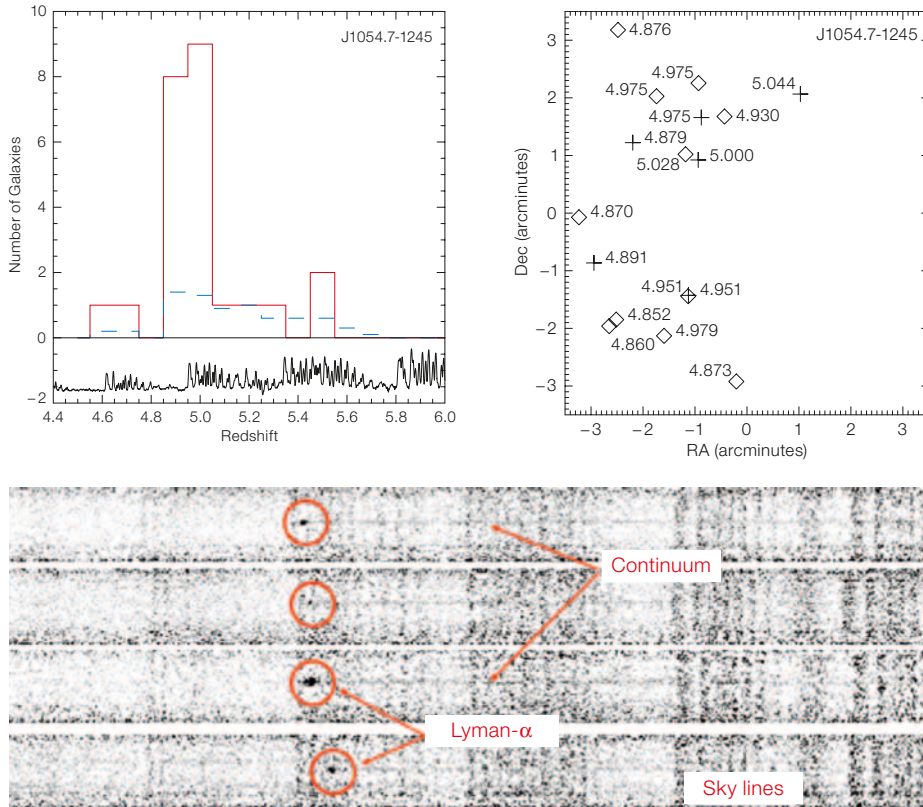


Figure 1. The redshift distribution of spectroscopically confirmed LBGs in one ERGS field, J1054-1245, is shown at upper left (in red) in comparison to the distribution of redshifts in the survey as a whole, normalised to the same area (in blue). The redshift “spike” at $z \sim 5$ is obvious. The night-sky strength as a function of redshift for Ly α is shown below the redshift distribution. The spatial distribution of the LBGs in this redshift spike across the FORS2 imaging field is shown at upper right. Four examples of two-dimensional spectra of LBGs in the spike are shown (lower plot). In each case wavelength increases to the right and position along the slit varies vertically. Objects show clear Ly α emission and continuum redward of the line.

unconfirmed subsample is sufficiently well understood that we can explore the distribution of Ly α equivalent widths in $z \sim 5$ LBGs. This distribution is an indicator of the underlying initial mass function (IMF) within the ongoing starburst that powers the UV emission from the LBGs. There has been recent discussion in the literature as to whether higher redshift systems have top-heavy IMFs (with a high ratio of massive to low-mass stars) as they may have restframe UV colours too blue for a standard IMF. Higher Ly α equivalent widths favour top-heavy IMFs. The distribution of equivalent widths for the spectroscopically-confirmed $z \sim 5$ sources is biased to higher values than the similar distribution for $z \sim 3$ LBGs. However, because of our careful assessment of the completeness and reliability of our sample, we can correct for the contribution of spectroscopically-unconfirmed $z \sim 5$ sources, which by definition have low or negative Ly α equivalent widths. When this is done, the $z \sim 5$ distribution is consistent with that seen at $z \sim 3$; there is no evidence for an evolution in the IMF between these redshifts.

We carried out FORS2 spectroscopy using twenty masks across the ten fields (totalling an effective area of about 450 square arcminutes), resulting in a sample of some 70 spectroscopically-confirmed LBGs at $z \sim 5$ and above. Approximately half of the spectra show Ly α emission plus a continuum break, the rest only a break in the continuum as the intervening intergalactic medium (IGM) scatters the continuum shortwards of restframe Ly α out of our line of sight. The objects are not distributed uniformly across the fields. Two fields in particular show clear three-dimensional clustering of LBGs; not only do the sources cluster spatially, their redshift distributions show clear “spikes” at particular redshifts, unlike the typical field (see Figure 1). The LBGs within these fields trace out coherent large-scale structures, not necessarily proto-clusters, but more likely rich sheets or filaments of matter seen when the Universe was approximately one billion years old. The density of LBGs within these structures makes them particularly suitable targets for follow-up studies with comparatively small-field future instrumentation such as ALMA and KMOS.

While this kind of structure in the LBG distribution might be expected if it were to eventually form massive galaxies, the structures are physically very extended and the LBGs must inhabit separate dark matter halos. This large scale, when taken together with the comparatively short-lived nature of typical $z \sim 5$ LBG starbursts (a few tens of Myr, Verma et al., 2007), make it unlikely that all the LBGs in the structure will eventually combine to form a single massive galaxy (or several such galaxies). For these to form, most of the baryons within them cannot be within the UV luminous LBGs at $z \sim 5$. The LBGs may trace regions where these reside, either in separate systems within the same large-scale structure, or in larger underlying galaxies within which the UV-luminous LBGs are embedded. The LBGs may well be the UV-luminous “tip of the iceberg” of a much larger over-dense structure, whether a sheet, filament or perhaps proto-cluster. This issue motivates our mm/sub-mm follow-up of these fields, discussed below.

Our spectroscopy is complete enough, and the likely contamination fraction of non $z \sim 5$ sources in the spectroscopically

The spectroscopy also reveals a difference between the restframe UV-optical spectral energy distributions of the line-emitting and the break-only populations. The break-only galaxies appear to have both redder observed $I-K$ colours and redder 1200–1700 Å restframe continuum slopes than the line-emitters, a difference that is difficult to explain purely by differences in the ages of their stellar populations. Allowing the metallicity or dust extinction to vary between these two subsamples may explain the difference, with the break-only subsample being more extinguished and/or having a slightly higher metallicity. Taken as a whole, if the correlation between metallicity and UV continuum slope identified at low redshift is applicable at

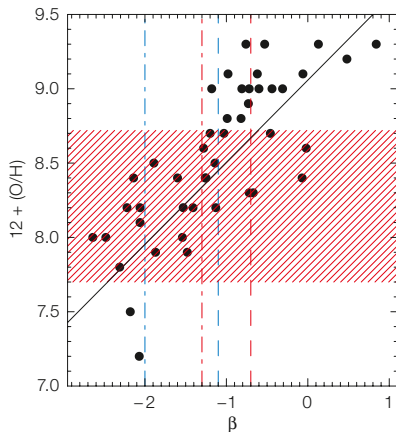


Figure 2. A plot of metallicity against UV spectral slope, β . Points show the correlation between the quantities for local galaxies (from Heckman et al., 1998). The dot-dashed vertical lines indicate the spectral slope of the galaxies with only spectral breaks (no line emission) in our sample (red) and for the whole sample with spectroscopic redshifts (blue), and the dashed vertical lines indicate the spectral slope of the galaxies with Ly α mostly in absorption (red) and galaxies with Ly α predominately in emission (blue) for LBGs at $z \sim 3$ (Shapley et al., 2003). Our objects appear to have steeper UV spectra than $z \sim 3$ LBGs, indicating lower typical metallicities, on average $0.3 Z_{\odot}$, but with some scatter. The red hatched area indicates the range of metallicity estimates in prior literature.

$z > 3$, the typical $z \sim 5$ LBGs have metallicities a factor of ~ 3 lower than those of LBGs at $z \sim 3$ (see Figure 2), a result consistent with that found in a photometric study of the GOODS–South LBGs by Verma et al. (2007).

Most of the EDisCS fields have been imaged in the restframe UV by the Hubble Space Telescope (HST). Many of the LBGs, both the candidates from the photometric sample and the spectroscopically confirmed objects, are imaged at kiloparsec-scale resolution. A majority of the spectroscopically confirmed objects covered by this imaging are resolved on this scale into two or more UV luminous components, while being unresolved in the ground-based imaging (typically corresponding to a scale of order ~ 10 kpc, see Figure 3). There has been some debate in the literature as to the nature of LBGs, particularly those with multiple UV components. Could these systems be UV-luminous super-star clusters embedded in individual, mostly obscured, more massive systems, or could they be indicative of merger events, potentially with each component being a complete system undergo-

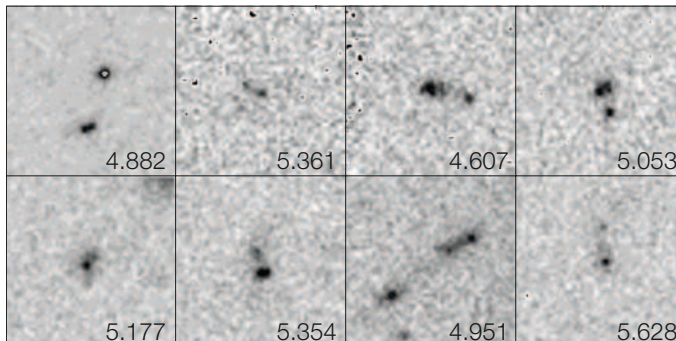


Figure 3. Eight examples of spectroscopically confirmed galaxies with multiple components. Each box is 5 arcseconds \times 5 arcseconds and the images were taken using the HST/ACS camera and the F814W filter. Redshifts are indicated in the bottom right-hand corners.

ing the merger? The nature of the larger-scale clustering seen in some of the fields might support the “embedded” hypothesis in order to account for sufficient baryons to form massive galaxies at lower redshifts. However, work on nearby analogues of LBGs (Overzier et al., 2008) indicates that, for these low redshift systems at least, the merger hypothesis is most likely. It is impossible to determine whether either of these scenarios account for the structure seen in the $z \sim 5$ systems from the optical imaging and spectroscopy data alone. However, this is exactly the type of issue that ERGS was designed to tackle through follow-up observations in other wavebands.

ERGS in other wavebands

Our first steps in following up ERGS have been carried out in the mm and sub-mm, in order to answer several questions raised by our optical and near-infrared results from the VLT. The mm and sub-mm allows us to trace cold molecular gas and dust. Since this is the material out of which stars form, ascertaining the amount of cold gas will allow us to, for example, determine the potential for these galaxies to keep forming stars. This also had the additional benefit of enabling us to prepare for future observations with ALMA.

We chose to follow up the two most clustered fields. Not only does this allow us to observe and characterise a comparatively large number of LBGs in relatively few deep pointings, but it has also allowed us to search for other non UV-luminous sources embedded in the same large-scale structures as the LBGs, as might be expected if these they are truly the progenitors of massive galaxies. Our initial

exploration in these wavebands have used LABOCA on APEX to image one field in continuum at $870 \mu\text{m}$ (about $150 \mu\text{m}$ in the restframe) and the Australia Telescope Compact Array (ATCA) to image two fields at 7 mm and 12 mm to search for redshifted CO(2–1) and CO(1–0) line emission respectively. The latter observations can be thought of as less sensitive and lower frequency pathfinders to future ALMA studies, with ALMA being able to target the same fields at higher frequencies, probing higher transitions of CO and potentially the key [C II] line which is the dominant coolant of the interstellar medium, amongst other lines.

The sub-mm observations with LABOCA (Stanway et al., 2010) targeted a field containing twelve spectroscopically-confirmed $z \sim 5$ LBGs. Ten lay in a region where the data had a 2σ limit of 3 mJy. To this level, no individual LBG was detected. Stacking the pixels corresponding to these $z \sim 5$ galaxies, a limit of < 0.85 mJy was placed on the $870 \mu\text{m}$ emission of the “average” $z \sim 5$ LBG. With an assumed dust temperature of 30 K, this places a limit on the typical dust mass of below $1.2 \times 10^8 M_{\odot}$, no more than $\sim 10\%$ of the stellar mass of the typical system. Higher temperatures lead to even lower masses. Future ALMA observations, will be orders of magnitude more sensitive, and thus individual galaxies are likely detectable in relatively short exposures.

The ATCA observations (Stanway et al., 2008; Davies et al., 2010) similarly targeted multiple LBGs in two clustered ERGS fields. No individual galaxy was detected in either CO(2–1) or CO(1–0). After stacking the spectra of eight LBGs in one field, we found a limit to the molecular gas content of the average $z \sim 5$ LBG of $< 3.1 \times 10^9 M_{\odot}$.

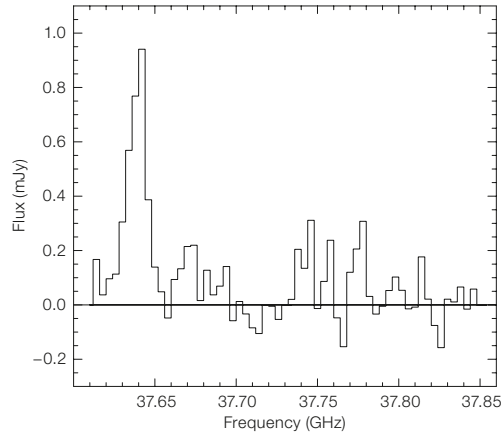
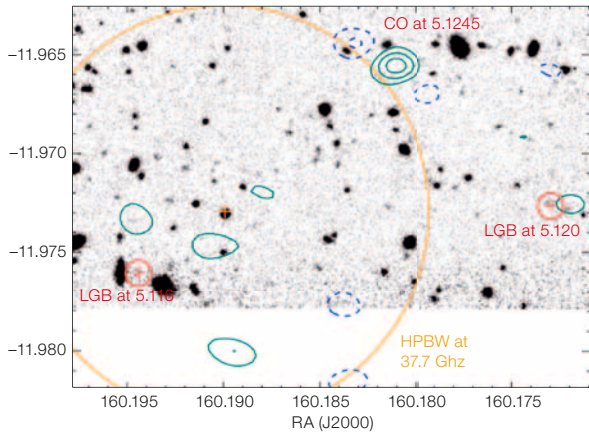


Figure 4. *I*-band image of part of one of our fields is shown (left) containing two LBGs at $z = 5.12$, indicated by the red circles with crosses inside, overlaid with (green) contours of radio emission at frequencies corresponding to the CO(2–1) line at the same redshift as the LBGs. An object with no obvious optical counterpart is detected at these frequencies close to the top of the image. The field centre and half-power beam width of the ATCA radio observations are indicated by the yellow cross and circle respectively. The 37.7 GHz-band ATCA spectrum of the source detected in the radio data, indicating a clear line at a frequency consistent with CO(2–1) at $z = 5.1245$, is shown at right.

This limit is comparable to the stellar mass of a typical source. Given the low conversion rate of molecular gas into stars, these systems are running out of fuel for their ongoing starburst; they are being observed a substantial way through and probably close to the end of the event. This agrees with previous determinations of the typical ages of the stellar populations of these sources and our own LABOCA results.

Taken together, these observations indicate that $z \sim 5$ LBGs are unlikely to be UV-luminous super-star clusters embedded in larger, more heavily obscured underlying systems, as these should have been detected in the mm/sub-mm observations. Consequently, they give strong support to the idea that the $z \sim 5$ LBGs are “switched on” by mergers and the resulting starburst uses up (or expels through driving strong winds) the available fuel, typically in a few tens of millions of years. The bias to observing the galaxies towards the end of the starburst phase would be a natural consequence of the merger trigger. Provided that the starburst lasts a length of time comparable to, or shorter than, the lifetimes of massive stars, we would only ever expect to predominantly select sources at the end of their starburst in a restframe UV-luminosity selected sample.

The data also indicate that the over-dense structures traced by these LBGs do not contain a large population of mm/sub-mm luminous starbursts. In the LABOCA field, there is a single convincing detection of a source away from the area covered by our optical imaging, consistent with the number of detections found in observations

of other fields to the same depth. No excess of sub-mm sources associated with the structure traced by LBGs are detected within the current dataset. While deeper observations with ALMA and other facilities will likely detect less luminous systems within such structures, the current observations do not indicate a significant association of the most luminous sub-mm galaxies with over-densities of LBGs at $z \sim 5$. In the single case where we have detected (Stanway et al., 2008, see Figure 4) and subsequently reconfirmed (Stanway et al., 2010, in preparation) CO emission from a galaxy embedded in the same structure as multiple LBGs, the ratio of CO to continuum luminosity indicates that the starburst within that galaxy is closer in nature to luminous starbursts seen in low redshift spiral galaxies, rather than to the ultra- or hyper-luminous sources selected in the sub-mm at intermediate and high redshifts.

Prospects

The ESO Remote Galaxy Survey has given us important clues about the nature of galaxies seen 1 Gyr after the Big Bang. ERGS has shown that $z \sim 5$ LBGs are young, relatively metal-poor, compact intense starbursts, apparently in the throes of merging, and which trace out large coherent structures. The key to obtaining this knowledge was the spectroscopic observations with FORS2 that allowed us to estimate contamination rates, determine if the galaxies had a top-heavy IMF, investigate their clustering properties and enabled us to make important follow-up observations with other facilities.

These initial follow-up studies of ERGS give an indication of the work on the most distant galaxies that will be made possible with future facilities. Rather than studying potentially atypical luminous sources, facilities such as ALMA and the E-ELT will allow us to study the more numerous and typical populations in all of their gaseous phases, from cold molecular to warm/hot ionised gas, and provide spectral energy distributions from the restframe UV out to the sub-mm. Such targeted observations will characterise the $z \sim 5$ LBGs (and by extension higher redshift systems) in the greatest detail along with other, as yet undetected, galaxies sharing the same structures. Fields containing a high density of spectroscopically-confirmed high redshift sources, such as those in ERGS, are the ideal targets for a detailed investigation of the early evolution of galaxies with the VLT and future facilities such as ALMA and the E-ELT.

References

- Davies, L. J. M. et al. 2010, MNRAS, in press, arXiv:1007.3989
- Douglas, L. S. et al. 2007, MNRAS, 376, 1393
- Douglas, L. S. et al. 2009, MNRAS, 400, 561
- Douglas, L. S. et al. 2010, MNRAS, in press, arXiv:1007.2847
- Lehnert, M. D. & Bremer, M. N. 2003, ApJ, 593, 630
- Poggianti, B. et al. 2009, The Messenger, 136, 54
- Stanway, E. R. et al. 2004, ApJ, 607, 704
- Stanway, E. R. et al. 2008, ApJ, 687, L1
- Stanway, E. R. et al. 2010, MNRAS, in press, arXiv:1007.0440
- Verma, A. et al. 2007, MNRAS, 377, 1024
- White, S. D. M. et al. 2005, A&A, 444, 365



Upper: Alan Moorwood (shown left) and Sandro D'Odorico (right) recently retired and became the first ESO astronomers emeriti. See Primas et al. p. 50 for more details.

Lower: The Chilean President Sebastián Piñera (centre left) and the Foreign Affairs Minister, Alfredo Moreno (right), recently received the ESO Director General, Tim de Zeeuw (left) and ESO Representative in Chile, Massimo Tarengi (centre right), to discuss the siting of the E-ELT on Cerro Armazones. See ann1038 for more details.



Central Massive Objects: The Stellar Nuclei – Black Hole Connection

held at ESO Garching, Germany, 22–25 June 2010

Nadine Neumayer¹
Eric Emsellem¹

¹ ESO

An overview of the ESO workshop on black holes and nuclear star clusters is presented. The meeting reviewed the status of our observational and theoretical understanding of central massive objects, as well as the search for intermediate mass black holes in globular clusters. There will be no published proceedings, but presentations are available at <http://www.eso.org/sci/meetings/cmo2010/program.html>.

This workshop brought together a broad international audience in the combined fields of galaxy nuclei, nuclear star clusters and supermassive black holes, to confront state-of-the-art observations with cutting-edge models. Around a hundred participants from Europe, North and South America, as well as East Asia and Australia gathered for a three-day meeting held at ESO Headquarters in Garching, Germany (see Figure 1). The sessions were of very high quality, with many very lively, interesting and fruitful discussions. All talks can be found online on the web page of the workshop¹.

The key scientific questions for this workshop were:

- What is the evolutionary/causal connection between nuclear clusters and black holes?
- What can the Galactic Centre tell us about the “nuclear cluster–black hole” connection?
- Where do we stand observationally for black holes, nuclear clusters and intermediate mass black holes?
- What do theoretical models tell us about star formation in the extreme gravitational potential near the black hole and under the extreme stellar densities in galactic centres?
- Do we understand the feeding of the central parsec? How are nuclear clusters replenished with fresh gas?
- What do theoretical models tell us about dynamics, evolution and migration of nuclear star clusters in galaxy centres?



Figure 1. Workshop participants assembled outside ESO Headquarters in Garching.

- Are intermediate mass black holes formed in nuclear clusters/globular clusters?
- How do the central massive objects relate to their host galaxies?

In the course of the workshop we walked through these science questions, starting from the best studied example of a supermassive black hole and its surrounding nuclear star cluster, at the heart of our own Galaxy. We indicate the authors of the contributions, which are highlighted in this summary, so that they can be traced in the presentations online¹.

The Galactic Centre black hole and nuclear star cluster

The known orbits of 30 stars around the central radio source in our Galaxy make Sgr A* the best case for a supermassive black hole, with a mass of $4.3 \times 10^6 M_{\odot}$ (Stefan Gillessen). Figure 2 shows a fit to the orbit of one of these stars (S2). The supermassive black hole resides in a very massive star cluster of about $3 \times 10^7 M_{\odot}$,

made up of several populations of stars. The existence of very young O and WR stars in the central few arcseconds around the black hole is puzzling. The currently favoured solution to this paradox of youth is *in situ* star formation in infalling gas clouds. This view is also supported by the fact that the Milky Way nuclear star cluster is rotating (Rainer Schödel). Resonant relaxation can explain the warp and the co-/counter-rotating dichotomy of the young stars (Bence Kocsis). However, the existence of S stars very close to the black hole is even more surprising. These are ordinary B stars with an age of about 10^8 years. Their observed properties can be best explained by a binary disruption scenario, called the Hills mechanism (Alessia Gualandris).

Where is the expected stellar cusp at the Galactic Centre? The formation timescale might be longer than 10^{10} years, i.e. the nuclear cluster is not old enough to have formed a cusp (Holger Baumgardt). The deficit of old stars around Sgr A* could be explained by the collision and destruction of giants with main sequence stars or stellar mass black holes (Melvyn Davies). Another possibility might be that a fraction of the stars get disrupted and accreted onto the central black hole.

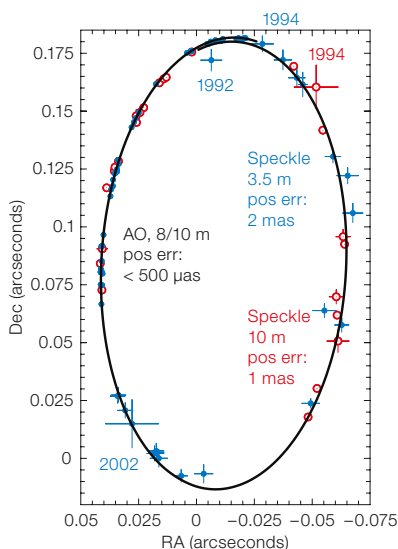


Figure 2. Result of the combined orbit fit for the Galactic Centre star S2. Blue: NTT/VLT measurements. Red: Keck measurements. The black line shows the Keplerian fit (after Gillessen et al., 2009).

Black holes and their scaling relations

Currently, dynamical black hole mass determinations exist for about 50 galaxies. These correlate tightly with the overall properties of their host galaxy’s bulge, e.g., its velocity dispersion σ . However, the low-mass end of the black hole–host galaxy scaling relations is still not well-sampled. Jens Thomas reported on the ongoing SINFONI programme to fill in the underpopulated regions in the M – σ relation using stellar kinematic modelling. Karl Gebhardt pointed out that getting any black hole mass to better than 20% accuracy is difficult and that taking systematic effects into account is very important. What counts when setting up the scaling relations is the robustness of the assumed uncertainties.

Jenny Greene presented accurate black hole mass determinations in galaxies with megamasers, along with measurements of their stellar velocity dispersion. These galaxies lie below the M – σ relation, showing a large scatter (see Figure 3). Moreover, active galactic nuclei (AGN) diagnostics help to measure black hole masses at the low-mass end. The future for black hole detections looks bright! Upcoming transient surveys may be able to detect many tidal disruption events of stars around low mass black holes (Linda Strubbe).

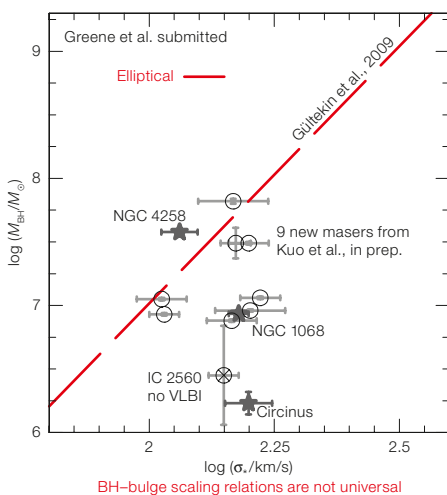


Figure 3. The relation between black hole mass and bulge velocity dispersion is shown for the maser galaxies presented by Greene et al. (2010). The maser galaxies trace a population of low-mass systems whose black holes lie below the M – σ relation defined by elliptical galaxies (red line).

Nuclear star clusters and their relation to black holes

Nuclear star clusters are very common. They are found in spirals, S0s and dwarf elliptical galaxies with an occupation fraction of about 50–75%. Nuclear clusters are compact and massive, with half-light radii of typically ~ 3 –5 parsec, and masses of 10^6 – $10^7 M_{\odot}$, and they show complex star formation histories (Jakob Walcher). Generally, nuclear clusters are seen in late-type galaxies and black holes in early-type galaxies, but often these two components coincide (Alister Graham). For the nearest nuclear star clusters, the stellar and gas kinematics are spatially well-resolved, and enable the dynamical detection of black holes inside the star clusters (Anil Seth, Nadine Neumayer). Some nuclear star clusters also show signatures of an AGN, making the co-existence of a black hole indisputable (Aaron Barth, Joseph Shields).

Nuclear star clusters observed in nearby (early-type) galaxies (in the Virgo and Fornax clusters) seem to have properties that vary continuously along the luminosity sequence (Laura Ferrarese). Although they represent a tiny fraction of the total light in a galaxy they can be rather prominent above the extrapolation of the outer light profile towards the centre in low-

luminosity objects. Nuclear clusters are similar but more compact stellar systems than ultra-compact dwarf galaxies, the latter having comparatively elevated mass-to-light ratios (Michael Hilker). Using spectrographs assisted by adaptive optics, the stellar populations and kinematics of both types of systems can be probed today (Mariya Lyubenova) to test, for example, whether or not they host massive black holes.

Feeding, star formation and feedback

The question of how galaxy nuclei are replenished with fresh gas was discussed on the third day of the conference. There are different mechanisms at work that make gas lose angular momentum and drive it from large to small scales (mergers, bars, unstable gravitational discs, three-armed spirals, turbulent viscosity and magnetic stress), all inferred from observations and simulations (e.g., Francisco Müller-Sánchez, Nozomu Kawakatu). However it is still unclear which mechanism dominates under which circumstances (Witold Maciejewski, Tessel van der Laan, Gaëlle Dumas, Rainer Beck).

Observations show a lag between the central starburst and AGN phase, due to a transition of fast supernova to slower mass-loss winds (Richard Davies). The mass loss from surrounding stars seems to be sufficient to grow a nuclear disc and to cause accretion (Marc Schartmann). We were reminded however that we still do not understand how black holes can be fed (Norman Murray, Rainer Beck), and how AGN feedback works, although a number of scenarios have been studied with detailed numerical simulations (Vincenzo Antonuccio-Delogu, Chris Power). Feedback from star formation could also be an important (and competitive!) contributor in regulating the feeding itself: in the Milky Way it seems to mostly be acting via radiative pressure, but it remains to be seen if this is true also in denser environments near the centre.

Are intermediate mass black holes formed in nuclear/globular clusters?

Theoretically, in young star clusters after core collapse, runaway collisions of stars

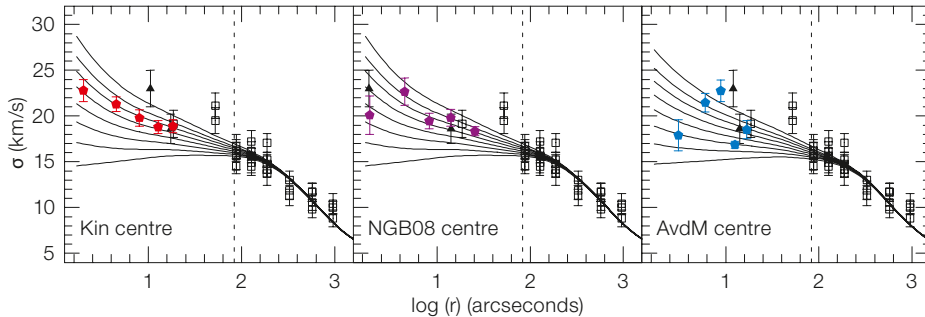


Figure 4. New velocity dispersion (σ) measurements of Omega Centauri shown as a function of radius. The left panel shows the measured σ assuming the kinematic centre, while the middle and right panels show the same for the centre derived by Noyola et al. (2008) and Andersen & van der Marel (2010). The solid lines show isotropic spherical models assuming various black holes masses (0, 1, 2, 3, 4, 5, 6 and $7.5 \times 10^4 M_{\odot}$). See Noyola et al. (2010) for details.

can result in the build up of massive objects of about $2000 M_{\odot}$. However, when including stellar evolution, stellar mass-loss winds limit the growth to a few hundred solar masses (Simon Portegies-Zwart).

Observationally there are a number of signatures for intermediate mass black holes (IMBHs) in globular clusters. Clearly, the most compelling evidence is the detection of non-thermal emission, seen, for example, for G1 in M31, but globular clusters have very little or even no gas and so the emission is very faint or absent.

The evidence from the density structure is still controversial, as the core radius and shallow density slope are not unique signatures for a black hole. These characteristics are influenced by binary heating and are also present around the time of core collapse. However, an IMBH in a globular cluster will suppress mass segregation by scattering the most massive stars, making the quenching of mass segregation a promising tracer to detect IMBHs (Stefan Umbreit, Michele Trenti).

Finally, there are several candidate clusters with suggestive dynamical evidence for an IMBH, e.g., M10 (Giacomo Beccari), M54 (Michele Bellazzini), NGC 6388 (Nora Lützgendorf), and of course, Omega Centauri, for which Behrang Jalali presented new integral field unit kinematics obtained with Argus/FLAMES, supporting the presence of a $4.7 \times 10^4 M_{\odot}$ black hole (see Figure 4).

Formation of black holes/nuclear clusters

Supermassive black holes observed at $z \sim 6$ are usually assumed to originate either from the remnants of the first stars (Pop III stars, Bernadetta Devecchi), or from intermediate mass black holes with up to $\sim 10^5 M_{\odot}$. To form massive intermediate mass black holes, the gas in primordial galaxies needs to collapse without fragmenting. Numerical simulations have great explorative power in this context. They enable the influence of different physical processes on the runaway collapse to be studied (Dominik Schleicher), can follow the evolution of complex systems, and moreover constrain the growth by mergers and/or accretion using statistical data on black hole mass, seed distribution and luminosity functions (Sandor van Wassenhove, Silvia Bonoli).

Various scenarios have been proposed to explain the formation of nuclear clusters, and David Merritt detailed some of the important dynamical principles that should be kept in mind while dealing with these. A nearly unavoidable process is the heating of the nuclear cluster if it is dynamically colder than its surrounding stellar environment, but this can be significantly slowed down if a central dark mass is present. David Merritt and Markus Hartmann reviewed the possibility of forming nuclear clusters from infalling (globular) cluster systems, which seems a viable hypothesis, mostly for bulge-dominated galaxies.

Relation to the host galaxy

The question of how the central massive objects relate to the properties of the host galaxy was discussed in the last session of the conference. Peter Erwin pointed out that black holes and nuclear

clusters do not seem follow the same scaling relations. While black hole mass correlates tightly with bulge mass (Dimitri Gadotti, Jian Hu), nuclear cluster mass correlates best with total stellar mass, at least in spiral galaxies.

But black hole mass not only correlates with its host galaxy's (bulge) mass, but also with the host galaxy's mid-infrared luminosity (Eleonora Sani) and tentatively also with the number of globular clusters in early-type galaxies (Andreas Burkert). The correlation with globular cluster number even challenges the claim that the $M-\sigma$ relation is the tightest among the scaling relations (Enrico-Maria Corsini).

The meeting was wrapped up by Ortwin Gerhard in an excellent summary talk that triggered a lively discussion. The topics covered during that week have recently gained quite a lot of momentum both on the theoretical and the observational sides, and the results presented at this meeting provided us with an impressive updated view of nuclear clusters, black holes and their potential links. A number of key presentations also pointed out how much we still have to discover and learn!

Acknowledgements

The success and smooth organisation of this workshop would have not been possible without the help and support of Christina Stoffer, as well as the other members of the LOC (in particular, Behrang Jalali, Davor Krajnović, Harald Kuntschner, Nora Lützgendorf and Svea Teupke). The organisers are most grateful to the SOC for their work and very relevant contributions. We thank the review speakers for their excellent talks introducing the topics, and all speakers for very interesting and enjoyable talks. We are grateful to the ESO education and Public Outreach Department (ePOD) for the beautiful and efficient work in producing the workshop poster and cups.

References

- Anderson, J. & van der Marel, R. P. 2010, ApJ, 710, 1032
- Gillessen, S. et al. 2009, ApJL, 707, L114
- Greene, J. E. et al. 2010, arXiv:1007.2851
- Noyola, E. et al. 2008, ApJ, 676, 1008
- Noyola, E. et al. 2010, ApJ, 719, L6

Links

- ¹ Workshop programme: <http://www.eso.org/sci/meetings/cmo2010/program.html>

The 2010 SPIE Symposium on Astronomical Telescopes and Instrumentation

Mark Casali¹

¹ ESO, SPIE Symposium co-chair

A brief overview of the 2010 SPIE Symposium on Astronomical Telescopes and Instrumentation, with emphasis on the ESO contributions, is presented.

The biennial SPIE meetings on Telescopes and Instrumentation provide a unique opportunity for people working in astronomical technology to meet, present developments and share ideas. The 2010 symposium was held from 27 June to 2 July in San Diego. It included over 2000 papers submitted to 12 different conferences covering a whole range of activities including space- and ground-based telescopes and instrumentation, adaptive optics, optical and infrared interferometry, observatory operations, modelling, systems engineering and project management, technologies for ground- and space-based astronomy, software and cyber infrastructure, and detectors for wavelengths from the millimetre to high energy. Formal conferences, talks and papers are of course only part of the event and one of the most important aspects of any SPIE conference is the large number of both planned and impromptu discussions between colleagues from all over the globe, crucial for the sharing of knowledge and experience and establishing new collaborations.

The organisation and logistics of such a large conference are important to achieving a successful outcome. Poor air conditioning or unclear audio can make attending the long sessions difficult and ruin the effective exchange of information. In this respect, the conference facilities in San Diego were of a very high standard, with excellent audio-visual equipment, including twin giant projection screens in the largest hall used for the plenary sessions (one screen for the presentation, one for a giant head-and-shoulders view of the speaker). The good organisation of catering and availability of quick lunches helped everyone keep to schedule. Even the wireless internet connections for such a large number of participants functioned reasonably well.



Figure 1. The ESO stand at the 2010 SPIE Symposium held in San Diego showing a model of the European Extremely Large Telescope.

SPIE symposia usually include plenary sessions in which all registered participants gather in one room to view presentations by invited speakers. The plenary session speakers this year were selected to give a scientific overview of many topical areas in astronomy and were asked to present these at a suitable level for the cross-disciplinary audience of astronomers, engineers and physicists. These sessions were very well attended with most of the several thousand symposium attendees present. Space astronomy was highlighted, with talks about ESA space science, Herschel, Hinode, Fermi, Chandra and XMM-Newton. Ground-based science was also covered with talks about ALMA science, ELT science (given by Roberto Gilmozzi of ESO), survey astronomy, and dark matter and energy.

Given the importance of astronomical technology for ESO, a large number of our staff attended the conference, and over 80 oral and poster papers were either prepared or contributed by ESO staff attending the symposium. I give a few examples here, showing the wide range of topics covered:

- 2010 update on the VLTI status at Paranal by Pierre Haguenaer et al.;
- A summary of the current X-shooter performance by Joel Vernet et al.;
- An overview of the science goals and possible performance of an extreme-AO planet-detection instrument (EPICS) for the E-ELT by Markus Kasper et al.;
- A digest of ten years of experience with the VLT operations and data-flow architecture by Francesca Primas;

- Ultra-stable operation of detectors for high resolution/stability spectrographs by Antonio Manescau et al.;
- Green alternatives to fossil-fuel power generation for modern observatories by Ueli Weilenmann et al.

In addition ESO staff played an important role in the symposium planning and organisation, contributing a symposium co-chair, five conference chairs, and many people within the programme committees for each conference. A novel aspect of SPIE is the availability of courses (typically half to one day) covering various important skills. This year courses included adaptive optics and systems engineering for astronomy projects. A course on scalable frameworks for observatory software was presented by Gianluca Chiozzi of ESO.

A particularly interesting part of any SPIE symposium is the exhibition by industry and astronomical institutes and organisations. Over 70 different exhibits were on show covering most technologies and manufacturing processes required for astronomical facilities. This was also a great opportunity to discuss progress and capabilities with manufacturers to try to get a glimpse over the technological horizon. An ESO display was set up (Figure 1) and staffed on hourly shifts by ESO personnel attending the symposium.

In summary, the San Diego meeting appears to have been a great success. SPIE meetings usually alternate across the Atlantic, so the next one returns to Europe in 2012 and will be held in Amsterdam.

Science with ALMA Band 5

held at INAF–Osservatorio Astronomico di Roma, 24–25 May 2010

Robert Laing¹
Roberto Maiolino²
Hans Rykaczewski¹
Leonardo Testi¹

¹ ESO

² INAF–Osservatorio Astronomico di Roma, Italy

A small complement of receivers for the ALMA Band 5 (163–211 GHz) is under construction. This workshop was devoted to the scientific potential and goals of a full set of Band 5 receivers for ALMA, with emphasis on the detection of water in the local Universe and the 158 μm emission line of C^+ from high redshift galaxies.

The Atacama Large Millimeter/submillimeter Array (ALMA) observatory is currently in the commissioning phase on Chajnantor, with expected release of the first call for proposals for Early Science in a few months. ALMA will be initially equipped with a subset of the receiver bands that are finally envisaged. The initial receiver bands selected were those deemed to be both feasible and of the highest scientific interest when construction was approved. ALMA Band 5 (163–211 GHz), although always considered to be scientifically important, was placed at lower priority, primarily because of the difficulty of observing close to the strong atmospheric water line at 183 GHz.

Following the accumulation of statistics showing that the transparency of the Chajnantor site around the water line is better than expected and the development of improved phase-correction techniques, a proposal to support the construction of six Band 5 receivers for ALMA was supported by the European Commission (EC) under the Framework Programme 6 (FP6). The main scientific motivation was the synergy between ALMA Band 5 and the HIFI instrument on the Herschel satellite, which is currently in full operation. ALMA Band 5 will allow us to resolve and image emission from water and its isotopes, which are being detected by Herschel at other (typically shorter) wavelengths invisible from the ground. The small complement of Band 5

receivers will be installed at the ALMA Observatory by 2012.

Since the initial proposal to the EC, the scientific case for Band 5 has strengthened and initial tests of the first receivers are very promising. In order to take full advantage of the development work already undertaken as part of the EC–FP6 project, it is timely to consider the production of a full set of Band 5 receivers. A necessary preliminary step is the re-evaluation of the scientific potential and goals of an ALMA fully equipped with Band 5: this was the primary aim of the workshop.

Over the last decade, and especially in the last few years, there has been an increasing interest in observations at the frequencies offered by the ALMA Band 5, for both Galactic and extragalactic science. Water is, of course, of intense interest because of its role in the origin of life. A key application for Band 5 is therefore high resolution imaging of the water line at 183 GHz in our own Solar System, Galactic and nearby extragalactic sources. In addition, the 158 μm line of C^+ from objects at redshifts between 8.0 and 10.65 will appear in the band, opening up the possibility of probing the earliest epoch of galaxy formation.

Workshop themes

The workshop was attended by representatives from the ALMA project, technical groups developing the ALMA Band 5 receivers for the EC–FP6 programme and by astronomers with a broad range of scientific backgrounds. The status, timeline and plans for the ALMA projects were presented together with the expected schedule for the ALMA Development Plan, from which the full production of ALMA Band 5 cartridges could potentially be funded. The science goals of the EC–FP6 project were also presented, highlighting the opportunities and limitations of the small complement of Band 5 receivers. The science sessions explored in detail the scientific potential of the ALMA observatory with a full complement of Band 5 receivers: this would provide a giant leap in sensitivity and image fidelity as compared to the initial system. The sessions were divided

into: Solar System, Late-type Stars, Star and Planet Formation, Nearby Galaxies and the High-redshift Universe. Keynote speakers reviewed the science in each area and were followed by contributed talks and extended discussion sessions.

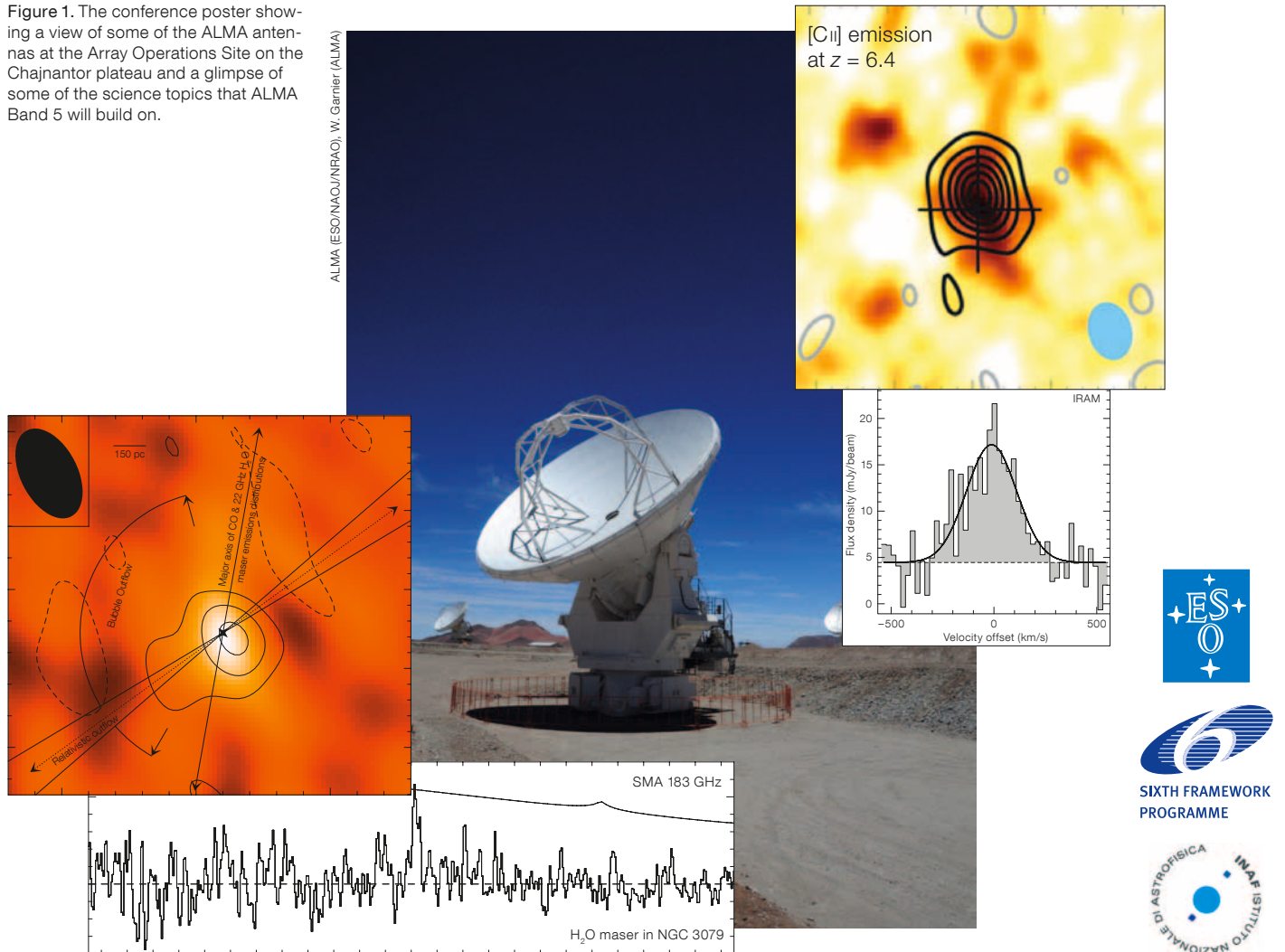
It became clear that the study of water and its isotopes, including deuterated species, in the Solar System is a major possibility offered by ALMA with Band 5 (H_2S , SO and SO_2 also have transitions in the band). Comets provide unique information on the physics and chemistry of the early Solar System and it will be possible to image them in the water lines and to constrain their water abundances. Seasonal variations of the water content of Mars, Venus and the atmospheres of the giant planets and their larger moons will also be extremely interesting.

Water is also a key molecule in star formation: its abundance is low in cold, quiescent regions, but increases at shocks, therefore acting as a tracer of energetic phenomena. It is also a principal constituent of grain ice mantles and the main reservoir of oxygen. Studies of H_2^{16}O and H_2^{18}O in star-forming regions with Herschel are producing extremely interesting results which hint at complex spatial and spectral structure which can only be resolved using ALMA Band 5. As well as water (which is also important to an understanding of oxygen chemistry) many other molecules have transitions in Band 5, particularly relevant to deuteration and chemistry at shocks. Herschel has found surprisingly little cold water vapour in some protoplanetary discs, suggesting that the water may be mostly locked up on the surfaces of dust grains. ALMA's full sensitivity will therefore be needed to deepen our understanding of water in star-forming regions.

One of the main reasons to study late-type stars is their key role in the formation of dust. Models suggest that 183 GHz maser emission may overlap the SiO and H_2O 22 GHz maser shells, which in turn straddle the dust formation zone.

The second main theme of the workshop was the observation of C^+ from the first galaxies. This line, observed for the first time by Alan Moorwood, is the main cooling line of the Milky Way and is expected

Figure 1. The conference poster showing a view of some of the ALMA antennas at the Array Operations Site on the Chajnantor plateau and a glimpse of some of the science topics that ALMA Band 5 will build on.



also to be the brightest line emitted by the first galaxies. It has so far been detected in quasars out to a redshift of 6.4 (corresponding to ALMA Band 6). The redshift range from 8.0 to 10.65, corresponding to Band 5, is a critical one: observations of the Gunn–Peterson effect show that the epoch of reionisation ends at around a redshift of 6. Detection of C⁺ at higher redshifts would allow measurement of gas masses and also constrain the star formation rate in the first galaxies. ALMA is likely to be the only instrument capable of resolving these primordial galaxies and hence of measuring dynamical masses as well as other kinematical properties (e.g., outflows). Although ALMA will not be able to survey large areas at Band 5, blind searches are expected to discover significant numbers

of high-redshift galaxies through their C⁺ emission. New results from Herschel suggest that the C⁺/CO ratio is likely to be very large, making ALMA Band 5 extremely competitive with observations of low-order CO transitions at cm wavelengths (the high-order CO transitions which can be observed at other ALMA bands are probably not excited).

Finally, the current status of the first ALMA Band 5 receiver cartridge, developed at Chalmers University, was presented. The design overcame a number of technical challenges, for example in the cold optics. The mixer noise performance already met ALMA specifications at the time of the meeting, and the combination of the cold cartridge and local oscillator (provided by the Rutherford

Appleton Laboratory in the UK) was tested successfully shortly thereafter.

The detailed programme of the workshop and electronic versions of all the presentations are available on the workshop webpage¹.

Acknowledgements

We thank Giuliana Giobbi from INAF–OAR for her support that made the organisation of this workshop possible. The workshop was sponsored by the EC–FP6 project.

Links

¹ Workshop web page: <http://web.oa-roma.inaf.it/meetings/AlmaBand5/Home.html>

Solargraphs of ESO

Robert Fosbury¹
Tarja Trygg²

¹ Space Telescope European Co-ordinating Facility, ESO

² Aalto University School of Art and Design, Helsinki, Finland

The recently developed technique of simple pinhole camera “solargraphy” enables images of the path of the Sun to be recorded over long periods. Solargraphy cameras have been installed at the three ESO observatory sites in Chile and at ESO Headquarters in Garching. These intriguing images are presented and described. They illustrate, in a very direct way, the clear skies at the observatories.

Introduction

The origin of the technique of “solargraphy” can be traced deep into the history of the photographic process when the first attempts were made to record sunlit scenes on a photosensitive surface (e.g., William Henry Fox Talbot, 1800–1877). The astronomer Edward Emerson Barnard (1857–1923) acquired his interest in photography by using sunlight through a negative to produce an image on print-out paper in a commercial studio. This contact process was the normal way of making prints in the 1870s. The technique that has recently been re-invented under the name of solarigraphy was, however, only born when images were published on the internet in November 2000 by the project Solaris¹, led by the inventors of this unique photographic technique, Slawomir Decyk, Pawel Kula and Diego Lopez Calvin. They called these images “solarigraphics”, and they are created with pinhole cameras (without lenses) and light-sensitive material exposed in such a way that the image is revealed directly, without the use of further chemical development processes.

These pinhole cameras, which have come to be called “cans”, are extremely simple and cheap to construct and have a sensitivity low enough to enable images to be taken of the path of the Sun across the sky with exposures lasting many months.

One of us (TT) was an early pioneer of this process, renaming it “solargraphy” and starting a project to collect exposures from interesting locations all around the world².

During 2009, we had the idea of placing cans at the three ESO observing sites in Chile: La Silla, Paranal and Chajnantor and exposing them for several months. Apart from the wish to obtain images from what are undoubtedly interesting locations, our thought was that this would be a graphic visual record of the clarity and largely cloud-free properties of the observatories.

Here we present the images from Garching and the three observatory sites and explain what they show³.

Process

The cans are constructed from small black plastic canisters used for storing 35 mm film cassettes (see Figure 1). A pinhole in a sheet of aluminium foil is placed over a small aperture drilled into the side of the can, normally at half-height. A rectangle of black and white photographic printing paper (not film) is curled and placed snugly around the inside of the can with sufficient gap to leave the inside of the pinhole unobscured. The can is then sealed with plastic tape to make it watertight (except for the pinhole!).

In order to capture the scene with an exposure of several months, the cans are mounted securely with tape and/or cableties in a position that can record a good fraction of the path of the Sun across the sky. At the end of the exposure, the camera is recovered and, in a dimly lit room, the undeveloped photographic paper is scanned on a colour scanner. The resulting image is transformed to a “positive” by having its intensity scale inverted, followed by some appropriate adjustment of levels and colour balance.

The colours in black and white photographic paper exposed to light come from finely divided metallic silver growing on the silver halide grains. The latent image, which is typically ~ 10 silver atoms per billion-atom grain is invisible, but on continued exposure the latent image clumps



Figure 1. A mounted solargraphy can with the “shutter” open.

grow so that the first visible signs of a print-out image are yellowish, darkening to sepia than a maroonish-brown as the particle size increases. Eventually the maximum exposure produces a slate-grey shade. Reversing an image with this natural range of variations will produce interesting colours, which are of course unrelated to the real colour of the scene. However, lightly exposed parts will be bluish and shades of green/cyan will likely appear in the mid-tones, both of which will lend the positive images a natural look.

The solargraphs

We have obtained multi-month exposure solargraphs in Garching, La Silla, Paranal and Chajnantor (APEX) with the help of a number of very willing ESO staff who are listed in the acknowledgements.

ESO Headquarters in Garching. This camera was exposed from 21 July–15 December 2009 from outside the entrance floor offices on the south side of the building looking southwest and pointing up at an altitude of 20 degrees (see Figure 2). The obscuration at the top left is the back of a small satellite dish on whose support the camera was mounted. Those familiar with the location will recognise the large, now unused, satellite dish at the left and the glass pyramid roof just left of centre. The ST-ECF offices can be seen to the right. The white solar trails reveal what we all know: there is a lot of cloud cover in Bavaria! The summer period was not bad, but the autumn and winter months are well broken up.

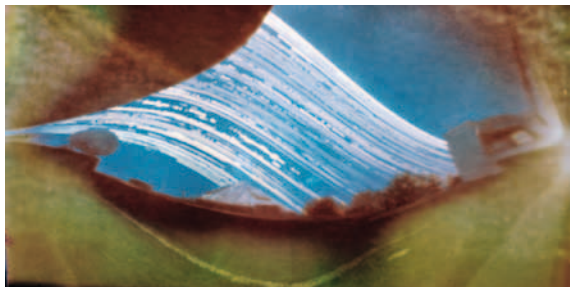


Figure 2. A five-month solargraph exposure at ESO Headquarters in Garching showing foreground objects, a satellite dish to the left and a pyramid roof left of centre.



Figure 3. Solargraph taken at La Silla looking northwest from the CAT telescope dome and showing three months of sunsets over the Pacific.

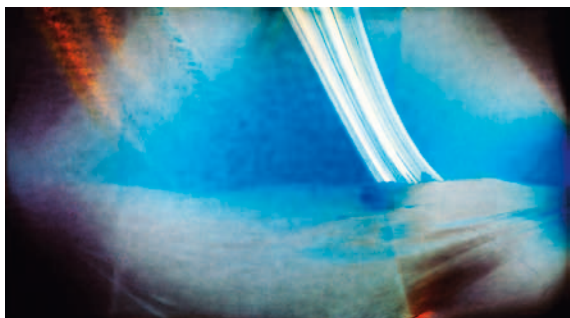


Figure 4. Sunrise behind the NTT at La Silla, exposed from the Danish 1.54-metre telescope catwalk, is shown on this solargraph.

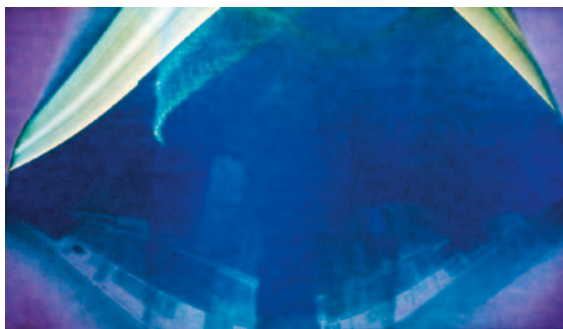


Figure 5. Solargraph taken at the VLT at Paranal, exposed for three months from the roof of the VLT building, pointing north between UT2 and UT3.



Figure 6. Solargraph taken from the control room roof of the VLT at Paranal looking north towards UT1.



Figure 7. Six months of exposure from the APEX enclosure gatepost looking west of north is shown on this solargraph. The moving antenna has created bright reflections that appear as a mottled white haze in the lower right of the image.

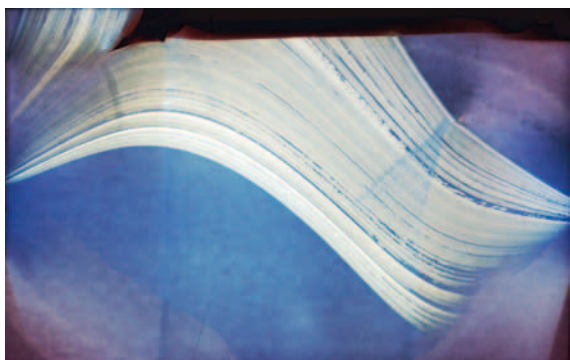


Figure 8. Looking east of north from the roof of the APEX generator building, this solargraph image shows sunrise over Cerro Chajnantor.

La Silla. Two cans were mounted at La Silla by Peter Sinclair and exposed from 6 October–28 December 2009. The first points northwest from the Coudé Auxiliary Telescope (CAT) dome and shows the New Technology Telescope (NTT), the Swiss 1.2-metre Leonhard Euler telescope and a number of other buildings and domes (Figure 3). The Pacific Ocean is on the horizon. The buildings appear blue because of the bright solar reflections from their white or metallic exteriors. The second can was mounted between the same dates and is looking east from the catwalk of the Danish 1.54-metre telescope and shows the NTT

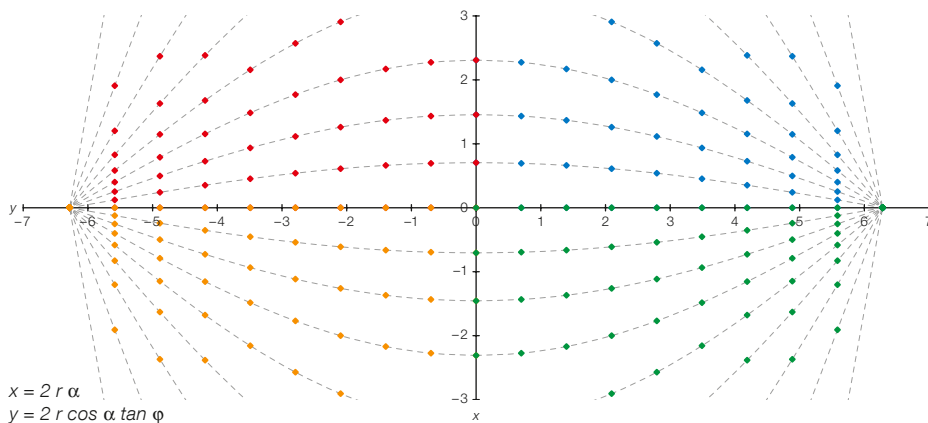


Figure 9. A representation of the projection of altitude and azimuth in a cylindrical pinhole camera is shown. The coloured points are separated by 10 degrees and the x and y scales are in units of cm for the solargraph cans used here. x and y are the horizontal and vertical coordinates, r is the radius of the can, and ϕ and α are the altitude and azimuth angles respectively.

backed by the rising Sun (Figure 4). The dark blue structure to the lower left of the NTT is the combination of the Schmidt and the 2.2-metre telescopes. The 3.6-metre and the CAT telescope domes cannot be seen — probably because they exhibited a similar brightness to that of the clear sky against which they were silhouetted. The solar trails in these images show that the weather is considerably better than in Garching — as we might have hoped!

Paranal. Gerd Hüpdepohl placed two cans on the VLT platform and exposed them from 5 October–26 December 2009. The first, placed on the roof of the Very Large Telescope Interferometer building, shows Unit Telescope 2 (Kueyen) on the left and UT 3 (Melipal) on the right with the VLT Survey Telescope on the far right (Figure 5). The second was placed on the control room extension roof facing north and shows UT1 (Antu) just left of centre (Figure 6). A remarkable feature of these two images from Paranal is that the solar trails are essentially unbroken. There was very little, if any, cloud cover during this period. Both of these solargraphs show a clear “ghostly” repeat of the solar trails, the origin of which is explained below.

Chajnantor (APEX). The cans at APEX were exposed for a full six months from mid-December 2009 until the winter solstice in June 2010. They were placed

by David Rabanus and both were pointed at an elevation of about 45 degrees. One was mounted on the gatepost to the enclosure, close to the antenna, and pointed west of north (Figure 7). Reflections of light from the antenna can be seen as a whitish, mottled haze on the mid-right of this image. The second can was on the roof of the generator powerhouse to the east of the enclosure and pointed east of north (Figure 8). It includes the tilted profile of Cerro Chajnantor on the right silhouetted against the trails of the rising Sun (note that the paper at the top of this image was damaged and produces an artificial split in the solar trails). There were some clouds at the ALMA site during this six-month period — but not many!

Some details

In order to interpret these images, it is necessary to understand the image geometry of cylindrical pinhole cameras. The projection of the altitude angle (ϕ) and the azimuth (α) onto the x,y -plane of the flattened photographic paper (with the angles in radians) is given by the formula in Figure 9. This figure shows a series of points, separated by ten degrees in altitude and azimuth, projected onto x and y . For a camera pointed horizontally with the cylinder axis vertical, this projection results in vertical lines remaining vertical. The x,y units in Figure 9 are in cm for a 35 mm film can camera.

An interesting feature of this kind of solargraph is noticeable in many published images, including especially the La Silla and Paranal examples shown here. The reflection of sunlight from the surface of



Figure 10. An illustration of how stiff paper forms itself inside a cylindrical tube. The straightening of the ends produces caustic reflections in the image.

the photographic paper (especially the glossy variety) results in a secondary image of the solar trails. For a perfect cylinder, this secondary image would appear at twice the distance of the primary image measured from the position of the pinhole just off the edge of the image. In reality, however, a rectangular sheet of stiff photographic paper curled inside a small cylindrical can does not form a perfect cylinder since the ends adopt a flatter form (see Figure 10). As can be shown by sketching the paths of light rays emerging from the position of the pinhole, reflections will describe a caustic along the lines where the paper makes a transition from a flat to a cylindrical profile. The position of this transition can be seen clearly in the Paranal images as approximately vertical dark blue lines.

Acknowledgements

We should like to thank Andreas Kaufer for taking the cans to Chile and distributing them to the three observatory sites. Olivier Hainaut and Carlos de Breuck helped us interpret the images and Olivier quickly solved the problem of the caustics by understanding how the paper flattened at the ends! Peter Sinclair, Gerd Hüpdepohl and David Rabanus did a great job in placing the cameras and documenting the pointing. David Malin kindly supplied the paragraph explaining the formation of the latent image and the resulting colours.

Links

- ¹ Solaris project: <http://free.art.pl/solaris/solaris/Solaris.html>
- ² Solargraphy project: <http://www.solargraphy.com/>
- ³ Further images and descriptions: http://www.flickr.com/photos/bob_81667/

The Experience of Two High School Students Doing Astronomical Research at ESO

Lia Sartori¹
Clara Pelloni¹

¹ Liceo Lugano 2, Savosa, Switzerland

As a project for diploma work at the end of Swiss high school, long-slit kinematic data for two giant elliptical galaxies, observed with the FORS1 spectrograph at the ESO VLT, were reduced by two students. The reduction of these data was our first research experience. The preparation and reduction of the long-slit data is outlined. We also describe our impressions of this first encounter with the scientific research world.

We are two Swiss students who started work on the high school diploma two years ago. In Switzerland the diploma includes a research project that takes place during the last two years of high school: the project can be done in any of the subjects taught in this kind of school. Usually professors propose a list of projects for the students to choose from. We decided to work in astronomy, one of the most fascinating fields of physics. Our project, entitled “Spectroscopic analysis of elliptical galaxies”, has led us to a whole new experience and to meet new people (including a few astronomers), but most importantly, has brought us to a mythical place in the astronomical world, namely the ESO observatories at La Silla, Paranal and Chajnantor (ALMA) in Chile, which are equipped with some of the world’s best telescopes.

During the entire project, we were guided by our physics teacher, Nicolas Cretton, astronomer and ex-ESO fellow. Together with Hans-Walter Rix, he wrote the original ESO observing proposals (65.N-0285 and 68.B-0590) on which our project was based. During the entire work, we received a lot of help and advice from Piero Rosati, an astronomer at ESO. When the spectra were all reduced, Eric Emsellem from the Observatoire de Lyon (and now at ESO) extracted the kinematical quantities for each axis of the galaxies.

We visited ESO Headquarters in Garching twice during the summer of 2008 and

could therefore learn a great deal about activities at ESO: telescope design and construction, observation preparation and realisation. At first, we felt a bit disorientated in this new world of scientific researchers. But soon we got acquainted with many nice and helpful astronomers who showed us the various research activities at ESO. We could also discuss our diploma project and get some precious advice. During this full immersion in the scientific world, something completely new for us, the impression was really positive and stimulating. At ESO, we found a nice and welcoming atmosphere: everybody was very helpful and the interactions between astronomers seemed to us very friendly. The desire to work one day in a research institute such as ESO has been an extra motivation for us to start, with even more enthusiasm, our university studies. During the visit to Garching, we also visited the outreach department where we were offered a lot of goodies: DVDs, posters, caps, postcards, etc.

The visits to ESO helped immensely in achieving the goals of the diploma project. Once the project was completed, we participated in various regional and national competitions. The most significant one was the national competition “Science and Youth” that took place in Geneva at the end of April 2009¹: four days of project presentations and discussions with experts, other participants and the public. Presenting our project to such a wide audience turned out to be challenging, since we had to adapt our explanations to the various levels of scientific expertise. But the Geneva competition was not only work: there was a lot of free time to get to know all the other participants, who came from all over Switzerland.

Preparatory theoretical work

Since the high school programme contains little astronomy, before starting the data reduction work we had to learn a few necessary astronomical concepts: stellar evolution (life cycle of stars, Hertzsprung–Russell diagram), galaxy structure and morphology, dark matter in galaxies, long-slit spectroscopy (emission lines, absorption lines, line-of-sight

velocity profiles, etc). A few technicalities, such as the working of telescopes, spectrographs and CCDs were also needed. This study constituted the first part of our project. The complete manuscript of our project report is available (in Italian) on the web².

Data reduction

The goal of our project was to fully reduce long-slit spectra of two giant elliptical galaxies, NGC 5018 and NGC 3706, and to obtain the corresponding kinematic quantities: mean line-of-sight velocities, velocity dispersions and higher order moments of the velocity profile. Figure 1 shows one of the target galaxies, NGC 5018. Spectra were obtained with the FORS1 spectrograph of the VLT in 2000 and 2001. The light of elliptical galaxies is dominated by the emission from red giant stars with spectral types such as our calibration templates stars. Visible absorption lines include the K, H lines of calcium, the H β , H γ and Mg b lines (see Figure 2). These two galaxies had already been observed (e.g., Carollo & Danziger, 1994a,b and Carollo et al., 1995), but never with such a large telescope as the VLT. With these data, we tried to confirm and extend to larger radii previously published data. For both galaxies there is an indication of dark matter in the outer parts, so very extended kinematic data (up to two to three effective radii, R_{eff}) could improve the confidence on the presence of a dark halo. Previous work has shown the importance of both increased radial extension and the calculation of higher order moments in quantifying the amount of dark matter in elliptical galaxies.

It is notoriously difficult to measure dark halos in elliptical galaxies, since one has to rely on absorption spectra, which are very hard to obtain beyond one R_{eff} due to the sharp drop in stellar luminosity and because of the absence of an extended gas tracer, as in spiral galaxies. One alternative to stellar kinematics is to use planetary nebulae that can be detected at large radii. The present study confirms and extends previously published kinematic data such as those obtained by Carollo & Danziger (1994a,b) and Carollo et al. (1995). It therefore constitutes an

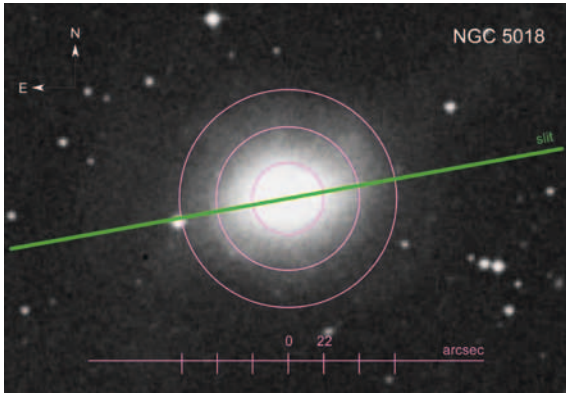


Figure 1. A Digital Sky Survey image of NGC 5018, with the position of the FORS1 long slit on the major axis (green) shown and the circles of radii 1, 2 and 3 R_{eff} overlaid (pink). Asymmetric features beyond $2 R_{\text{eff}}$ are probably the sign of a past merger in this galaxy.

improved basis for the dynamical modelling that is needed to study the amount and distribution of dark matter in giant elliptical galaxies; such modelling is however outside the scope of our diploma project.

With the GRIS-600B+12 grism and a 1.31 arcsecond-wide slit, we had an instrumental spectral resolution σ_{instr} of 200 km s^{-1} , similar to the galaxy velocity dispersion, which is just sufficient to obtain good kinematic measurements. The wavelength resolution was 1.2 \AA per pixel, which corresponds to 7.8 \AA for the CCD pixels and slit size we used. The total exposure times for NGC 5018 are 200 minutes for the major axis and 150 minutes for the minor axis, whereas

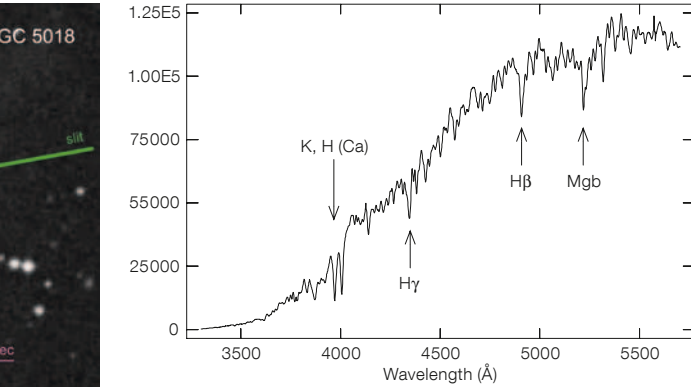


Figure 2. The central major axis spectrum of NGC 5018 is shown from the FORS1 observations. The major absorption lines of calcium, hydrogen and magnesium are indicated.

for NGC 3706 they were 135 minutes for the major axis, 90 minutes for the intermediate (45-degree) axis and 225 minutes for the minor axis.

As the first step, we obtained the raw data (science and calibration frames) for the FORS1 programme from the ESO Archive. From there, a lot of effort and time went into understanding: 1) the nature of the imaging and spectroscopic data and corresponding calibrations; 2) the methodology to remove instrumental signatures; and 3) the calibration procedures to go from instrumental to physical units. For all these tasks, we were also introduced to IRAF³, which we ran on a Linux laptop as part of the ESO Sci-software package⁴.

All raw spectra were bias-subtracted, flat-fielded, sky-subtracted and wavelength-calibrated following the various steps described in Massey et al. (1992) and Massey (1997). Particular attention

was given to the sky subtraction, since we wanted to obtain reliable kinematic data at large distances from the galaxy centres. In this respect, the 408-arcsecond long FORS1 slit was very useful. We also reduced in the same manner spectra of calibration template stars observed at the same telescope: as templates we used the following giant stars, indicated with their respective spectral type: HR 4595 (K3III), HR 4790 (G3III), HR 4801 (K5III), HR 4818 (K4III).

Results: stellar kinematics of NGC 5108 and NGC 3076

To quantify the line-of-sight velocity distributions along the principal axis of the galaxies, Eric Emsellem computed the Gauss-Hermite moments with dedicated software (a C version of a penalised pixel-fitting routine, described by Cappellari & Emsellem, 2004): mean rotation velocity, velocity dispersion sigma, and

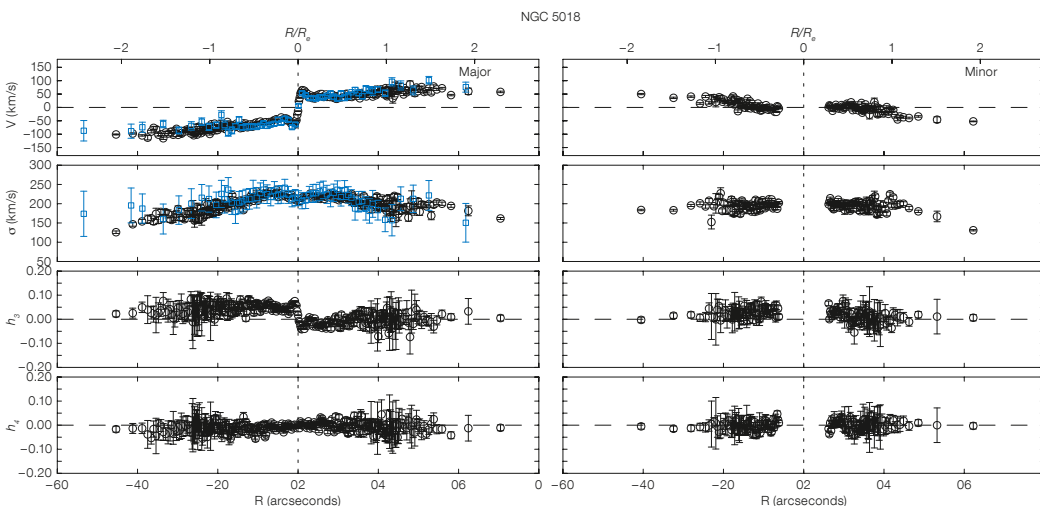


Figure 3. The stellar velocity, velocity dispersion, h_3 and h_4 profiles as functions of distance from the galaxy centre (in arcseconds) are shown along the major axis of NGC 5018, from top to bottom respectively and for the major and minor axes (left and right). Blue points are the data from Carollo & Danziger (1994b). For the minor axis, systematics on the detector prevented us from extracting the kinematics in the central few arcseconds for this galaxy. The top axes are labeled in effective radii R_{eff} ($1 R_{\text{eff}} = 22$ arcseconds). The velocity dispersion (around 200 km s^{-1}) dominates the mean rotation (around 60 km s^{-1}) and decreases only slowly towards the outer parts.

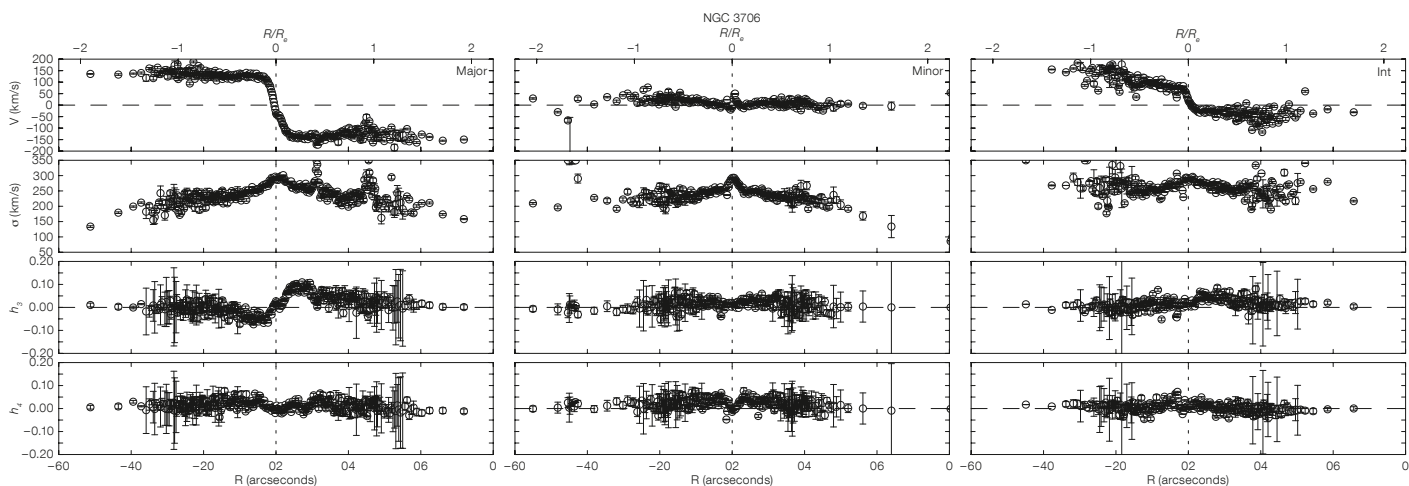


Figure 4. The stellar velocity, velocity dispersion, h_3 and h_4 profiles as functions of distance from the galaxy centre (in arcseconds) are shown along the major axis of NGC 3706, from top to bottom respectively and for the major, minor and intermediate axes (left, middle and right respectively). The top axes are labelled in effective radii R_{eff} ($1 R_{\text{eff}} = 27$ arcseconds). This galaxy rotates faster than NGC 5018: it has a mean rotation of around 150 km s^{-1} . As for NGC 5018, the velocity dispersion shows a slow decline with radius. A few foreground stars happen to lie on the slit and explain some of the observed disturbances in the profiles.

moments h_3 and h_4 . Figures 3 and 4 show the results of such computations for the two galaxies: in both cases we go further than $2 R_{\text{eff}}$. In NGC 5018 (Figure 3), there is some asymmetry between the left and the right side, which could be interpreted as a signature of a past merging event. Indeed NGC 5018 displays some tidal tails in the outer parts (see e.g., Rothberg & Joseph, 2006). There is central drop in the velocity dispersion, associated with a sharp rise in the mean velocity curve, probably the sign of a so-called “sigma-drop” interpreted as the result of past gas accretion in a central disc (Emsellem, 2006). In NGC 3076 (Figure 4), the stellar velocity reaches higher amplitudes and is quite regular except for a central feature also revealed by the h_3 profile. The dispersion is dropping slowly in the outer part. In both galaxies the h_4 moment is mostly consistent with zero.

The trip to Chile

Our data was obtained in service mode so we did not use the VLT ourselves to observe the two galaxies. Fortunately, at

the end of our diploma work we were able to submit it to the national competition “Science and Youth”, which in 2009 had a special prize for astronomical projects in honour of the International Year of Astronomy. This prize could not have been better chosen for us since it was a trip to Chile to visit the three ESO sites, La Silla, Paranal and Chajnantor in early September 2009 and a night of observations at the Swiss 1.2-metre Leonhard Euler telescope at La Silla. Together with another student, Andreas Cuni, we won the special prize and went to Chile to visit the famous telescopes. Below we describe our impressions of this trip.

Chile has many wonderful landscapes, but our trip was mostly enlightening from

a scientific point of view. Indeed we could meet astronomers and engineers and see how they live and work. This experience was very useful in view of a possible future career in the scientific research world.

We first visited the observatory of La Silla, near La Serena (see Figure 5). We had to submit a proposal for a night of observations at the 1.2-metre Leonhard Euler telescope (2 September 2009). Since for our diploma we had worked exclusively on spectra, we decided to do photometry of galaxies and globular clusters in various

Figure 5. From left to right, Andreas Cuni, Clara Pelloni and Lia Sartori on their visit to the La Silla Observatory.



Figure 6. The authors Clara Pelloni and Lia Sartori (centre left and right) between Pierre Dubath (the organiser of the trip to Chile) at left, and Andreas Cuni (the other prize-winner), at right, shown in Paranal at the gate of the road leading to the VLT. Pierre Dubath (Geneva Observatory) had the idea of creating the special prize in astronomy and found the necessary funding for the trip to Chile.



filters. The idea is to use the globular cluster observations to construct a Hertzsprung–Russell diagram in order to compute their ages and distances. Due to time constraints, we could only observe two globular clusters (47 Tuc and NGC 362) and one barred spiral galaxy (NGC 1300). The clusters were observed in the *B*-, *V*- and *I*-filters, while the galaxy in *R* and *I*. The results were satisfactory, even if the full Moon and some clouds reduced the image quality. For us, it was particularly rewarding to work on the practical aspects of astronomical observations, such as the telescope preparation, the setting of coordinates and other parameters and to be able to see the results after a few minutes.

We went further, to Paranal, to visit the mighty VLT (see Figure 6). ESO astronomers showed us the various telescopes at the Paranal site, their instruments and the control room. It was particularly exciting to see the aperture opening of the dome of one of the four Unit Telescopes of the VLT. First the telescope is put horizontal, to reduce dust falling onto the primary mirror while the dome is opening. Then the dome opens, together with the various lateral windows. It is hard to imagine the real dimensions of such an instrument only from pictures; having been there in person is an unforgettable experience!

Last but not least, we went to Chajnantor to visit the ALMA site, near San Pedro de Atacama, at an altitude of 5000 metres. The final project will have 66 radio antennas, built to observe the cold Universe. At that time, only one telescope was ready and functioning (the ALMA Pathfinder Explorer, APEX). Other antennas are ready on the ALMA site, but without instrumentation they do not work yet. Here as well, it was possible to speak with the people working there and to get detailed explanations on the working of the radio telescopes.

Conclusions

During our diploma project at the end of high school, we fully reduced spectra of two elliptical galaxies, using the same professional software that astronomers use in their daily work. We could derive extended kinematics (up to about $2.5 R_{\text{eff}}$) for NGC 5018 and NGC 3706, two giant elliptical galaxies. The derived mean velocity, velocity dispersions, and higher order moments h_3 and h_4 could be signposts for the presence of dark matter halos around these galaxies. For instance, at large distances from the galaxy centres, the velocity dispersions do not drop as sharply as naïvely expected on the basis of the distribution of the luminous matter. However, to quantify the amount of dark matter, detailed dynamical modelling is needed. This is outside the scope of our project, but our data constitute an excellent basis for such an analysis.

Our research project was our first encounter with the world of scientific research. It was a truly fascinating experience, thanks to the visit to ESO Garching and the various ESO telescopes in Chile and

mostly thanks to the warm welcome, patience and enthusiasm of all the astronomers, engineers and technicians we met. After high school, we will continue studying science: physics for Lia and mathematics for Clara, both at the Zurich ETH institute.

References

- Cappellari, M. & Emsellem, E. 2004, *PASP*, 116, 138
- Carollo, C. M. et al. 1995, *ApJ*, 441, 25
- Carollo, C. M. & Danziger, I. J. 1994a, *MNRAS*, 270, 523
- Carollo, C. M. & Danziger, I. J. 1994b, *MNRAS*, 270, 743 (CD94b)
- Emsellem, E. 2006, in *Mapping the Galaxy and nearby galaxies*, eds. Wada, K. & Combes, F.
- Massey, P. 1997, *A User's Guide to CCD Reductions with IRAF*, NOAO
- Massey, P. et al. 1992, *A User's Guide to Reducing Slit Spectra with IRAF*, NOAO
- Rothberg, B. & Joseph, R. D. 2006, *AJ*, 132, 976

Links

- ¹ Science and Youth: <http://www.sjf.ch/>
- ² Diploma project report: http://www.nicolascrétton.ch/Astronomy/index_LAM.html
- ³ IRAF: <http://iraf.noao.edu>
- ⁴ Scisoft: <http://www.eso.org/sci/data-processing/software/scisoft/>

ESO Astronomers Emeriti — Sandro D’Odorico and Alan Moorwood

Francesca Primas¹
Mark Casali¹
Jeremy Walsh¹

¹ ESO

In May and June 2010, Sandro D’Odorico and Alan Moorwood, both driving forces behind many ESO instruments and very active in research, retired after three decades at ESO. The ESO Director General, Tim de Zeeuw, elevated both to the newly inaugurated position of ESO Astronomer Emeritus. Celebrations on their transition to these esteemed positions were held and are briefly described.

Sandro D’Odorico

Sandro joined ESO as a fellow in 1980, becoming a staff member in 1981. He has been an inspiring force behind many instruments, including CASPEC, EMMI, UVES and, most recently, X-shooter, and has guided optical detector development for many years. Sandro stands out not just because of his zeal for instrumentation, but his passion for using those instruments for the research in which he was most interested — namely active galactic nuclei, and quasi-stellar object (QSO) absorption lines studies in particular. Despite a very active career in instrumentation he has kept up a strong research career with many dedicated collaborators. He was persuaded to allow a meeting in his honour, which was organised by Francesca Primas and Luca Pasquini and was held over two days (31 May–1 June 2010) at ESO Headquarters.

The meeting was themed to interweave Sandro’s achievements in both instrumentation and astronomical science. Talks were given by the majority of the participants, who had collaborated in one way or another with Sandro. Long-term collaborators, such as Adriano Fontana, Emanuele Glallongo, Stefano Cristiani and Paolo Molaro, talked about how scientific questions triggered ideas for new instruments; others had used the instruments that Sandro had led, including Bruno Leibundgut, who described



Figure 1. Sandro D’Odorico sharing the amusement over his optical instrument sculpture with Mark Casali at his retirement party.

the early reduction of EMMI spectroscopy. A highlight of the meeting was the talks given by some of those who are usually behind the scenes, spending most of their time on ray tracing and in the optics laboratory. Bernard Delabre described the optical design of the many ESO instruments in which he has been involved during the time that Sandro has been at ESO, Gerardo Avila expounded on working with fibres, showing some examples of the hardware, and Olaf Iwert covered the exciting years of CCD development at ESO. In the field of QSO absorption lines there was a full morning session of talks, including one by Wal Sargent describing spectroscopy of $z \sim 6$ targets with the Keck instrument HIRES, and one by Max Pettini on detecting outflows from high- z galaxies with high resolution spectroscopy. Two threads running through many of the talks were personal memories and football — with many speakers showing photographs of non-professional football teams in which Sandro had played. Two of his closest collaborators at ESO, Hans Dekker and Jean-Louis Lizon, were in Chile during the meeting and contributed many stories and memories over the video link. Noteworthy was the presence of Sandro’s daughter, Valentina D’Odorico, also a professional astronomer, and Francesco Bertola, who supervised Sandro’s

Master’s thesis. In the closing ceremony Sandro was presented with a present by Tim de Zeeuw (see the photo on the Astronomical News section page) and a “sculpture” made by Jean-Louis Lizon from spare X-shooter parts (see Figure 1).

Alan Moorwood

Alan was the longest serving astronomer at ESO — until May 2010, that is. He joined in 1978, when ESO was still based in Geneva, and throughout his career he has specialised in infrared instrumentation. He was an early pioneer of infrared (IR) spectroscopy, starting from the days when IR detectors had only one pixel. A chronicle of the IR instruments, among them IRSPEC, IRAC and IRAC2, ISAAC, SOFI and CRIRES, to which he has been a central contributor is given in the *Messenger* article on personal recollections (Moorwood, 2009). Alan was Head of Instrumentation from 2004, and for the last two years, Head of the Directorate of Programmes, and so had a steering influence on the design work for the E-ELT and its instrumentation.

A retirement party, or Emeritus welcoming party (!), was held for Alan on 18 June 2010 at ESO Headquarters. There were warm appreciations by Gert Finger,



Figure 2. Alan Moorwood enjoying the intricacies of his IR instrument sculpture with Mark Casali at his retirement party.

who has developed the state-of-the-art in infrared detectors under Alan's leadership and by Jean-Louis Lizon, who has assembled or maintained much of the VLT instrumentation. Roberto Gilmozzi, the current Head of the Telescope Division, recounted time spent with Alan at the VLT in the very early times, when ISAAC was being commissioned. Mark Casali, the current Head of Instrumentation, presented Alan with another of Jean-Louis Lizon's sculptures, based on parts from different IR instruments (see Figure 2). This sculpture was interactive and a set of hex-keys was provided to release one of the stuck mechanisms! Alan, whose memory is renowned in ESO, recounted extensively many experiences on and off the telescopes (see the photo on the Astronomical News section page).

References

Moorwood, A. 2009, *The Messenger*, 136, 8

New Staff at ESO

Adrian Russell

I am originally from Sheffield in England, and sadly still find myself supporting Sheffield United football club despite the fact that they never win! When I am not working I am also a keen photographer. My wife Lilie and I have two girls Elizabeth (8) and Victoria (5); they will both start at the Munich European School in September and are looking forward to learning to speak German.

Having started life as an electronics engineer, I rapidly became hooked on astronomy and did my PhD at the University of Cambridge (at the Mullard Radio Astronomy Observatory, MRAO), working on mm-wave heterodyne instrumentation

and molecular line studies of outflows in star formation regions.

In 1987 I joined the Royal Observatory Edinburgh (ROE) and my wife and I went on a three-year tour of duty in Hawaii, where I was a support scientist on the newly commissioned James Clerk Maxwell Telescope (JCMT). During this time I supported many of the instruments on the telescope. In 1990 we moved to Garching and I spent a two-year sabbatical with Reinhard Genzel's group at the Max-Planck-Institut für extraterrestrische Physik where I worked on very high frequency sub-mm instrumentation for the JCMT. In 1992 I returned to the ROE and became the Head of the JCMT Instrumentation Programme. This involved



Adrian Russell

managing the international development programme carried out in the UK, Canada and the Netherlands.

In 1995 I made a massive change in direction to become the UK Project Manager for the Gemini project and moved into the optical/infrared world. Following the most radical reorganisation of British astronomy in decades, I was privileged to become the first Director of the UK Astronomy Technology Centre in Edinburgh in 1998. In January 2005 we moved to Charlottesville Virginia and I joined the National Radio Astronomy Observatory (NRAO) as North American ALMA Project Director/Project Manager.

Now, 20 years later, we are back in Germany! My family and I have just arrived at ESO and already it is very exciting. From my perspective the opportunity to become Director of Programmes at ESO was compelling. It is hard to imagine a better time to join ESO. As I see it there are three overriding priorities for ESO in the coming years: to continue to successfully operate and develop the existing ESO facilities; complete ALMA and ensure it fulfils its scientific potential; and establish the European ELT as the world's foremost optical-infrared facility. The prospect of playing a key and defining role in these areas, especially the E-ELT, is incredibly exciting. There can be little doubt that opportunities like this come very rarely indeed.

Elena Valenti

In June 2004 I had my first experience with ESO telescopes. At that time I was a PhD student at Bologna University and I was visiting UCLA Astronomy and Astrophysics Department in Los Angeles for several months to work on high resolution infrared spectra of cool giants in the Galactic Bulge. I flew from a hot and noisy LA to Santiago for my first observing run as PI at La Silla Observatory, three nights with SOFI on the New technology Telescope (NTT). I remember being a bit worried, not only because I had no previous experience, but also because I knew that an important part of my PhD thesis, aimed at studying the Bulge stellar populations in the near-infrared, actually depended on those three nights. I think I fell in love with



Elena Valenti

the place from the very first night. I still believe there is nothing more beautiful than the southern sky on a clear winter night in the Chilean desert! The observations went absolutely fine; I had good seeing and great support from ESO staff, astronomers and telescope operators. I went back to LA not only with my data, but also with the feeling that something important had actually happened. I found myself enjoying observation much more than I could imagine and I started considering the idea of applying for the ESO fellowship in Chile, as I wanted to learn much more about telescopes and instrumentation, in particular in the near-infrared.

In October 2006 I joined ESO as fellow with duty at Paranal. During the first year I was assigned to the VLT Unit Telescope 1 (UT1), which at that time was equipped with ISAAC and CRILES, so I could take advantage of my previous, first experience as an observer with an infrared imager (SOFI at the NTT) and spectrograph (NIRSPEC at the Keck II telescope), and largely improve on it. With CRILES I also had the chance to have a closer look at the adaptive optics (AO) systems. Of course I already knew what an adaptive optics system should do in principle, but the first time I saw live, in real time, a fuzzy and confused crowded field in the centre of our Galaxy becoming clear once the NAOS loop closed, I was so amazed that I immediately asked to be trained on UT4 instruments as well. Working with NACO and SINFONI allowed

me to become more and more familiar with AO systems, an experience that turned out to be extremely useful for my scientific activity. It gave me the chance to explore new possibilities and start new collaborations in the study of resolved stellar populations, which is one of my main research interests. I honestly don't see that there is anywhere else quite like ESO, where one can have both the chance to acquire such different expertise and get in touch with the most up-to-date observational facilities.

Since the beginning of my fellowship I have been amazed by the enormous number of things — related to instruments, telescopes, meteorology, software, data handling, etc — that I could learn. I was always extremely pleased by the great generosity of the people working in all divisions (astronomers, telescope operators, engineers, electricians, software people) in sharing their knowledge and hence allowing me to significantly increase my knowledge of observational astronomy. During the fourth year of my fellowship, I moved to the Astronomy Department of the Pontificia Universidad Católica in Santiago to work full time on scientific research. It was another great experience, and possible because of the ESO Chile fellowship rule that allows fellows to spend one year of pure research in a Chilean or ESO member state university. If I could go back in time I would certainly re-apply for the fellowship in Chile. I would like to take advantage of the opportunity now to thank, one more time, all the people I have met and worked with in Paranal and Santiago, because they all contributed to my scientific and personal growth.

Since April 2010 I have moved back to Europe to take up a position with the USD staff at ESO Headquarters in Garching. This is an extremely stimulating and scientifically active environment that allows young astronomers to work in areas of frontline technology and astronomy, and potentially to keep in touch with all branches of astrophysics. Now I can use the experience acquired at the telescopes to support astronomers on many different kinds of observations. It is a slightly different job but one that I really enjoy. There are many new colleagues who are always willing to share their expertise and with whom it is a pleasure to work.

Fellows at ESO

Pamela Klaassen

Picture it: the first day of school in suburban Toronto, 1996. A physics teacher at the front of the classroom with a bow tie and monotone voice (think Ben Stein in *Ferris Beuller's Day Off*), and a 17 year old girl sitting down at her desk saying, "Well, let's see if I like this, 'cause it's what I'm doing with the rest of my life". And so, my career as an astronomer began.

A few years later, I did my undergraduate and Master's degrees at the University of Calgary. As an undergraduate, I did manage to do a few nights of observing at an optical telescope, but I soon swayed over to the dark side (radio astronomy), and haven't really looked back since.

Then one day, on the road up to the summit of Mauna Kea to start some observations on the JCMT, my supervisor (Rene Plume) asked me where I wanted to do my PhD. I think he was trying to get rid of me. Apparently though, some good decisions CAN be made at 4000 m, because I contacted Christine Wilson later that evening, and started as her PhD student about a year later; with the caveat that she would be on sabbatical for my second year. This gave me license to go on a sort of graduate student sabbatical of my own, and I headed to the Harvard-Smithsonian Center for Astrophysics for a one year Sub-mm Array (SMA) pre-doctoral fellowship (with Eric Keto). Instead of being one of three radio astronomers on campus, I was in a building dedicated to radio astronomy. It was great! After that year, I dutifully returned to McMaster University with a new-found appreciation for radio interferometry. Two years later (which takes us to 2008), I finished my PhD, and moved to ESO.

For most of my career, I've been studying the gas dynamics in regions of our Galaxy forming massive stars. I started out only studying the large-scale outflow structures. But, as I gained knowledge, I started asking more questions, and writing more observing proposals, and asking more questions, and... the cycle continues to this day. I've now broadened my research interests to studying the dynamics of the gas in a variety of ways. This includes not only looking at the outflowing gas, but the infalling gas and rotation in and around the star-forming regions. I do



Pamela Klaassen

this by looking at the small-scale structures with interferometers, and the large-scale structures both with single-dish telescopes and combinations of interferometers and single dishes (to see the large-scale structures at high resolution). Recently, I've started probing the relationship between the ionised and molecular gas in regions forming massive stars, and how the bulk gas kinematics described above change across the ionisation boundary. (FYI — it doesn't look like much changes!)

Since arriving at ESO, I've become involved in the ALMA project, and have had the opportunity to learn all about the software under development by becoming a tester of the Observing Tool, and giving lectures on how to use the data reduction software (CASA). I'm really looking forward to putting the skills I've learned here at ESO to good use when ALMA comes online next year.

Rodolfo Smiljanic

When I was eleven years old, I had the chance to do a course on basic astronomy at the planetarium in my home town in Brazil. There I also looked through a telescope for the first time. The images I saw that night are still imprinted on my mind. Two years later, I read in a magazine an article entitled: *How to become a professional astronomer*. That was the true turning point, where the path to becoming a professional astronomer became clear to me.

This path first led me to the Valongo Observatory of the Federal University of Rio de Janeiro for an astronomy undergraduate degree. I first wanted to be a cosmologist, but that changed in my first month of studies. During a class I was told that it was possible to infer the chemical composition of the stars from their spectra! I was so excited by this amazing idea that I immediately knew that my days as a cosmologist were over; I would become a stellar astrophysicist. There I had my first research experience, studying the abundance of heavy s-process elements in chemically peculiar barium giant stars. For this research I analysed FEROS spectra, and that was probably the first time I heard about ESO. The years I spent at the Valongo Observatory were very important for me and I cherish them a lot.

Later I moved to the University of São Paulo, first for an MSc in astrophysics and then for a PhD. During those years I changed my focus from the heavy elements to the lighter ones. It was during my PhD that I had my first chance to come to ESO. In 2006, I came with a Brazilian studentship to stay for one year and work on the use of stellar beryllium abundances as a cosmochronometer. The scientific environment in ESO made a great impression on me. I went back to Brazil to finish my PhD, hoping that one day I would be able to come back to ESO.

Rodolfo Smiljanic



The chance for that appeared one month after my PhD defense. On the day before my birthday I received the fellowship offer, which I promptly accepted. I started as a fellow in Garching in October 2009, after a nine months postdoc in Brazil. In my research, I use high resolution spectroscopy to determine stellar chemi-

cal abundances and investigate the physical processes affecting the structure and the evolution of low- and intermediate-mass stars. I am also interested in understanding the chemical evolution of the Galaxy better. For my functional duties I joined the User Support Department. I am now helping to support service

mode observations using UVES at the VLT. It was a long and challenging, but also rewarding, path from a small telescope and a planetarium to being part of ESO, a world-leading observatory where I can work with one of the largest and most modern telescopes ever built.

Announcement of the ESO Workshop

Dynamics of Low-Mass Stellar Systems: From Star Clusters to Dwarf Galaxies

4–8 April 2011, ESO Santiago, Chile

At the low-mass end of stellar systems, there used to be a well-known dichotomy. On the one hand, there are star clusters with typical sizes of a few parsecs (pc), whose internal dynamics can generally be well described by the Newtonian gravity law. On the other hand, there are the much more extended dwarf galaxies with sizes of several hundred pc, whose dynamics appear to be dark matter dominated and which are usually related to cosmological substructures. These classical boundaries have been blurred by the recent discovery of new classes of stellar groupings, such as ultrafaint dwarf spheroidal galaxies (dSphs), ultramassive super star clusters, ultra compact dwarf galaxies (UCDs), and dark-matter-poor tidal dwarf galaxies (TDGs). These discoveries and the confirmation of multiple stellar populations in a number of Galactic globular clusters have reinforced the question, to which extent star clusters and dwarf galaxies actually share common origins and are intimately linked in their dynamical evolution.

In this context, recent years have seen a particularly large effort in the astronomical community to thoroughly investigate the internal dynamics of low-mass stellar systems in the Milky Way and Andromeda. Extensive measurements of dwarf spheroidal galaxy kinematics have yielded crucial input for structure formation theories, particularly on the clustering properties of dark matter on small scales. Similar observing campaigns regarding Milky Way

star clusters are providing strong constraints on theories of modified gravity and on the shape of the black hole mass–sigma relation at low masses. Proper motion studies of the Galactic halo have revealed a marked phase-space correlation of dSph orbits, which is challenging canonical structure formation paradigms, and alternative explanations to dark matter have been put forward regarding the large velocity dispersions found for dSphs.

Beyond the Local Group, space-based imaging has been extensively used to investigate the dynamical evolution of star cluster populations in a number of star-forming galaxies. The initial cluster mass function is distinctly different from the mass function of old globular clusters, which is still not very well understood. Also, star clusters and dwarf galaxies have been used as dynamical tracers in galaxies and galaxy clusters, constraining the gravitational potential on large scales. Finally, peculiar internal dynamics were found for UCDs — objects at the phase transition between star clusters and dwarf galaxies — suggesting either dark matter clustering on scales below those suggested for dSphs, or a significant variation of the initial mass function.

All this shows that the dynamics of low-mass stellar systems is not only an interesting subject in its own right, but is also intimately linked to global theories of structure formation, the physics of gravity, and

the shape of the stellar initial mass function. Given the wealth of new information gathered most recently in this field, the time is ripe to hold a dedicated meeting on this topic. We aim at bringing together a mix of astronomers from both observations and theory who work on the dynamics of dwarf galaxies and star clusters.

The scientific organising committee consists of: Holger Baumgardt, Australia; Giovanni Carraro, ESO; Michael Fellhauer, Chile; Mark Gieles (co-chair), UK; George Hau, ESO; Michael Hilker, ESO; Helmut Jerjen, Australia; Steffen Mieske (co-chair), ESO; Yazan Momany, ESO; Ivo Saviane, ESO; Michael West, ESO; Mark Wilkinson, UK.

The local organising committee consists of: Karla Alamo, María Eugenia Gómez, Valentin Ivanov, Lucie Jilková, Paulina Jirón, Renee Mateluna, Steffen Mieske.

The workshop, limited to 60–80 participants, will take place at the ESO premises in Santiago, Chile.

Further details are available at <http://www.eso.org/sci/meetings/dynamics2011/>.

The deadline for registration is 15 January 2011. Further information can be obtained from dynamics2011@eso.org.

Evolution of Compact Binaries

6–11 March 2011, Valparaíso, Chile

Compact binaries divide into many classes depending on the mass of either component, the mass transfer rate, the magnetic fields involved and whether the primary star is a white dwarf, neutron star or black hole.

However, the evolution of all these objects is driven by a common mechanism: angular momentum loss. This process controls the change of the orbital period as well as, in the phases of interaction, the mass transfer rate. This means that the basic physics behind all these objects is the same, and, by comparing the results found for one class, we might be able to understand similar problems in another. Some of the open questions that are common to all classes of compact binaries are, for example:

- the impact of the common envelope phase;

- the role of rotation in the evolution of the secondary;
- the role of magnetic fields in binary evolution;
- possible braking mechanisms and their efficiency;
- physical mechanisms to increase the mass of the compact component to finally reach a point of ignition.

With this workshop we plan to bring together people from different communities; and in this sense it is a very broad and open workshop. On the other hand, it will also be focused as it concentrates on one specific problem, namely binary evolution, which, over the last decade, has emerged as one of the most active fields within the compact binary communities.

The deadline for registration is 15 January 2011.

Scientific Organising Committee: Jarrod Hurley, Australia; Andrew King, UK; Ulrich Kolb, UK; Mario Livio, USA; Félix Mirabel, France; Linda Schmidtobreick, ESO; Matthias Schreiber, Chile.

Local Organising Committee: Moira Evans, Centro de Astrofísica de Valparaíso; María Eugenia Gómez, ESO; Paulina Jirón, ESO; Elena Mason, ESO; Kieran O'Brien, UCSB; Retha Pretorius, ESO; Alberto Rebassa, Univ. de Valparaíso; Linda Schmidtobreick (co-chair), ESO; Matthias Schreiber (co-chair), Univ. de Valparaíso; Claus Tappert, Univ. de Valparaíso; Maja Vuckovic, ESO; Mónica Zorotovic, ESO–PUC.

Further information can be found at http://www.eso.org/sci/meetings/Binary_Evolution2011/ and more details can be obtained by e-mail: binary-evolution-2011@eso.org.

Personnel Movements

Arrivals (1 July–30 September 2010)

Europe

Bonzini, Margherita (I)	Student
Cortese, Luca (I)	Fellow
Delorme, Alain (F)	Senior Contract Officer
Diaz Trigo, Maria (E)	Operations Scientist
Dietmann, Evelina (I)	Administrative Assistant
Echaniz, Juan Carlos (E)	System Engineer-Product Assurance
Hamilton, Robert (GB)	ERP Consultant
Lagerholm, Carina (S)	Student
Motalebi, Fatemeh (IR)	Student
Munding, Silvia (D)	Librarian
Pineda, Jaime (RCH)	Fellow
Pontoni, Cristian (I)	Mechanical Engineer
Randall, Suzanna (GB)	Operations Scientist
Russell, Adrian (GB)	Director of Programmes
Wallace, Jane (GB)	Executive Assistant

Chile

Brammer, Gabriel (USA)	Fellow
Hau, George (GB)	Operations Staff Astronomer
Lombardi, Gianluca (I)	Fellow

Departures (1 July–30 September 2010)

Europe

Chereau, Fabien (F)	Software Engineer
Conn, Blair (AUS)	Fellow
De Silva, Malcolm (GB)	Contract Officer
Gladysz, Szymon (PL)	Post Doctoral Researcher
Justen, Benedikt (D)	Student
Korhonen, Heidi (FIN)	Fellow
Lind, Karin (S)	Student
Martinez, Patrice (F)	Optical Engineer
Schmidt, Sandra (D)	Secretary/Assistant
Snodgrass, Colin (GB)	Fellow
Wicenc, Andreas (D)	Software Engineer
Ziegler, Bodo (D)	User Support Astronomer

Chile

Evatt, Matthew (USA)	Mechanical Engineer
Gallenne, Alexandre (F)	Student
Mason, Elena (I)	Operations Astronomer
Oestreich, Martin (D)	Electrical Engineer
Ritz, Andre (RCH)	Procurement Officer
Robert, Pascal (F)	Instrumentation Engineer
Wehner, Stefan (D)	Software Engineer
Zorotovic, Monica (RCH)	Student

ESO, the European Southern Observatory, is the foremost intergovernmental astronomy organisation in Europe. It is supported by 14 countries: Austria, Belgium, the Czech Republic, Denmark, France, Finland, Germany, Italy, the Netherlands, Portugal, Spain, Sweden, Switzerland and the United Kingdom. ESO's programme is focused on the design, construction and operation of powerful ground-based observing facilities. ESO operates three observatories in Chile: at La Silla, at Paranal, site of the Very Large Telescope, and at Llano de Chajnantor. ESO is the European partner in the Atacama Large Millimeter/submillimeter Array (ALMA) under construction at Chajnantor. Currently ESO is engaged in the design of the 42-metre European Extremely Large Telescope.

The Messenger is published, in hard-copy and electronic form, four times a year: in March, June, September and December. ESO produces and distributes a wide variety of media connected to its activities. For further information, including postal subscription to The Messenger, contact the ESO education and Public Outreach Department at the following address:

ESO Headquarters
Karl-Schwarzschild-Straße 2
85748 Garching bei München
Germany
Phone +49 89 320 06-0
information@eso.org
www.eso.org

The Messenger:
Editor: Jeremy R. Walsh
Design, Production: Jutta Boxheimer;
Layout, Typesetting: Mafalda Martins;
Graphics: Roberto Duque
www.eso.org/messenger/

Printed by Peschke Druck
Schatzbogen 35, 81805 München
Germany

Unless otherwise indicated, all images in The Messenger are courtesy of ESO, except authored contributions which are courtesy of the respective authors.

© ESO 2010
ISSN 0722-6691

Contents

Telescopes and Instrumentation

M. Kenworthy et al. – A New Coronagraph for NAOS–CONICA – the Apodising Phase Plate	2
P. Martinez et al. – On the Difference between Seeing and Image Quality: When the Turbulence Outer Scale Enters the Game	5
F. Kerber et al. – Balloons over the La Silla Paranal Observatory	9

Astronomical Science

M. A. Barucci et al. – The Outer Frontiers of the Solar System: Trans-Neptunian Objects and Centaurs	15
F. Schuller et al. – The APEX Telescope Large Area Survey of the Galaxy (ATLASGAL)	20
R. Saito et al. – VISTA Variables in the <i>Vía Láctea</i> (VVV): Current Status and First Results	24
G. Giuffrida et al. – A Wide-angle VIMOS Survey of the Sagittarius Dwarf Spheroidal Galaxy	29
M. Bremer et al. – Studying the Properties of Early Galaxies with the ESO Remote Galaxy Survey	32

Astronomical News

N. Neumayer, E. Emsellem – Report on the ESO Workshop “Central Massive Objects: The Stellar Nuclei – Black Hole Connection”	37
M. Casali – The 2010 SPIE Symposium on Astronomical Telescopes and Instrumentation	40
R. Laing et al. – Report on the ESO Workshop “Science with ALMA Band 5”	41
R. Fosbury, T. Trygg – Solargraphs of ESO	43
L. Sartori, C. Pelloni – The Experience of Two High School Students Doing Astronomical Research at ESO	46
F. Primas et al. – ESO Astronomers Emeriti – Sandro D’Odorico and Alan Moorwood	50
New Staff at ESO – A. Russell, E. Valenti	51
Fellows at ESO – P. Klaassen, R. Smiljanic	53
Announcement of the ESO Workshop “Dynamics of Low-Mass Stellar Systems: From Star Clusters to Dwarf Galaxies”	54
Announcement of the ESO/Universidad de Valparaíso Workshop “Evolution of Compact Binaries”	55
Personnel Movements	55

Front Cover: Near-infrared colour composite image taken with the VISTA telescope of the core of the Large Magellanic Cloud, showing the nebula NGC 2070 containing the R136 star cluster. The image was formed from exposures in *Y*, *J* and *Ks* filters (as blue, green and red) with exposure times of 40, 47 and 81 minutes respectively. These images form part of the VISTA Magellanic Cloud Survey. See Release 1033 for more details. Credit: ESO/M.-R. Cioni/VISTA Magellanic Cloud Survey. Acknowledgement: Cambridge Astronomical Survey Unit.